UCLouvain

École polytechnique de Louvain

Simulating human walking to virtually develop and test new methods for locomotion assistance

Authors: **Matthieu AUSSEMS, Nicolas DINEUR**
Supervisor: **Renaud RONSSE**
Readers: **Paul FISETTE, Greet KERCKHOFS, Henri LALOYAUX**
Academic year 2022–2023
Master [120] in Mechanical Engineering

Abstract

Walking is a fundamental human activity that contributes to physical and mental well-being. However, physical impairments and gait disorders can significantly hinder walking ability, impacting an individual's quality of life and social participation. Developing innovative technologies, such as prostheses, active orthoses, and exoskeletons, to enhance locomotion is crucial. The design of effective assistive control strategies is a critical factor for the proper functioning of these devices. Virtual simulations provide a valuable approach to test control strategies before human experiments, offering time-saving and safer conditions.

This thesis aims to address these challenges by replicating and implementing Geyer's walking model in a widely accessible programming language and the Robotran platform. The thesis follows a three-stage approach: a theoretical understanding of the 2 dimensions human locomotion model, implementing it using Robotran, and validating the results against Geyer's Simulink model.

The findings from the 2D Robotran model demonstrate human walking dynamics, closely resembling Simulink simulation results for an entire left foot gait cycle. The results encompass kinematics, muscle actuation, and neural control, providing conclusive evidence. Limitations and areas for improvement are explored in the context of the contact model. The thesis concludes by highlighting the significant findings and the potential for virtual testing of locomotion assistance methods. The model developed represents a step forward in bio-mechanical research, laying the foundations for future investigations into the bio-mechanics of human walking.

Acknowledgement

We would like to thank Renaud Ronsse, professor at the Institute of Mechanics, Materials and Civil Engineering at UCLouvain. As our thesis promotor, he passed on very useful knowledge, advised and guided us along this project.

We would like to extend our thanks to Henri Laloyaux, PhD student and assistant for the Mechatronic, Electrical Energy, and Dynamic systems division, for his exceptional availability, invaluable advice, extensive knowledge, and unwavering support and optimism throughout the entire year.

Furthermore, we would like to take this opportunity to thank the members of the iMMC. Their expertise and fresh look at the project were key to bringing the project to conclusion.

Finally, we would like to express our deepest thanks to our families and friends who have been a constant source of support and encouragement throughout this journey and who have kindly agreed to proofread this document.

Acronyms

- AFO : Adaptative frequency oscillator-based
- BE : Buffer element
- BCI : Brain-computer interface
- CPG : Central pattern generator
- CE : Contractile element
- COM : Center of mass
- EEG : Electroencephalography
- GAS : Gastrocnemius
- GLU : Gluteus
- GRF : Ground reaction force
- HAM : Hamstring
- HFL : Hip flexor
- MBS : Multibody system
- MTC : Muscle tendon complex
- PE : Parallel element
- SCI : Spinal cord injury
- SE : Serie element
- SOL : Soleus
- TA : Tibialis anterior
- VAS : Vasti

Contents

1 Introduction **2**
- 1.1 Analysis of the Human Gait 3
  - 1.1.1 Anatomical Planes 3
  - 1.1.2 Gait cycle 4
- 1.2 Introductory Summary 5

2 State of the Art **7**
- 2.1 Mathematical Models 7
  - 2.1.1 Executor: Skeletal Subsystem 7
  - 2.1.2 Actuator: Muscle Subsystem 9
  - 2.1.3 Controller: Nervous Subsystem 10
  - 2.1.4 External Environment: Ground Contact Model 11
- 2.2 Complete Model of Human Locomotion 11
  - 2.2.1 Geyer Model 11
  - 2.2.2 COMAN Simulation 12
  - 2.2.3 OpenSim Models 12
- 2.3 Methods for Locomotion Assistance 13
  - 2.3.1 High-Level Controllers 14
  - 2.3.2 Mid-level Controllers 14
- 2.4 Testing of Assistance Methods 16

3 Simulation Tools **18**
- 3.1 Simulation Environment 18
  - 3.1.1 Simulink Software 18
  - 3.1.2 Robotran Software 18
  - 3.1.3 Simulator 19
- 3.2 Body Mechanics Model 20
  - 3.2.1 Inertial Frame, Reference Angles and Positions 20
  - 3.2.2 MBsyspad Description 20

4 Bio-inspired 2D Model of Human Gait **22**
- 4.1 Muscle Actuation Layer 23
  - 4.1.1 Characterization of the Leg Muscles 23
  - 4.1.2 Hill's Muscle Model 24
  - 4.1.3 Muscle Length and Torque applied to the Joints 27
- 4.2 Neural Control Layer 28

4.2.1 Reflex-based Control Laws 28
4.2.2 Leg Muscles Stimulation Laws during Human Walking 30
4.3 External Environment : Ground Contact Model 33

5 Specific Implementation Choices for the Bipedal Model 35
5.1 Muscle Actuation Layer 36
5.1.1 Excitation-Contraction Coupling 36
5.1.2 Selection of an Integration Method 36
5.1.3 Impact of the Implementation Choices on the Muscle Actuation Layer's Outputs 37
5.2 Neural Control Layer 38
5.2.1 Weight Supported by the Contralateral and Ipsilateral Leg . . . 38
5.2.2 The Neuromuscular Delay 39
5.2.3 Impact of the Implementation Choices on the Neural Control Layer's Outputs 40
5.3 External Environment: Ground Contact Model 41
5.3.1 Results of a Non-actuated One-leg Robotran Model 42
5.3.2 Results of a Non-actuated Two-leg Robotran Model 44
5.4 Conclusion 46

6 Robotran Model: Results and Analysis 48
6.1 Simulation Results in Robotran 48
6.1.1 Gait Cycle 50
6.1.2 Left Joint Positions 50
6.1.3 Right Joint Positions 52
6.1.4 Collapse of the Model 53
6.2 Muscle Actuation Layer 54
6.2.1 Conclusion 55
6.3 Neural Control Layer 55
6.3.1 Left Stimulations 55
6.3.2 Right Stimulations 57
6.3.3 Conclusion 59
6.4 External Environment: Ground Contact Model 60
6.4.1 Vertical Ground Contact Forces 60
6.4.2 Horizontal Ground Contact Forces 62
6.4.3 Conclusion 64

7 Limitations and Future Perspectives 65
7.1 Limitations and Potential Improvements 65
7.1.1 External Environment: Ground Contact Model 66
7.1.2 Optimization of Stimulation Parameters 67
7.1.3 Phase Detection Conditions 68
7.2 Future Perspectives 69

8 Conclusion 71

A Body Mechanics Characterization **73**

B Hill Muscles Characterization **74**
B.1 Useful Parameters for Muscle Characterization 74
B.1.1 Individual MTC Parameters 74
B.1.2 MTC Attachment Parameters 74
B.2 Force-length and Force-velocity Relationships of an MTC 75

C Neural Control Characterization **76**
C.1 Synthesis of Stimulations 76
C.1.1 Laws of Control based on Reflexes 76
C.1.2 Reflex Parameters 77
C.2 Representation of Muscle Activity during a Gait Cycle 78

D Stimulations Results **79**

E Ground Contact Model Results **82**
E.1 One-leg Unactuated Model 82
E.2 Two-leg unactuated model 83

Chapter 1

Introduction

Walking is a fundamental human activity, often taken for granted. Beyond allowing us to explore our environment, perform daily tasks, engage in social interactions, walking plays a crucial role in maintaining our overall physical and mental well-being. From simple walks in the park to high intensity physical activities, walking is central to living life to the fullest.

Alas, physical impairments or gait disorders can significantly impact the ability to walk, turning this seemingly basic action into a tremendous challenge. They can be congenital or acquired and are caused by various factors: neurological conditions such as Parkinson's disease or strokes, musculoskeletal disorders or deformities, injuries leading to limb amputations or paralysis but also because of natural aging. Population aging is, nowadays, one of the most important challenges for industrialized countries. It is expected that 40 years from now, more than 20 % of the European population will be older than 60 years [1]. The aforementioned conditions can manifest as unsteady, altered gait, difficulties to initiate movements, imbalance, or reduced speed for instance. This poses a genuine handicap, affecting both the individual's quality of life and their ability to participate fully in society.

It is therefore of utmost importance to develop innovative technologies aimed at enhancing locomotion. Prostheses, active orthoses, and exoskeletons emerge as promising devices that can potentially fulfill these requirements. Nevertheless, a critical factor in the proper functioning of these devices is the design of the assistive control strategy. The behavior of the user's response to the provided assistance is often uncertain, it needs to be perfectly understood. One way to mitigate this uncertainty is to conduct simulations virtually to test various strategies and opt for the most suitable one before engaging in experiments with human users. This approach offers multiple advantages, including time-saving and safer experimental conditions. Of course, reliable and consistent human locomotion models that can accurately represent the dynamics and kinematics of the gait cycle are crucial to virtually test control strategies.

Shaped by millions of years of evolution, human locomotion involves intricate coordination of numerous muscles, guided by a complex neural circuitry. For this reason, Hartmut Geyer, associate professor at Carnegie Mellon University's Robotics Institute, developed a simplified model involving seven muscles per leg and relying on muscle reflexes. With his model, Geyer obtained consistent results with regard to electromyographic observations of leg muscles [2].

The existing implementation of Geyer's model in MATLAB/Simulink, accessible on his website [3], has one limitation. It requires additional packages not covered by the basic MATLAB license, compelling individuals to purchase an expensive supplementary license. This narrows the accessibility of the model to a larger public.

Hence, the objective of this thesis is to replicate and adapt Geyer's model of human walking using the Robotran platform, a multibody simulation environment, developed at UCLouvain [4]. By doing so, the aim is to address the limitations associated with the availability of the model and make it more accessible for researchers and engineers working on locomotion control strategies. The use of the Robotran platform provides a viable alternative and expands the range of researchers who can utilize and contribute to the advancement of locomotion modeling and assistive technology.
Ths thesis is composed of three main stages. The first step is to gain a theoretical understanding of Geyer's model. The second step is the implementation of Geyer's model using Robotran. Finally, the results obtained from Robotran are validated and discussed by comparing them with the results obtained by Geyer on Simulink.

All graphs, tables and codes presented in this thesis are generated or written in Python. The entire code used, and the final simulation result are publicly available on GitHub [5]. A video showcasing the animation generated by the model is also available on the GitHub repository. Note that the artificial intelligence tool ChatGPT has been used to facilitate text correction and reformulation, in line with the EPL position on this subject.

1.1 Analysis of the Human Gait

1.1.1 Anatomical Planes

The three anatomical planes are defined with respect to the standing position of the bipedal model. By convention, the z-axis points upwards, the y-axis points to the left side of the model and the x-axis points forwards. The three anatomical planes as well as the geometrical axes are represented in Figure 1.1

- The frontal or coronal plane is perpendicular to the ground and parallel to the yz-plane. It separates the body into an anterior and posterior part.

- The sagittal plane is perpendicular to the ground and parallel to the xz-plane. It separates the left part from the right part of the body.

- The transverse or horizontal plane is parallel to the ground and the yx-plane. It separates the body into the upper and lower body.

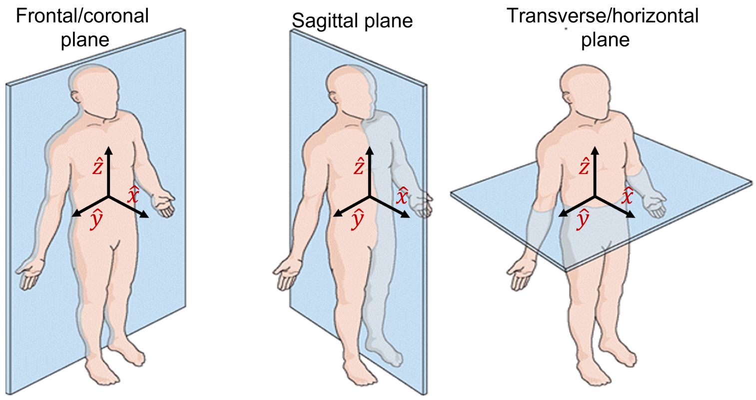

Figure 1.1: Anatomical planes and axis for a biped. Adapted from [6]

1.1.2 Gait cycle

A leg gait cycle can be divided in two phases: a stance and a swing phase. According to Kharb [7], the stance phase corresponds to the time-lapse during which the leg is in contact with the ground and supports the weight of the biped while the swing phase corresponds to the duration the leg is moving forward in the air. Over one walking gait cycle, each leg completes one leg cycle. During the gait cycle, they are therefore in stance for 60% of the time and in swing for 40%.
For 20% of the cycle, the biped is in a double support phase. This refers to the situation where both feet are simultaneously in contact with the ground.
Starting by convention with a right heel contact with the ground, a walking cycle can be divided into four phases.

1. **The double support phase I:** both feet are in contact with the ground.
2. **The simple support phase I:** the left leg starts its swing phase after the left toes lift from the ground while the right leg remains in a stance phase.
3. **The double support phase II:** the left heel reaches the ground. Both feet are in contact with the ground.
4. **The simple support phase II:** the right leg starts its swing phase after the right toes lift from the ground while the left leg remains in a stance phase.

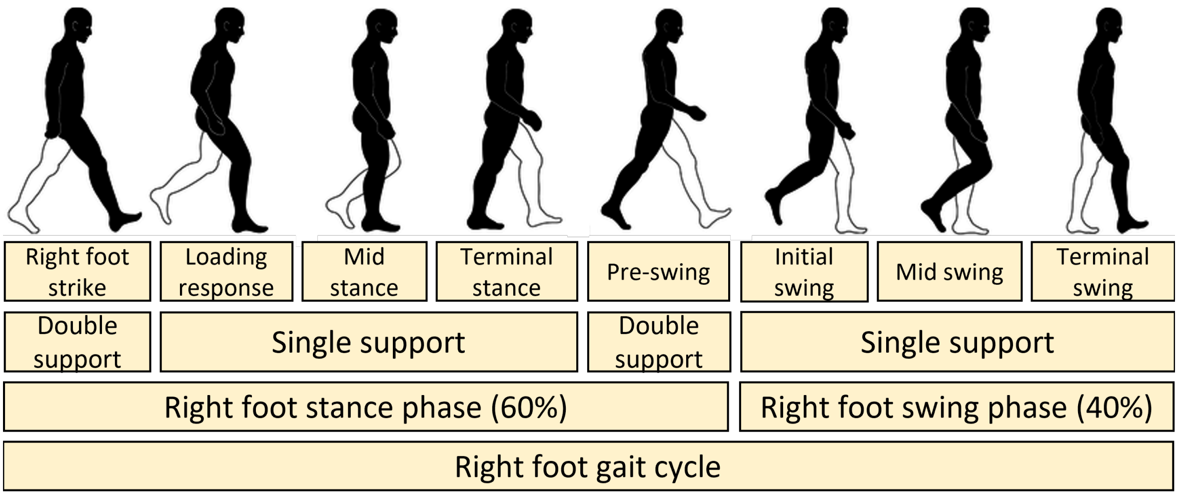

Figure 1.2: Right foot gait cycle. Image adapted from [8]

1.2 Introductory Summary

After presenting the background and objectives of this work and a general description of the gait cycle, this section briefly reviews its various chapters.

Chapter 2 - State of the Art

In this chapter, a review of the current state of knowledge, previous research results, and current research trends in the field of human gait modeling and locomotion assistance strategies is presented.
First, the different models used to model walking, with a focus on the role of the muscle subsystem, the neural subsystem, and the skeletal subsystem are outlined.
Then, the methods for assisting locomotion are discussed, focusing on the existing possibilities in terms of high-level and mid-level controllers, as well as on the methods for testing these assistance methods.

Chapter 3 - Simulation Tools

The purpose of this chapter is to introduce the tools used in this thesis.
First, the simulation environments are presented. The Simulink environment of Matlab, used by Geyer, and the Robotran environment, used for the implementation of the model.
Then, the bio-mechanical model of the body is described, as well as its representation in the Robotran environment.
Finally, an overview of the Robotran simulator is provided, focusing on the integrator used to solve the dynamic equations and its comparison with the Simulink integrator used by Geyer.

Chapter 4 - Bio-inspired 2D Model of Human Gait

This chapter is devoted to the presentation of the 2D model used. First, the Geyer model is described by presenting the modeling of the 7 muscles by Hill's model, as well as the reflex control laws that are used to obtain the muscle stimulations.
Finally, the contact force model based on spring-damper elements and friction model is described.

Chapter 5 - Specific Implementation Choices for the Bipedal Model

This chapter will present the implementation choices of some blocks/functions of the model, with explanations of the motivations and the impact on the output results. This will be accomplished for the muscle actuation layer, the neural layer, and the external forces.

Chapter 6 - Robotran Model: Results and Analysis

In this chapter, the results of the simulations are presented and analyzed. The results of walking are then compared with Simulink data to evaluate it. Various data are presented to analyze the model of walking: The joint positions, the stimulations of each muscle, the torques on each articulation and the ground reaction forces.

Chapter 7 - Limitations and Future Perspectives

This chapter focuses on the limitations encountered during the research and presents several strategies to address these limitations. Additionally, potential avenues for future research are explored, based on the outcomes and findings of the study.

Chapter 2

State of the Art

2.1 Mathematical Models

To accurately reproduce human locomotion, a thorough understanding of the neuromusculoskeletal system is crucial. This system encompasses the nervous, skeletal and muscular system interconnected as follows [**Human_gait**],[9]:

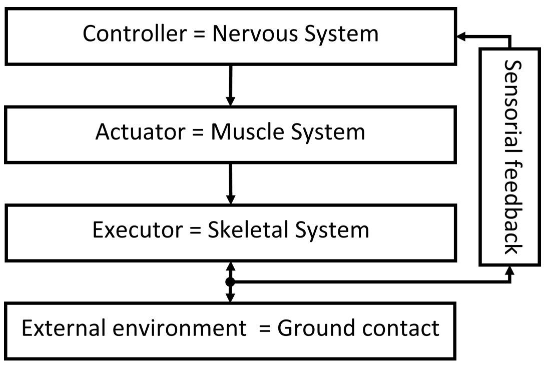

Figure 2.1: Diagram representing the structure of arrangement of the 3 subsystems within the total neuromusculoskeletal system and their relations with the environment. Figure from [**Human_gait**].

2.1.1 Executor: Skeletal Subsystem

The executor subsystem, also referred to as the skeletal system, is the internal framework of the human body. It is composed of rigid elements and joints i.e., bones and articulations and, plays a crucial role in supporting the body's weight and enabling diverse body movements. The movements are generated through the forces produced by the muscles creating torques at the joint level.

2.1.1.1 Bipedal Spring-mass Model

The bipedal spring-mass model embodies the fundamental concept of leg control during bipedal walking and running.
The model consists of a point mass connected to 2 springs representing the legs. During

the swing phase, the point mass follows a ballistic trajectory, while the springs come into play during the stance phase, when the force generated by their contractions against the ground counteracts gravity.
This model captures two essential characteristics of walking: bipedalism and leg compliance. Although simplistic, this model provides an accurate dynamic profile of the center of mass as observed experimentally and enables the unification of both running and walking under a single mechanical behavior. The bipedal spring-mass model serves as a template for the development of more sophisticated models (see Figure 2.2(a)) [10], [11].

2.1.1.2 Trunk Segment and Three-segmented Leg Model

In the analysis of human walking, the segmentation of the upper body into rigid bodies is no longer the most relevant factor. Therefore, models composed of a segment representing the trunk and two "three-segmented legs" have been developed (see Figure 2.2(b)).

The three-segmented leg model is composed of three segments corresponding to the thigh, the shank and the foot, connected by joints corresponding to the hip, knee, and ankle. Quasi-elastic torque characteristics at the ankle and knee can resolve possible kinematic redundancy problems induced by this model. [12].
The trunk is modeled as a segment that require to be balanced during the movement. The balance is achieved through multisensory integration that involves visual information, information from the vestibular organs, and proprioception of the legs. While this integrative control can be complex when standing up right, it is not necessary during walking [13].

2.1.1.3 Whole Body Model

The human skeletal structure can be modeled using a 33-rigid bodies model, which are connected by revolute and universal joints in such a way that 16 major anatomical segments can be identified (Figure 2.2(c)) [14]. This approach provides a detailed and accurate characterization of the human skeletal structure, allowing for precise analysis of the human gait.

The full body system has 44 degrees of freedom resulting from 38 rotational degrees of freedom from 26 revolute joints and 6 universal joints, as well as 6 degrees of freedom from the free rotations and translations of the base body. Each body is described using parameters commonly used in multibody studies, namely : the mass of the body, the position of its center of mass, and the inertia matrix.
The description of the body is completed by the following geometrical characteristics: the length of the segments, and the position of the proximal joint from the distal end. Since the whole body model has no spherical joints, it is particularly useful in inverse dynamics applications, although it can also be used for kinematic and forward dynamics analysis applications.

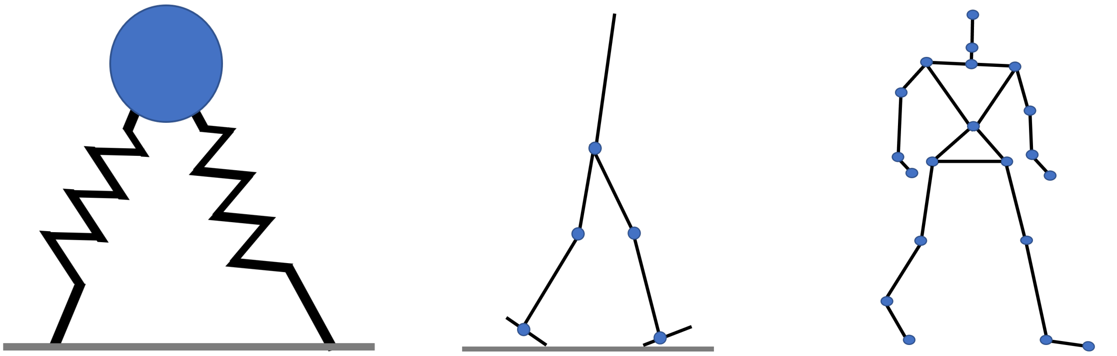

(a) Spring-mass model. (b) Three segmented leg model. (c) Full body model.

Figure 2.2: Skeletal subsystem models. Figures inspired from [2] and [14].

2.1.1.4 Foot Model

Due to its complexity and its significant impact on the overall gait pattern as a result of its interaction with the ground during locomotion, studying existing models representing the foot is key.

The human foot can be modeled as a rigid element or as a compliant element respecting the human foot proportions and the ankle position. In the first variant, the foot is represented as a single rigid element that is either flat (Figure 2.3(a)) or curved (Figure 2.3(b)) to approximate its shape. The second variant consists of 2 plates, respectively the hindfoot and the forefoot, connected by springs (Figure 2.3(c)). The configuration of the compliant model allows to represent the foot and the deformations the foot is subjected to during contact with the ground [9].

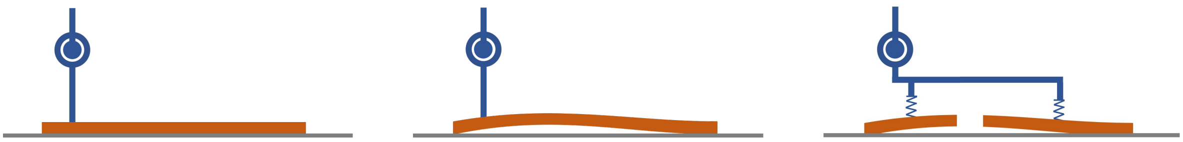

(a) Flat rigid foot. (b) Curved rigid foot. (c) Compliant foot model.

Figure 2.3: Foot models. Figures adapted from [9]

2.1.2 Actuator: Muscle Subsystem

The skeletal muscle subsystem consists of muscles that are attached to the skeleton. The contractions of these muscles, in combination with the masses and inertia of the moving bodies and the external reaction forces of the ground, generate the movements of the different parts of the body. The skeletal muscles produce forces inducing torques that actuate the joints. This subsystem is defined by the muscle tissues dynamics, which can be further subdivided into activation dynamics and contraction dynamics.

Activation dynamics describe the time lag between the electrical signal sent to the muscle and the resulting activation of the muscle fibers.
This relationship can be modeled as a low-pass filter represented mathematically by a first-degree differential equation [15].
The contraction dynamics correspond to the transformation of the muscle activation into muscle force. The most widely used model to describe contraction dynamics is the muscle-tendon Hill Model (see Figure 2.4). It is composed of a contractile element (CE) in series with an elastic element (SE). These 2 elements together form the motor unit in normal operation. If CE stretches beyond its optimal length, another elastic element (BE) engages. This elastic element prevents CE from collapsing if SE is slack [16], [2].

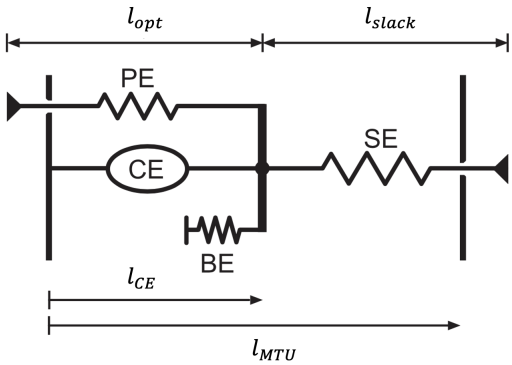

Figure 2.4: Muscle-tendon Hill model. Figure from [2]

2.1.3 Controller: Nervous Subsystem

The coordination and control of human locomotion are highly dependent on the nervous system.
In vertebrates, two different processes control human locomotion: a forward control called the central pattern generator (CPG) and a feedback control known as a sensory reflex-based system.

The CPG, located in the spinal cord, generates rhythmic patterns of activation of extensor or flexor muscles leading to cyclic movements such as walking or running.
Taga et al., introduced this system into the human locomotion model using distributed nonlinear oscillators, resulting in robust walking and running movements [17].
Another approach, using a hierarchical system, provides stable 3D results from walking and running [18].

A gait cycle similar to that obtained in the experiments either in terms of positions or in terms of torques on articulations can be generated by simple control laws based on muscular reflexes [2].
Muscular reflexes are a response to afferent sensory information from the muscle spindles such as the length of the contractile elements, the speed of contraction, or the forces developed by the motor unit.

Moreover, the reflex-based control, is able to integrate ground disturbances and to adapt to slopes.

2.1.4 External Environment: Ground Contact Model

When it comes to modeling human walking, it is important to consider how feet interact with the ground. To model stable and efficient locomotion, it is fundamental to understand the contact mechanics between the foot and the ground. Therefore, various models of foot-ground contact have been proposed and studied over the years.

According to Farley and Gonzales, measures of the displacement of the global center of gravity allow to compute the ground reaction forces (GRFs) [19].

Several compliant models allow for the representation of foot and ground deformation during contact. One method of replicating these deformations involves spring-damper elements to compute the GRFs [20], while other models utilize deformable 2D or 3D spheres, allowing for accurate estimations of the GRFs [21].

Compliant models require an experimental measurement of the compliance between the foot and the ground, whose value might change from one subject to another. In contrast to inverse dynamics simulations, the use of compliant models for direct dynamics simulation is quite successful. It should be noted that other models exist for inverse dynamics which are not addressed in this paper given they are less relevant in light of this study [22].

2.2 Complete Model of Human Locomotion

The aforementioned sections have outlined existing models to mathematically describe the three subsystems of the human neuromusculoskeletal system. The next three points are examples of the end-to-end implementation of human locomotion.

2.2.1 Geyer Model

Geyer's 2D model, described in [2], is composed of the following subsystems:

- The skeletal subsystem comprises the segment for the trunk and the three segmented legs is used for the skeletal subsystem.
- The muscular subsystem is composed of 7 hill muscles that act in the sagittal plane. In a 3D version of this model, 2 hill muscles are added in the coronal plane [23].
- The nervous system is modeled by sensory reflexes based on force and length feedback control.

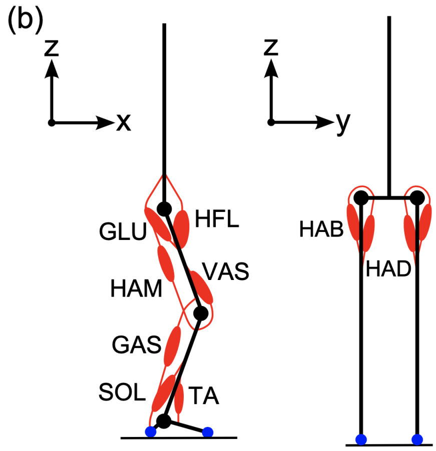

Figure 2.5: Geyer's human musculoskeletal model. Figure from [23]

2.2.2 COMAN Simulation

In addition to the Geyer model, Nicolas Van der Noot uses CPG on the COMAN humanoid robot. The controller used to model the nervous system is a combination of reflexes and CPG to control the muscles in Geyer's model. The CPG is realized with a Matsuoka oscillator network of 6 neurons.
This control enhances Geyer's model by incorporating the ability to adjust the walking speed over a wide range of speeds (0.4m/s - 0.9m/s), to predict the timing of the next contact with the ground, and to modulate the frequency of the steps.[9]

2.2.3 OpenSim Models

OpenSim is a powerful software platform used for biomechanical modeling of the human body. It allows researchers to create sophisticated models of the musculoskeletal system, which can be used to simulate human movements and study the effects of different conditions on the body.

OpenSim excels especially in modeling human walking as it provides the software to create detailed models of the muscles, bones, and joints involved in walking, and simulate the interworking of those structures during the different stages of the gait cycle.
These models can be used to study a wide range of topics related to human movement, including the effects of injuries or diseases on gait, the impact of different rehabilitation strategies, and the design of prosthetic devices.

For example, the model of Rajagopal et al. is a full body musculoskeletal model with muscle-actuated lower extremity and torque-actuated torso/upper extremity used in dynamic simulations of human movements [24].

Overall, OpenSim is an essential tool in biomechanics or human movement research. It has advanced capabilities for modeling human gait that make it particularly valuable for studying the complex and important aspect of human locomotion [25].

2.3 Methods for Locomotion Assistance

Human locomotion assistance devices refer to a range of equipment and devices designed to aid individuals with mobility impairments. These devices aim to improve mobility, independence, and quality of life for individuals with mobility impairments caused by lower limb pathologies or age-related conditions. The two primary categories of gait assistance devices currently available are those designed for full mobilization and those intended for partial mobilization. Full mobilization devices are primarily used to restore mobility to individuals experiencing severe motor control loss or disorders. On the other hand, partial assistance devices are designed to address the needs of patients with less severe conditions or for rehabilitation purposes.

Selecting the appropriate assistive device among exoskeletons, orthoses, and prostheses requires a thorough analysis of the individual's motor capabilities, visual abilities, cognitive functions, as well as their living environment and social interactions.

According to Aaron and Heer, an exoskeleton can be defined as an active mechanical device essentially anthropomorphic encompassing at least two joints, is "worn" by an operator, fits closely to the body, and works in concert with the operator's movements. They use the term orthosis to describe an assistive device primarily used to enhance the ambulatory capacity of individuals experiencing pathologies affecting a single articulation. [26] Lower limb prostheses are artificial devices designed to replace missing or amputated limbs to restore mobility and enhance life quality [27],[28].

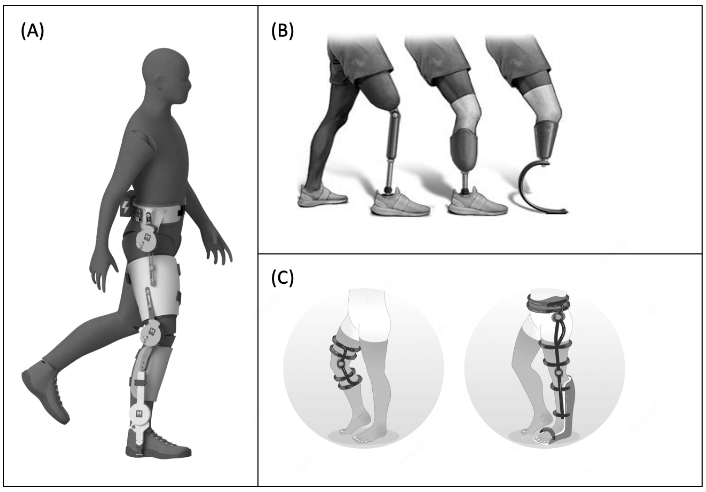

Figure 2.6: (A) Exoskeleton (active mechanical design "worn" by an operator). Figure from [29], (B) Prosthesis (devices replacing limbs). Figure from [30], (C) Orthosis (assistive device). Figure from [31].

Notwithstanding the difference in the end goals of the various assistance devices, similarities exist in the techniques used for their control. The following sections will focus on high-level controllers and mid-level controllers of the common 3-level structure (consisting of high, middle, and low levels) distinguishing the identification of terrain or user intention (high level) and the continuous behavior (middle level) from the relation between position/torque control and devices actuation control (low level).

2.3.1 High-Level Controllers

The high-level controller determines the general behavior of an assistive device choosing a mode of operation based on the user's desired activity and environment. Inputs to these controllers originate from the user through input devices and sensors, from the environment, or a combination of both.

The brain-computer interface (BCI) consists in measuring the patient's brain activity and detecting specific brain patterns to determine an operation mode. BCIs mainly rely on electroencephalography (EEG). The brainwaves can be detected in a non-invasive way by placing electrodes on the patient's scalp [32]. In 2016, López-Larraz et al. proposed a closed-loop BCI system using EEG to distinguish between rest and movement attempts while using the H2, a 6 DOF wearable lower-limb exoskeleton [33].
A second possibility is to use explicit user input. The task of selecting the mode of operation is left to the patient using voice commands [34] or buttons usually positioned on crutches [35]. Commonly used for spinal cord injury (SCI) patients since no input can be obtained from their legs, this kind of control is used in the TWIICE exoskeleton [36], the Ekso suit [37], or the CUHK-EXO [37].

The behavior of the device can also be adjusted automatically based on the user's movements or intended movements. Movement recognition is achieved through joint sensors and inertial measurement units [38], ground reaction forces signals [39], electromyography [40].

Finally, scientists are seeking to develop terrain identification to plan the gait pattern in consequence. Among the current techniques, the most developed include the estimation of the ground elevation through the contact surface between the ground and the limb as done in the mechanical department of Yonsei University [41], and the recognition of depth, stairs, and instances from 2D images [42] and [43].

2.3.2 Mid-level Controllers

Mid-level refers to the continuous behavior of the robot, where it translates the desired behavior or task specified by the high-level controller into a set of control commands during each time step of the main control loop. The mid-level controller can be divided into two separate blocks, namely the "detection/synchronization" block and the "action" block. The former block estimates the current gait phase and enables synchronization between the device and the user, while the latter calculates the corresponding desired physical outputs.

2.3.2.1 Detection/Synchronisation Blocks

The simplest way to impose the gait phase consists in increasing linearly the gait phase over time knowing in advance the time step duration. This method is called the "simple linear increase of the gait phase" [44] and is, for instance, used by the Walkon suit controller [45]. Jackson and Collins developed a customized ankle orthosis in 2014, which also utilizes a similar controller. However, in the latter case, the duration of the gait cycle is estimated based on the duration of the previous step (time-based gait phase interpolation) [46].

A frequent method used in exoskeletons control is the manual trigger by the user. This method is similar to the one described in the previous section.

Assistive devices such as the ReWalk [47] or the ATLAS [48] project continuously impose the movement hereby making the user responsible to remain in synchronization with the device [49]. For this purpose, a pre-recorded joint trajectory from a healthy individual or a trajectory extrapolated from gait analysis data, is typically used. The desired trajectory can be tuned according to different postures to improve flexibility and functionality [50].

The phases of a walking step can be determined by expected gait events. For example, the MIT powered ankle-foot prosthesis uses the heel or toe strike. Mooney et al. use the moment when the shank angular velocity is crossing zero in his ankle orthoses [51]. Specific peak angle of a joint can also be used, as in the MINDWALKER exoskeleton [52].

The concept of adaptive frequency oscillators-based control (AFO) has been extended to wearable robotics by Ronsse et al. to capture periodic signals related to locomotion during cyclic rehabilitation exercises or walking [53]. It is an assistance method that is not linked to the movement and that does not require other sensors than the own encoders of the assistance robot. It is used in the treadmill-mounted LOPES exoskeleton and the hip orthosis ALEX II for instance.

The analysis of the angle-speed graph of a single joint has been established as a viable approach to determining the phase of gait, as demonstrated by the developers of the UT Dallas knee-ankle prosthesis [54]. Accurate identification of the specific gait phase can be achieved by interpreting the direction of the speed on the graph.

Kang paved the way in 2019 for the use of machine learning models to determine the user gait phase by successfully validating a phase estimator based on a sensor fusion-based neural network in an active hip orthosis [55]. Other methods exist such as decision trees [56], support vector machines [57], or random forest algorithm classification [58].

2.3.2.2 Action Blocks

The function of the action block is to generate a motor command of either kinetic (torque or force) or kinematic (angle or speed) nature.

The simplest method used for providing partial assistance is through the utilization of torque profiles.
As timing is a determinant factor for the efficiency of an assistive device [26], the imposed torque profile may be tuned over time.

The user can be assisted to move in synchronization with a completely predefined trajectory based on gait data obtained from healthy people. It is used in the MINDWALKER [52], the H2 exoskeleton or in the rehabilitation knee orthosis AGoRA [59].

The lower-limb assistance field is a virtual field where the mechanical interactions between the user and the environment are significant. Therefore, impedance control is widely used in particular in partial assistance devices, where the limbs can be considered as active elements. Impedance control is often referred to as "assisted as needed" control [60]. The C-Brace knee ortheses was designed based on this principle for instance [61].

The detection of muscular activity with an EEG can be used to impose a proportional torque on a specific joint. Some papers propose to generate a position command by feeding an admittance model with the muscle signals [62]. Muscle activity amplification is typically used in the ankle [62], knee [63], and hip orthosis [64]. Concerning the lower-limb prosthesis, despite the effort to integrate EMG signals as control strategies, no commercially available prosthetic leg exists yet [65].

One type of bio-inspired controller seeks to emulate the human neuromuscular system, consisting of virtual neurons and muscles. The virtual muscles are Hill-type muscles, producing torques function of the activation signal and the current muscle states. The total torque for each joint is then determined by summing the torques generated by the virtual muscles that affect that joint. Some of these controllers are based on the neuromuscular reflex model proposed by Geyer and Herr, which relies on feedback loops, or "reflexes", that receive joint position data, ground contact, and virtual muscle lengths as inputs, and generate activation signals for the virtual muscles [2]. Often used to control prostheses [66], exoskeletons can also benefit from this controller [67].

2.4 Testing of Assistance Methods

There is a rich pool of tools and methods to evaluate robot-assisted locomotion methods. The evaluation criteria can be divided into 3 categories: kinematic/kinetic metrics, human/device interactions, and goal-level indicators [68].
The most popular evaluation human/device interaction method is the quantification of muscular fatigue.
However, other interaction indicators exist to quantify muscular fatigue, for instance, EMG analysis [69], the most popular and used indicator seems to be the metabolic cost. Various metabolic energy expenditure models using Hill muscles are available.
Bhargava et al. established an empirical model to quantify muscle energy consumption, which is characterized as the conversion of chemical energy into mechanical work and

heat liberation [70].
Several models using muscle states, joint moments and angular velocities exist [71].

F. M. Silva and J. A. Tenreiro Machado used the position of the hip joint as a spatial indicator to minimize the power needed in a walking bipedal model [72]. The center of mass (COM) excursion can also serve as spatial indicator to compare the performance of one device to another [73].

Another method of assessing rehabilitation devices is to compare the kinematic and kinetic patterns during device usage and when it is not used or, with the average pattern in able-bodied subjects [74].

Chapter 3

Simulation Tools

3.1 Simulation Environment

3.1.1 Simulink Software

Simulink is a graphical programming environment based on pre-built blocks. These blocks represent signals, mathematical functions or filters for instance. Therefore, Simulink is the language of predilection when it comes to signal processing and control modelling. Simulink offers various add-ons modules. Simscape is recommended to be used when physical systems need to be modeled. This module enables to construct multibody systems among other physical systems by incorporating a wide range of physical components including rigid bodies, springs, dampers, joints, and more.

To achieve a virtual replication of human walking, both the modeling of physical components, such as the legs and ground contact, and control laws to coordinate the body movement is required. Therefore, Geyer used Simulink and Simscape together to develop his model.

3.1.2 Robotran Software

The Robotran environment (see Figure 3.1), developed at UCL-MEED, is a powerful tool that allows for the generation of dynamic and kinematic equations of multibody systems (MBS) through a symbolic approach. From a graphical description of the system in MBsysPAD, the multibody equations can be generated in PYTHON using the symbolic translator MBsysTran. These equations can then be accessed via the interface in MBsysSIM and a 3D animation can be performed in the 3D illustrator.

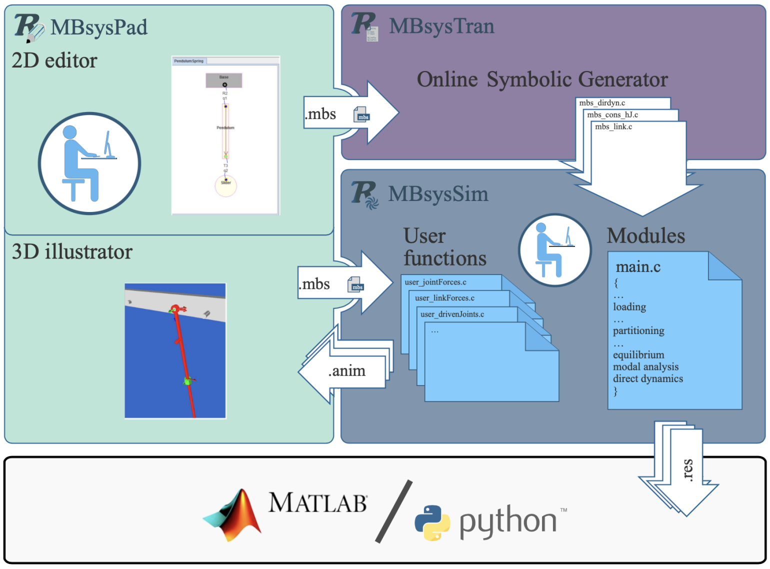

Figure 3.1: The ROBOTRAN program from (https://www.robotran.be)

3.1.3 Simulator

The selection of an appropriate integrator is dependent upon the specific characteristics of the problem being solved.

For its locomotion model, Geyer uses the *ode15s* integrator within Simulink, a variable integration step method. The *ode15s* solver computes the model states using variable-order numerical differentiation formulas and incorporates solutions from multiple preceding time points to determine the current solution, making it particularly efficient for stiff models such as the ground contact model (see section 4.3).

When implementing Geyer's model in Robotran, the choice was made to use a fixed time-step integrator over a variable time-step one despite its drawbacks, such as increased computational cost and lower accuracy. This decision was made with the awareness that this thesis represents the starting point for a larger goal: virtually develop and test new methods for locomotion assistance. Indeed, in this particular case, the constant time-fixed step integrator was deemed necessary to enable efficient real-time calculation to allow an assistive device to react in real-time to its user movements.
Specifically, the explicit Runge-Kutta method of order 4 (RK4) was selected with a time step fixed at $12.5\mu s$. The time step was determined after multiple trials to ensure the accuracy of the ground reaction forces while ensuring a reasonable computation time. The RK4 method is based on the principle of iteration, i.e. a first estimate of the solution is used to calculate a second more accurate estimate and so on.

3.2 Body Mechanics Model

As the aim of this thesis is to model human walking, the human body is modeled based on Geyer and Herr simplified seven-segments model. The body is considered to be composed of one trunk and two three-segmented legs (2.1.1.2). The latter are actuated by Hill-type muscles as described in section 4.1. The modeled body weighs 80 kg and measures 1.80 m, representing the typical characteristics of an average adult in Europe [75]. Given the emphasis has been placed on a two-dimensional walk, the walking motion is restricted to the sagittal plane.

3.2.1 Inertial Frame, Reference Angles and Positions

The reference inertial frame for measuring motion is established at the left foot's toes. Since the inertial frame is not placed at the hip, the angular references differ between the left and the right leg. Each joint angle is defined positively in the direction of the purple arrow in Figure 3.2. As for the hip angle, it is positive in the counterclockwise direction for the left leg, whereas for the right leg, it is positively in the clockwise direction. All positions are measured with respect to the ground, where the model assumes a zero position. When the model stands completely straight, with absolute ankle angle at 90 degrees and absolute hip and knee angles at 180 degrees, the upper end of the trunk is located at a height of 1.80 meters ($z = -1.8$ [m]).

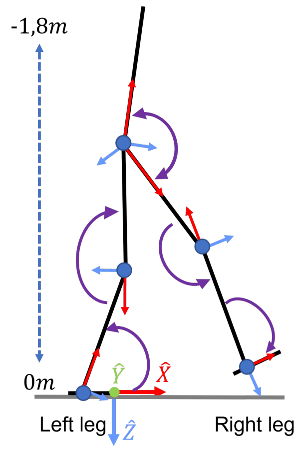

Figure 3.2: Definition of the inertial reference frame and the reference angles of the sagittal joints.

3.2.2 MBsyspad Description

A multibody system is a complex mechanical system composed of various interconnected bodies interacting with each other through joints. The motion and dynamics of each body in the system are influenced by the forces and torques exerted on them by the other bodies and by external forces. The multibody system of interest for this thesis is represented in Figure 3.3. The data utilized to characterize the different bodies can be found in Appendix A.
Each leg is equipped with three revolute joints whose rotation axes are perpendicular to the sagittal plane. The legs are connected to the trunk by one more sagittal revolute joint.

The thigh segment has been separated into two segments (i.e, the lower and the upper thigh), connected by a prismatic transversal joint. This is necessary to determine the mass distribution of the complete body between its two legs in order to calculate muscle stimulations. Further explanation regarding this matter is presented in section (4.2.2). The model is connected to the inertial frame (i.e., Base) by three prismatic and three rotational joints providing six degrees of freedom, although 4 joints suffice in the case of a 2D model. Two sensors are placed on each foot: one at the heel and the other in the toe area. The two sensors provide continuously information on the feet position hereby, facilitating the real-time calculation of external forces (4.3). Two additional sensors are located on the trunk to determine its pitch angle.

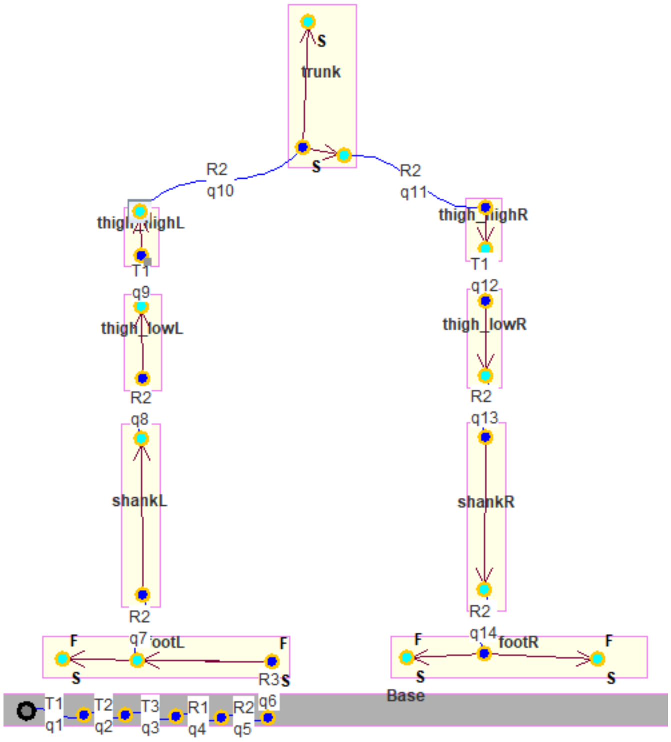

Figure 3.3: Robotran representation of the multi-body system representing the lower limbs and the trunk of a human via MBSysPad.

Chapter 4

Bio-inspired 2D Model of Human Gait

This section presents the layout of the model structure, subject of this thesis. This structure is summarized in Figure 4.1.

The final goal is to provide appropriate torques to the multibody system joints, in order to achieve locomotion.
The model is divided into three parts: (i) the multibody system, (ii) the muscle actuation layer, and (iii) the neural control layer.

The multi-body system representing the human body receives torques from the muscle actuation layer and external forces from the ground contact model and allows to obtain the evolution of the positions and velocities of the joints.

The neural control layer allows to obtain muscle stimulations from delayed positions and speeds of the articulations based on reflex control laws (see section 4.2).
The muscle actuation layer first computes the force developed by the muscles and subsequently obtains from the length of the insertions of the muscles, the torques applied on the joints (see section 4.1).

The ground contact model computes external forces that are contact forces directly sent to the multibody system (see section 4.3).

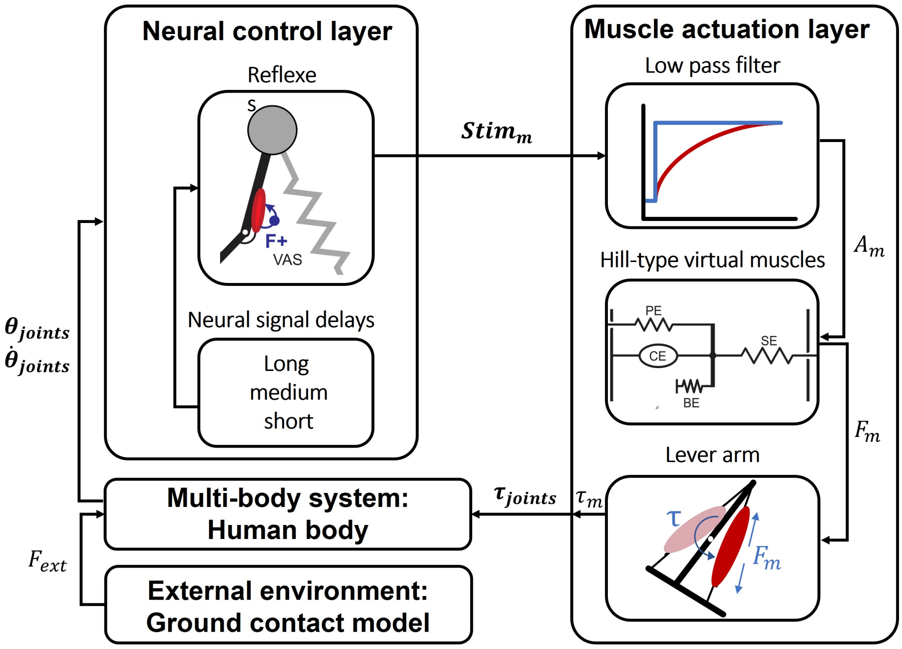

Figure 4.1: General structure of the Geyer's model.

4.1 Muscle Actuation Layer

4.1.1 Characterization of the Leg Muscles

To create a 2D model of human walking, the implementation and characterization of seven muscles that act in the sagittal plane were used. These implementations and characterizations are based on [2]. The seven muscles are illustrated in a schematic drawing of the human body, which can be seen in figure 4.2.

- The *Soleus* (SOL) acts on the ankle. Its role is the plantarflexion of the ankle, i.e., to point the toes downwards. It is a mono-articular muscle.
- The *Tibialis anterior* (TA) acts on the ankle. Its role is the dorsiflexion of the ankle, i.e., to bring the toes towards the leg. It is a mono-articular muscle.
- The *Gastrocnemius* (GAS) acts on the ankle and on the knee. Its role is the plantarflexion of the ankle and the flexion of the knee. It is a bi-articular muscle.
- The *Vasti* (VAS) acts on the knee. Its role is the extension of the knee. It is a mono-articular muscle.
- The *Hamstring* (HAM) acts on the knee and on the hip. Its role is the flexion of the knee and the extension of the hip. It is a bi-articular muscle.
- The *Gluteus* (GLU) acts on the hip. Its role is the extension of the hip. It is a mono-articular muscle.

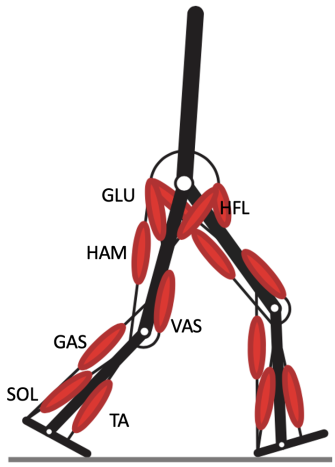

Figure 4.2: Representation of the 7 muscles acting in the sagittal plane. Figure modified from [2].

- The *Hip flexor* (HFL) acts on the hip. Its role is the flexion of the hip. It is a mono-articular muscle.

4.1.2 Hill's Muscle Model

In accordance with the explanation provided in the introduction of chapter 4, starting from the appropriate stimulations of the muscles resulting in their contraction, the objective is to obtain the production of a muscular force that causes torque on the joints on which muscles act.
To represent the seven muscles described in the previous section, Hill's muscle model is employed as in [16]. This section describes the mathematical framework that enables us to obtain the muscle force and the variation of the contractile element's length. This mathematical development is inspired from [15] and [76].

4.1.2.1 Muscle Tendon Complex

Each muscle is represented by a "Muscle Tendon Complex" (MTC). Each MTC is made up of an active contractile element (CE) which models the muscle fiber, a serial element (SE) which models the tendon connecting the muscle to the bones, a parallel elastic element (PE), and an elastic buffer element (BE). During normal operation only the CE and SE are activated. The PE is activated when the CE extends beyond its optimal size. Similarly, the BE is activated when the length of the SE falls below a certain threshold. These elements can be found in Figure 4.3.
Hill's muscle model is easily adaptable to different muscle types and situations, making it a versatile tool for human movement studies.

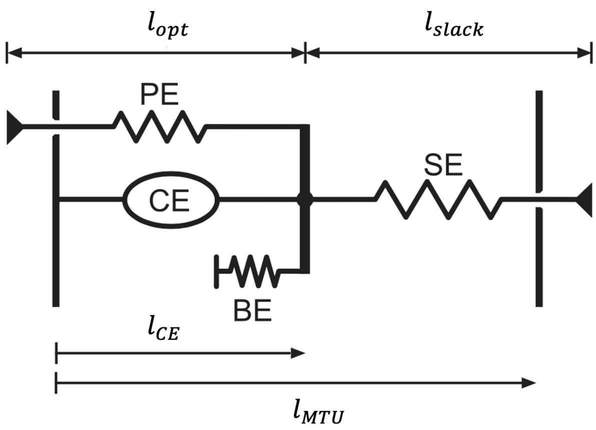

Figure 4.3: Muscle-Tendon Complex (MTC) of Hill's model. Figure from [2]

4.1.2.2 Mathematical Development

The data required to mathematically characterize the MTC (i.e., obtain the muscle force and the contractile element's length) are the stimulation of the muscle and the length of the MTC.
The stimulation is obtained using control laws described in section 4.2.2.
As each MTC is attached to fixed points of the body, its length can be obtained from the angles of the joints as explained in section 4.1.3.

The forces of the elements (SE, PE, and BE) can be obtained from the lengths of the different elements ($l_{se} = l_{mtc} - l_{ce}$).
The force of the CE can be expressed using the following formula:

$$F_{ce} = A_m \cdot F_{max} \cdot f_l(l_{ce}) \cdot f_v(v_{ce}) \tag{4.1}$$

Where F_{max} is the maximum isometric force, and $f_l(l_{ce})$ and $f_v(v_{ce})$ are the force-length and force-velocity relationships which are represented in Figures 4.4 and 4.5 (for the formulation of these curves, see Appendix B.2).

Then, the force developed by the muscle is obtained by $F_m = F_{se} = F_{ce} + F_{pe}$.

Figure 4.4 illustrates that the force generated is maximized when the length of the contractile element (CE) approaches its optimal length (l_{opt}) and diminishes when the muscle is either compressed or extended beyond this optimal length. The muscle's force-producing capacity decreases during rapid contraction and is enhanced during extension. For further details on this model see [15].

To obtain the length of the contractile element (l_{ce}), once $f_l(l_{ce})$ is obtained, the force-velocity relationship is computed using the following equation:

$$f_v(v_{ce}) = \frac{F_{se} + F_{be}}{A_m \cdot F_{max} \cdot f_l + F_{pe}} \tag{4.2}$$

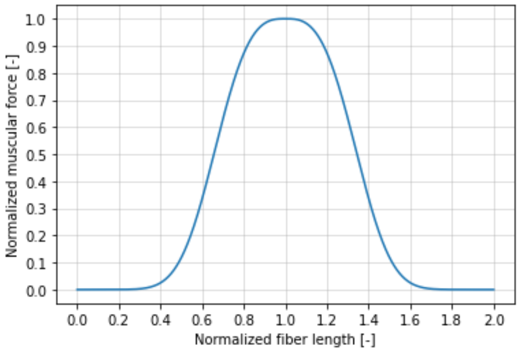

Figure 4.4: F-l relationship

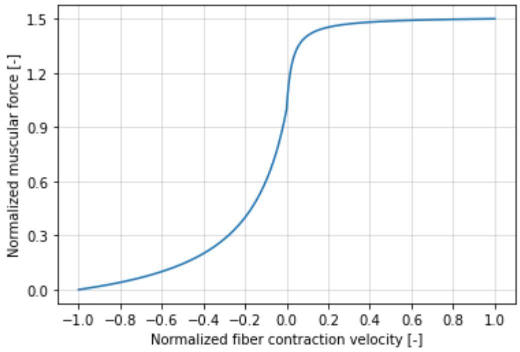

Figure 4.5: F-v relationship

The inverse force-velocity relation is then used to obtain the contraction speed of the contractile element (v_{ce}) which can be integrated to obtain the length of the contractile element (l_{ce}).

4.1.2.3 Computation of Muscle Activation

Muscle activation (A_m) is obtained from muscle stimulation (S_m) after a slow electro-chemical process. The time delay caused by this process can be modeled using a first-order differential equation representing the "excitation-contraction coupling":

$$\tau \cdot \frac{dA_m(t)}{dt} = S_m(t) - A_m(t) \tag{4.3}$$

This differential equation represents a low pass filter with a time constant τ of 0.01 s. The dynamic response of muscle activation is represented in Figure 4.6.

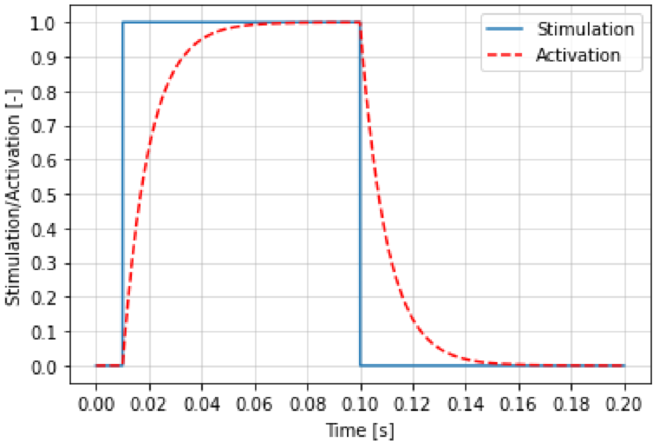

Figure 4.6: Dynamic response of muscle activation

4.1.3 Muscle Length and Torque applied to the Joints

Depending on the muscle type (mono or bi-articular), each MTC contributes to the movement of one or two joints. The conversion of the muscle force (F_m) into a joint torque (τ_m) is modeled as $\tau_m = \pm r_m(\phi)F_m$.
The instantaneous lever (r_m) is a constant value for the hip joint and a cosinus relation for knee and ankle joints.

$$r_m(\phi) = \begin{cases} r_0 & \text{for hip} \\ r_0 \cdot cos(\phi - \phi_{max}) & \text{for knee and ankle} \end{cases} \tag{4.4}$$

Where r_0 is the distance between the muscle attachment point and the articulation, ϕ and ϕ_{max} refer respectively to the joint angle and to the joint angle producing the maximal lever.
The torque applied to each joint is the sum of the contributions of the torques resulting from the muscles attached to it.

Hill's muscle model does not take into account the biological constraints imposed by the ligaments. Their action, in addition to maintaining 2 bones together, is to maintain the angle of the joints within a given range. Therefore, Geyer introduced a joint soft limit concept [2]. This approach consists in modelling the ligaments as nonlinear spring damper and computing a proportional additional torque if the joint angle is out of its normal range to prevent overextension such that the total torque applied at the joint is expressed as $\tau = \tau_m + \tau_{extra}$.

$$\tau_{extra} = -c_{joint} \cdot (\phi - \phi_{lim}) \cdot (1 + \frac{\dot{\phi}}{\omega_{max}}) \tag{4.5}$$

Where c_{joint} is the spring damper stiffness, ϕ_{lim} is the joint limit angle, $\dot{\phi}$ is the joint angular velocity, and ω_{max} is the reference angular velocity. τ_{extra} is different from 0 only if $\phi - \phi_{lim} > 0$ and $\frac{\dot{\phi}}{\omega_{max}} > -1$.

In practice, it is of interest to note that, only the knee is impacted by this limit during a normal gait cycle. Ankle joint limits are involved in the first moment of the simulation when the stable gait cycle has not yet been reached.

The approach used to determine the MTC length (l_{mtc}) is based on an estimation of the changes in the MTC length induced by changes in the joints angles. The variation of l_{mtc} can be expressed using the following model:

$$\Delta l_{mtc} = \begin{cases} \rho \cdot r_0 \cdot sin(\phi - \phi_{ref}) & \text{for hip} \\ \rho \cdot r_0 \cdot [sin(\phi - \phi_{max}) - sin(\phi_{ref} - \phi_{max})] & \text{for knee and ankle} \end{cases} \tag{4.6}$$

Where the reference angle ϕ_{ref} is the joint angle at which $l_{mtc} = l_{opt} + l_{slack}$ and ρ is the pennation factor used to consider the misalignment of muscle fibers with respect to the attachment position of the muscle.

4.2 Neural Control Layer

The muscle stimulations that activate the muscles, as outlined in [2] and [76], are derived from the control laws explained in [15]. In this section, the control laws used for stimulating the seven muscles that operate in the sagittal plane will be presented. These muscle stimulations depend on the phase of walking, i.e., specific stimulations are required for both the stance and swing phases. Additionally, variations arise during double support.
Furthermore, we will detail the effects of muscle stimulations in the context of walking.

4.2.1 Reflex-based Control Laws

Muscle stimulation can be based on 2 principles of control laws: Feedback control and PD control of the joint position. These control laws are based on a delay that represents the propagation of afferent signals from the muscle spindles and GTOs to the joint.

4.2.1.1 Feedback Control

Stimulations signals based on feedback control are obtained from a pre-stimulation ($STIM_0$) to which a feedback component ($\pm G \cdot P(t - \Delta t)$) is added:

$$STIM(t) = \begin{cases} STIM_0(t) & \text{if } t < \Delta t \\ STIM_0(t) \pm G \cdot P(t - \Delta t) & \text{if } t > \Delta t \end{cases} \tag{4.7}$$

where P is the sensory information, G is the gain factor and Δt is the signal propagation time delay.
The presence of $\pm$, stems from the fact that the feedback can be positive or negative corresponding to an excitatory or inhibitory post-synaptic potential at the α motor neuron.

The signal P corresponds to the sensory information coming from the muscle spindles and the GTOs. This signal can be of 2 different natures: A signal of the MTC's force (F_{mtc}) or a signal of the length of the MTC contractile element (l_{ce}).

Force signal-based feedback component of a MTC m is defined by the following formula[1]:

$$S_m^F = G_m \cdot \frac{F_m(t - \Delta t_m)}{F_m^{max}} \tag{4.8}$$

Where $F_m(t - \Delta t_m)$ is the MTC's generated force at time $(t - \Delta t_m)$, F_m^{max} is the maximal isometric force of the muscle and G_m is a constant positive gain parameter. The gain is an essential parameter that needs to be optimized for each MTC. [2]

[1]The way of representing equations in this section is inspired by [77]

[2]In the Robotran model, the gain values used are based on Geyer's model in Simulink, as some values indicated in [2] were found to be incorrect.

When a change in a muscle's stimulation comes from the feedback of the force generated by the muscle itself, it creates a positive feedback loop. This means that the more force the muscle generates, the more it will be stimulated resulting in the generation of an even higher force. However, the force-length and force-velocity relationships, which are described in 4.1, make the relation between force and stimulation non-linear. This non-linearity means that the force generated by the muscle does not increase indefinitely.
Conversely, when the force generated by the muscle decreases due to the aforementioned relationships, the stimulation also decreases. These two phenomena lead to highly non-linear trends of stimulations and forces.
The force feedback control law is mainly used in the stance phase to represent the VAS, SOL and GAS stimulations.

Length signal-based feedback component of a MTC m is defined by the following formula:

$$S_m^l = [G_m \cdot (\frac{l_m^{ce}(t - \Delta t_m)}{l_m^{opt}} - l_{off,m})] \tag{4.9}$$

Where $l_m^{ce}(t - \Delta t_m)$ is the length of the contractile element at time $(t - \Delta t_m)$, l_{off_m} is the optimal length of the contractile element, l_m^{opt} is an offset for the length and G_m is a constant positive gain parameter. The offset and the gain are parameters that need to be optimized for each MTC.

This control law implies that the muscle will be stimulated when the length of the contractile element exceeds a fixed length.
This length feedback control law is mainly used in the stance phase to represent the TA stimulation and in the swing phase to represent the TA and HFL stimulations.

4.2.1.2 PD Control of Joint Position

Stimulations signals based on the proportional-derivative control of the joint position are obtained from the following formula:

$$S_m^\theta = |[K_m \cdot (\theta(t - \Delta t_m) - \theta_m) + D_m \cdot \dot{\theta}(t - \Delta t_m)]| \tag{4.10}$$

Where the proportional component is composed of K_m the proportional gain, $\theta(t - \Delta t_m)$ the angle of the joint at time $(t - \Delta t_m)$, and θ_m the reference position. The derivative component is composed of D_m the derivative gain and $\dot{\theta}(t - \Delta t_m)$ the angular speed of the joint at time $(t - \Delta t_m)$.

This is a conventional PD controller that aims to move the joint position θ towards the reference position θ_m by damping the joint's angular velocity.
This PD control law is mainly used in the stance phase to represent the HAM, GLU and HFL stimulations from the trunk inclination and for the VAS with only the proportional component using the knee position.

4.2.2 Leg Muscles Stimulation Laws during Human Walking

To obtain each stimulation, the control law components are added to a pre-stimulation that is not dominant relative to the added components. This pre-stimulation is a parameter that needs to be determined and optimized [3]. These pre-stimulations are specific to the phase of walking, stance phase pre-stimulations will be noted $S^{St}_{m,0}$ and swing phase pre-stimulations $S^{Sw}_{m,0}$.
The stimulations that will be described in this section are motivated by [2] and are shown in Figure 4.7.

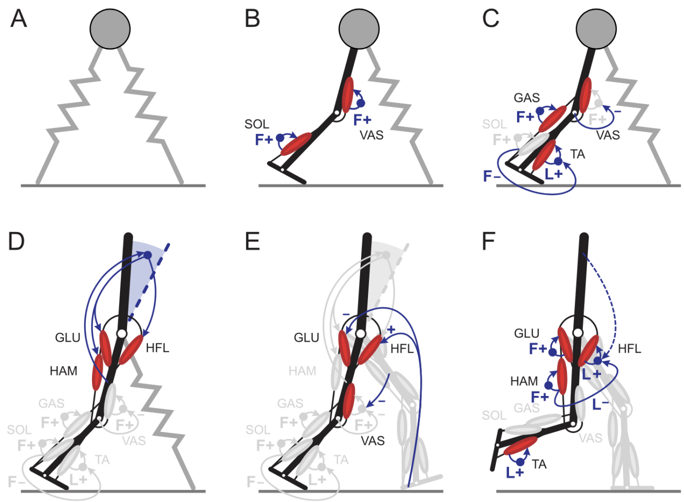

Figure 4.7: (A) Bipedal spring mass model, (B) F+ of SOL and VAS, (C) F+, L+ and F- of TA, GAS and PD control of VAS, (D) PD control of GLU,HFL and HAM, (E) Double support for GLU, HFL and VAS, (F) F+, L+ and L- of TA, HAM, GLU and HFL. Figure from [2]

The stimulations described in this section are based on the following legged mechanics principles:

- Mechanical self-stability: Legged locomotion self-stabilizes.
- Compliant leg behavior: Legs behave similar to springs in stance.

4.2.2.1 Stance Phase Reflexes

Compliant behavior in neuromuscular legs can be generated from positive force feedback (F+) of the extensor muscles (i.e., soleus muscle (SOL) and vasti muscle group (VAS)).

$$S_{SOL} = S^{St}_{SOL,0} + S^{F}_{SOL} \tag{4.11}$$

$$S_{VAS} = S^{St}_{VAS,0} + S^{F}_{VAS} \tag{4.12}$$

[3]In our Robotran model, the gain values used are based on Geyer's model in Simulink, as some values indicated in [2] were found to be incorrect.

To avoid the tendency of the leg to overextend at the knee and at the ankle, positive force feedback (F+) of the gastrocnemius (GAS) and positive length feedback (L+) of the tibialis anterior muscles (TA) are used.

$$S_{GAS} = S^{St}_{GAS,0} + S^{F}_{GAS} \tag{4.13}$$

$$S_{TA} = S^{St}_{TA,0} + S^{l}_{TA} \tag{4.14}$$

In addition to preventing knee hyperextension, the GAS reflexes contribute to generating an overall compliant leg behavior.

The reflexes of the TA based on length feedback is not required if sufficiently active extensors preserve the torque equilibrium between the knee and the ankle. Therefore, a negative force feedback (F-) from the SOL which will inhibit the TA is added.

$$S_{TA} = S^{St}_{TA,0} + S^{l}_{TA} - S^{F}_{SOL} \tag{4.15}$$

An inhibiting reflex is added to the VAS to protect the knee from hyperextension if the knee extends beyond 170°. This reflex is based on a proportional control of the knee position.

$$S_{VAS} = S^{St}_{VAS,0} + S^{F}_{VAS} - K \cdot (\theta_{knee}(t - \Delta t_m) - 170°)^{4} \tag{4.16}$$

The HAM, GLU, and HFL muscles are responsible of mechanical self-stabilization by maintaining the orientation of the trunk through PD control. If the trunk is excessively tilted forward (relative to the reference trunk angle), the HAM and GLU muscles are activated, otherwise, the HFL muscle is activated.

$$S_{HAM} = S^{St}_{HAM,0} + S^{\theta_{trunk}}_{HAM} \tag{4.17}$$

$$S_{GLU} = S^{St}_{GLU,0} + S^{\theta_{trunk}}_{GLU} \tag{4.18}$$

$$S_{HFL} = S^{St}_{HFL,0} - S^{\theta_{trunk}}_{HFL} \tag{4.19}$$

A modulation of hip muscle stimulations (HAM, HFL and GLU) proportionally to the amount of weight the ipsilateral leg[5] is bearing is needed to stabilize the trunk as hip torques can only balance the trunk if the legs bear sufficient weight on the ground.

$$S_{HAM} = S^{St}_{HAM,0} + S^{\theta_{trunk}}_{HAM} + k_{bw} \cdot |F^{ipsi}_{leg}(t - \Delta t_m)| \tag{4.20}$$

$$S_{GLU} = S^{St}_{GLU,0} + S^{\theta_{trunk}}_{GLU} + k_{bw} \cdot |F^{ipsi}_{leg}(t - \Delta t_m)| \tag{4.21}$$

[4] $K \cdot (\theta_{knee}(t - \Delta t_m) - 170°)$ is added only if $\theta_{knee} > 170°$

[5] Refers to the leg on the same side of the muscle

$$S_{HFL} = S^{St}_{HFL,0} - S^{\theta_{trunk}}_{HFL} - k_{bw} \cdot |F^{ipsi}_{leg}(t - \Delta t_m)| \tag{4.22}$$

The aforementioned stimulations are shown in Figure 4.7: $(A) \rightarrow (D)$.

4.2.2.2 Variation of Stance Reflexes in Double Support

Before entering the swing phase, the ipsilateral leg reduces its weight-bearing load, causing a decrease in its functional importance until it transitions into the swing phase. This is achieved by inhibiting the VAS muscle of the ipsilateral leg in proportion to the weight that the contralateral[6] leg is bearing.

$$S_{VAS} = S^{St}_{VAS,0} + S^{F}_{VAS} - k_{bw} \cdot |F^{contra}_{leg}(t - \Delta t_m)| \tag{4.23}$$

During walking, this inhibition is used to coordinate movement. This allows the knee to bend and the ankle to extend, pushing the leg forward and off the ground. This ankle push-off is an important principle of walking, especially for the transition from the double support phase to the swing phase.

In addition to the ankle push-off, the swing phase is initiating in double support by the increase in HFL stimulation and by the decrease in GLU stimulation. These variations are based on a fixed constant amount (ΔS).

$$S_{HFL} = S^{St}_{HFL,0} - S^{\theta_{trunk}}_{HFL} + \Delta S \tag{4.24}$$

$$S_{GLU} = S^{St}_{GLU,0} + S^{\theta_{trunk}}_{GLU} - \Delta S \tag{4.25}$$

These stimulations are shown in Figure 4.7: (E).

4.2.2.3 Swing Phase Reflexes

During swing phase, the locomotion of the leg is based on a leg's ballistic motion. This ballistic motion is modelized in two ways.

First, the HFL is stimulated by a positive length feedback (L+) allowing leg protraction during swing.

$$S_{HFL} = S^{Sw}_{HFL,0} + S^{l}_{HFL} + k_{lean} \cdot (\theta - \theta_{ref})_{TO} \tag{4.26}$$

Where the length feedback is biased by the trunk's pitch θ at take-off (TO) to represent the dependance between required protraction speed and trunk's forward lean.

Secondly, the gait stability is ensured by the swing-leg retraction. The mechanical self-stability of the locomotion is more robust to disturbances if the legs retract

[6]Refers to the leg on the other side of the muscle

before landing. This retraction can be obtained by negative length feedback (L-) of the HFL from the HAM and positive force feedback (F+) of the GLU and the HAM.

$$S_{HFL} = S^{Sw}_{HFL,0} + S^{l}_{HFL} + k_{lean} \cdot (\theta - \theta_{ref})_{TO} - S^{l}_{HAM} \tag{4.27}$$

$$S_{GLU} = S^{Sw}_{GLU,0} + S^{F}_{GLU} \tag{4.28}$$

$$S_{HAM} = S^{Sw}_{HAM,0} + S^{F}_{HAM} \tag{4.29}$$

The other muscles (SOL, VAS, GAS) are silent in swing phase and TA remains active to allow foot clearance with the ground.

These stimulations are shown in Figure 4.7: (F)).

A summary of these stimulations and the parameters used can be found in Appendix C, more specifically a schematic representation of the phases in which the different muscles are activated can be found in Appendix C.1.

4.3 External Environment : Ground Contact Model

To model the forces of contact with the ground, a mesh is applied to the foot where each point undergoes the contact model. For the characterization of the 2D contact of a point, four data points are necessary, which include the position and velocity in the vertical axis (z and v_z with z-axis oriented downwards) and the position and velocity in the horizontal axis (x and v_x with x-axis oriented towards the front of the foot).

A point is considered to be in contact with the ground when its vertical position satisfies the following condition with regard to the ground elevation (z_{ground}):
$\Delta z = z - z_{ground} \geq 0$.

For each point that in contact with the ground, the vertical force (F_z) and horizontal force (F_x) are computed based on the model described by Günther and Ruder in [78].

A non-linear spring-damper model is used to model the normal ground reaction force F_z :

$$F_z = -k_z \cdot \Delta z \cdot (1 + \frac{v_z}{v_{max}}) \tag{4.30}$$

Where k_z is the normal contact stiffness coefficient (8150 kN/m), Δz is the ground penetration and $\frac{v_z}{v_{max}}$ is the ground penetration velocity normalized to $v_{max} = 3\ cms^{-1}$. This reaction force is non-zero if $\frac{v_z}{v_{max}} > -1$.

In the horizontal direction, there are reversible transitions between visco-elastic adhesion (static dry friction) and friction (dynamic dry friction).

For static dry friction, the tangential force ($F_{x_{st}}$) is modeled as follow:

$$F_{x_{st}} = -k_x \cdot \Delta x \cdot (1 + sgn(\Delta x) \cdot \frac{v_x}{v_{max}})) \tag{4.31}$$

Where k_x is the tangential contact stiffness coefficient ($8200 N/m$) and Δx is the difference between the initial and current position of the contact point.

If the condition $F_{x_{st}} > |\mu_{st} \cdot F_z|$, with μ_{st} the static friction coefficient ($\mu_{st} = 0.9$), is reached the point starts to slide and the tangential force ($F_{x_{dyn}}$) is subject to the following dynamic dry friction law:

$$F_{x_{dyn}} = sgn(v_x) \cdot \mu_{sl} \cdot F_z \tag{4.32}$$

Where μ_{sl} is the dynamic fiction coefficient ($\mu_{sl} = 0.8$).

Adhesion is reached again and the point returns to static dry friction (See equation 4.31) when $v_x < v_{x,crit}$ with $v_{x,crit} = 1cms^{-1}$.

Chapter 5

Specific Implementation Choices for the Bipedal Model

As explained in the general overview of section 4.1, the system works in a closed loop. The inputs of the multi-body system (joint torques) are obtained from the outputs of this same system (joint positions and velocities) and through the neural control layer and the muscle actuation layer.

This section presents the specific implementation choices of certain blocks/functions of the model, explains the thought process that led to these choices, and their impact on the output results.

The methodology employed to derive the results presented in sections 5.1 and 5.2 is outlined as follows: the input signals from each Simulink block were exported and passed through the corresponding custom blocks independently of Robotran (see Figure 5.1). These results are used to verify the functionality of each block by comparing the output signal obtained from Simulink and the output obtained from the custom blocks.

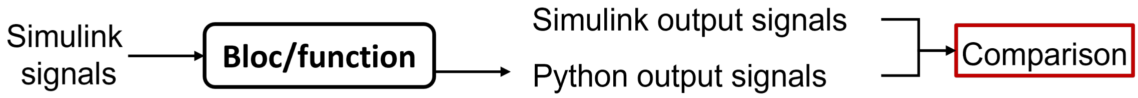

Figure 5.1: Representative diagram of the comparison of results between Python and Simulink models.

5.1 Muscle Actuation Layer

5.1.1 Excitation-Contraction Coupling

As explained in section 4.1.2.3, the transition from muscle stimulation to muscle activation is achieved by solving the following first-order differential:
$\tau \cdot \frac{dA_m(t)}{dt} = S_m(t) - A_m(t)$. This equation is solved using a first order low pass filter.

$$y_i = \alpha \cdot x_i + (1 - \alpha) \cdot y_{i-1} \tag{5.1}$$

The filter takes in a stimulation signal (x_i) and produces an activation signal (y_i) that is influenced by the previous activation level (y_{i-1}). The filter works by attenuating the effect of the previous activation level over time. Figure 5.3 shows the time delay induced by the filter, while Figure 5.2 represents the difference between the stimulation of the *Vasti* obtained using Simulink's filter block and the filter previously described.

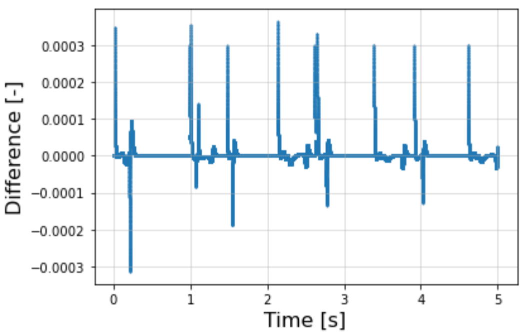

Figure 5.2: Difference between the activation obtained with low pass filter and the one obtained with Simulink.

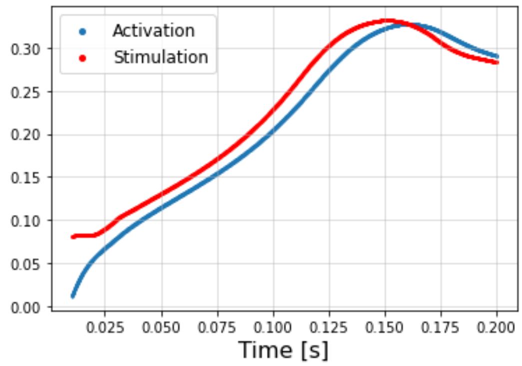

Figure 5.3: Stimulation and activation for the left *Vasti*.

5.1.2 Selection of an Integration Method

As presented in section 4.1, the CE length (l_{ce}) is essential to characterize the muscle and calculate its muscular force (F_m). This l_{ce} can be obtained by the integration of the CE contraction velocity (v_{ce}), which is determined by the forces of the different elements in Hill's model. A feedback loop is established, where the l_{ce} is utilized to determine the forces. These forces are then employed to calculate the length at the subsequent time step through the integration of the contraction velocity between these two-time steps.

In this section, the choice of the integration method used to implement the muscle model is outlined by comparing the l_{ce} signals of the *Vasti* obtained with the custom muscle layer block to the signal obtained with the integrator block of Simulink.

The choice between 2 integration methods, namely Euler iteration and Runge Kutta 4 is presented to determine which approach yields the most conclusive results.

Euler iteration is a method that consists in estimating the value of the variable at each intermediate time step using the previous value and the variable derivative at that point. The number of intermediate time steps is dictated by the number of iterations chosen. The graph of Figure 5.4 shows the difference between l_{ce} obtained with the Euler iteration with 3, 5 and 10 iterations per time step and l_{ce} obtained with Simulink from v_{ce} signals exported from Simulink. The difference is proportional to the number of iterations used for the integration method.
Runge Kutta 4 is a method that uses a combination of 4 different approximations to estimate the value of the variable at each time step, results are presented in Figure 5.5.

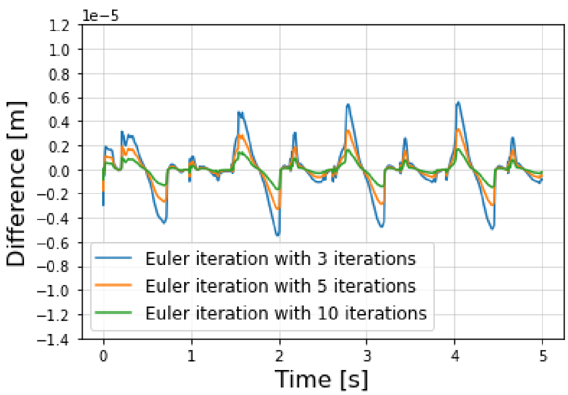

Figure 5.4: Difference between l_{ce} obtained with Euler iteration method of integration and l_{ce} obtained with Simulink integration.

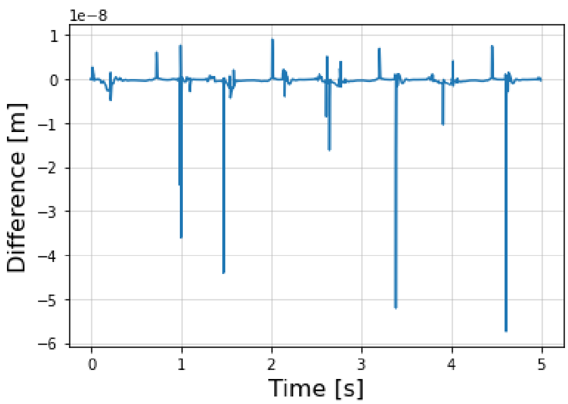

Figure 5.5: Difference between l_{ce} obtained with Runge Kutta 4 method of integration and l_{ce} obtained with Simulink integration.

The Runge-Kutta method not only provides more accurate results but also requires less computational time compared to the Euler iteration method. The Runge-Kutta method has therefore been selected for the model.

5.1.3 Impact of the Implementation Choices on the Muscle Actuation Layer's Outputs

This section highlights the impact of the implementation choices of the excitation-contraction coupling and the integration method used to obtain l_{ce} on the outputs of the muscle activation layer.
The overview of the model, depicted in Figure 4.1, introduces the role of the muscle actuation layer, i.e., to obtain torques from muscular stimulations.
Figure 5.6 illustrates the torques for the left leg obtained with our implementation of the muscle actuation layer based on muscular stimulations exported from Simulink. The figure also presents the difference between the obtained torques and the torques exported from Simulink. It can be concluded that the implementation choices made in section 5.1.1 and 5.1.2 are acceptable.

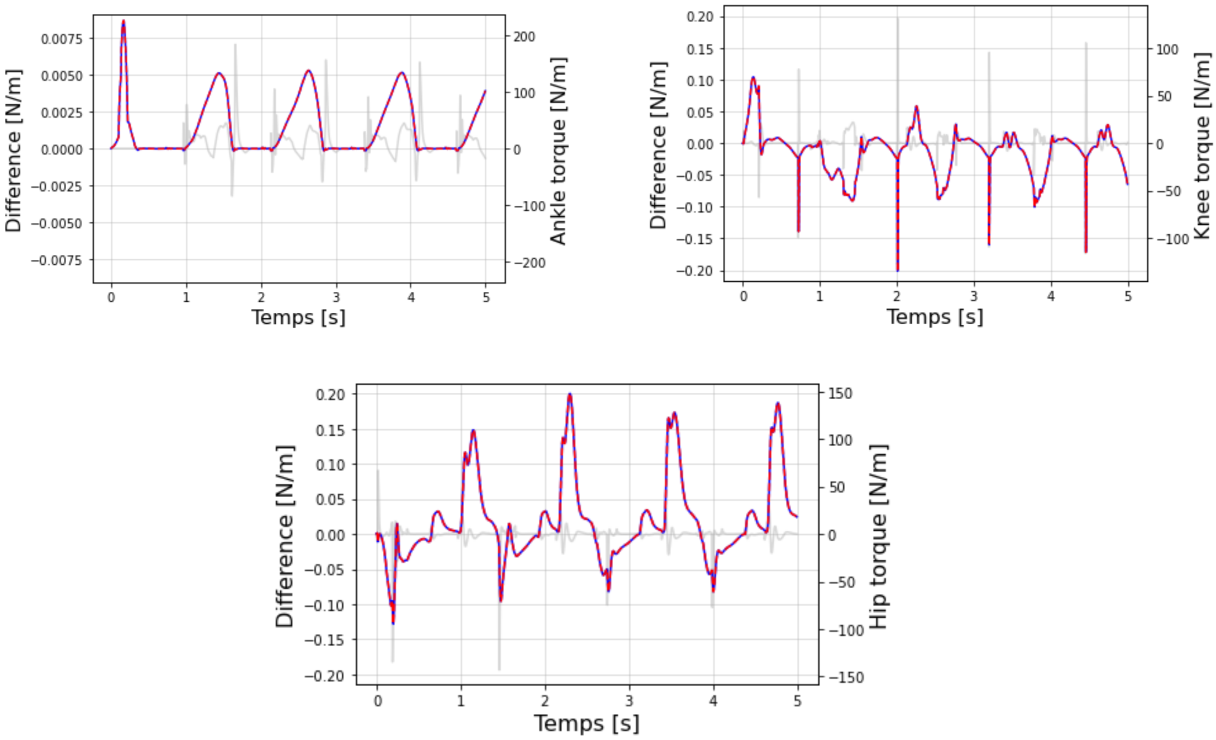

Figure 5.6: Torques on articulations of the left leg. The blue lines represent the torques obtained with our implementation of the muscle actuation layer, the red dashed lines represent the Simulink torques, and the grey lines represent the differences between the obtained and Simulink torques.

5.2 Neural Control Layer

5.2.1 Weight Supported by the Contralateral and Ipsilateral Leg

In section 4.2.2, the inhibition of the stimulation of particular muscles is presented. Depending on the muscle, the inhibition is either proportional to the weight supported by the contralateral leg or the weight supported by the ipsilateral leg. Concerning this crucial point of the model, a significant distinction arises when comparing Geyer's article [2] with the actual implementation of his model. In the article, Geyer expresses the distribution of the load between the two legs as a force whereas in Simulink, the load distribution is computed as a distance variation.

To uphold a scientific reproducibility approach, every aspect related to the load distribution has been computed in a manner consistent with that employed in Simulink.

Each thigh is composed of an upper and lower segment connected by a pressure sheet element represented by a prismatic joint. Depending on the body movements, the prismatic joint slides either in the positive or negative direction. To restrict the impact of this motion on the overall kinematics, the prismatic joint is actuated in force. This force acts in opposition to the movement, proportional to the velocity and the displacement of the slider.

$$\vec{F} = -A \cdot dx \cdot (1 + sgn(dx) \cdot B \cdot v) \tag{5.2}$$

With A and B constants, v the sliding velocity and dx the sliding distance. It is this last variable that multiplies the muscle stimulation and therefore acts as an inhibitory factor. This prismatic joint is modeled as a strain gauge.

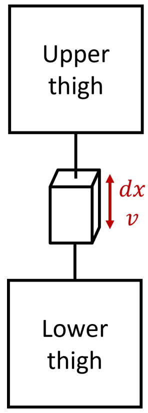

Figure 5.7: Representation of the thigh.

In his implementation, Geyer applies a filtering process to the obtained sliding distance signal. The specific purpose behind this filtering is not clear since he does not explain it. While filtering helps in obtaining smoother results, it also introduces a temporal shift that lacks any biological justification. In our implementation of the model, the same filter is used as in section 5.1.1 with another time constant ($\tau = 0.02\ s$). Nonetheless, it is noteworthy that the application or omission of the filter in Geyer's implementation does not appear to significantly perturb the overall kinematics of the model, as depicted in Figure 5.8. A similar behavior can be observed in the Robotran implementation, see Figure 5.9.

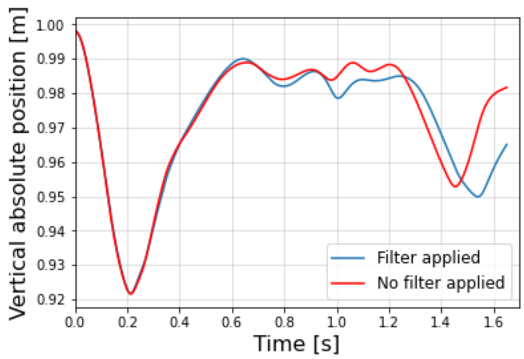

Figure 5.8: Hip vertical position in the Simulink model with and without the application of the filter.

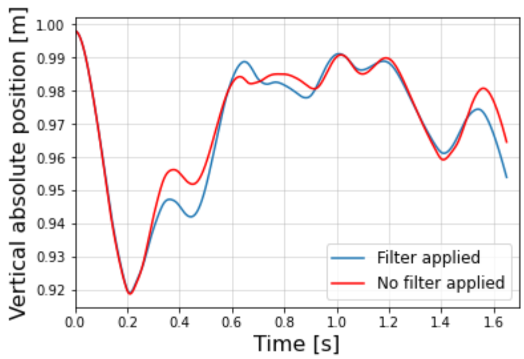

Figure 5.9: Hip vertical position in the Robotran model with and without the application of the filter.

5.2.2 The Neuromuscular Delay

The concept of neuromuscular delay is introduced in 4.2. Introducing a brief delay allows time for the sensory receptors to transmit feedback about the state of the muscles and joints to the nervous system. This feedback loop permits to modulate the muscle

activations, enabling the coordination of muscle contractions preventing simultaneous activation of antagonistic muscles.
To apply the delay, relevant variables are added in matrices. The values after the delay are retrieved by taking the matrix element corresponding to the index:

$$i_{delayed} = i_{current} - \frac{\Delta t_{delay}}{timestep}$$

5.2.3 Impact of the Implementation Choices on the Neural Control Layer's Outputs

This section highlights the impact of the implementation choices for the inhibition of the stimulations and the delay on the outputs of the neural control layer.
The overview of the model, depicted in Figure 4.1, introduces the role of the neural actuation layer, i.e., to obtain the muscular stimulations from the joint positions and velocities.
Figure 5.10 illustrates the difference between stimulations obtained with our implementation of the neural control layer and stimulations obtained with Simulink from joints data exported from Simulink for the VAS, GLU, HAM and HFL. Although a marginal difference is observed, it is not expected to have a significant impact on the overall kinematics.
As SOL, GAS and TA are not inhibited, their stimulation remains unchanged compared to the values obtained in Simulink (see appendix C).

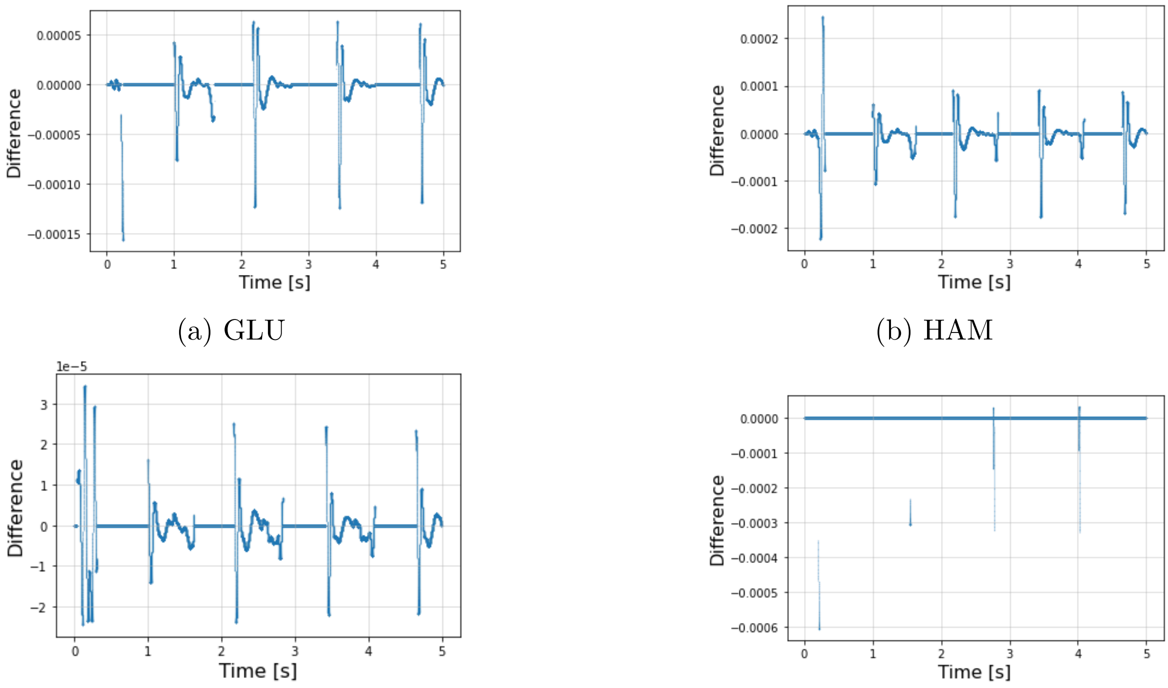

(a) GLU (b) HAM

(c) HFL (d) VAS

Figure 5.10: Difference between the obtained and the Simulink's muscle stimulations for the GLU, HAM, HFL and VAS.

5.3 External Environment: Ground Contact Model

This section describes the implementation of the ground contact model (GCM) block based on the description presented in section 4.3. A schematic representation of the GCM is available in Figure 5.11.

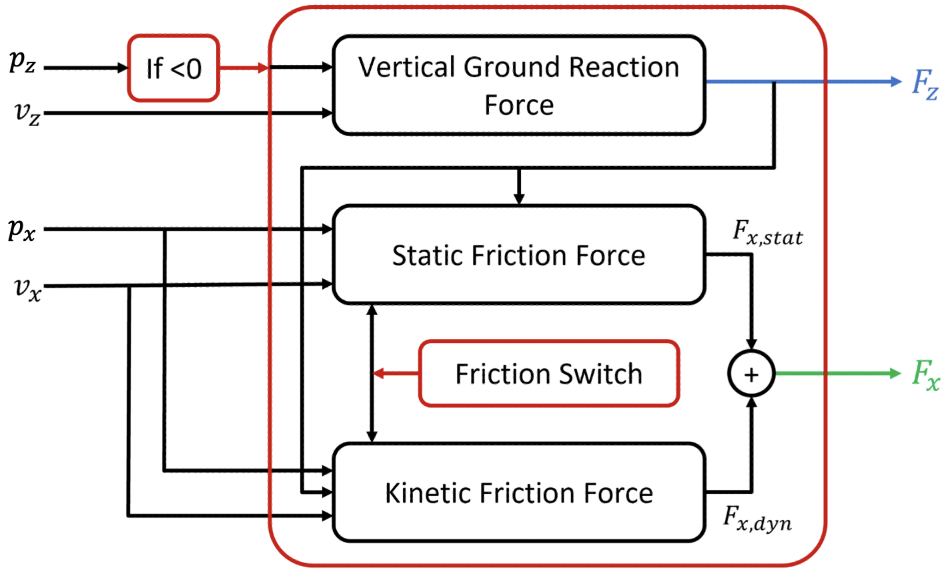

Figure 5.11: Schematic representation of the GCM model implementation. Black arrows represent the inputs of the block and the data flows within the block, red arrows represent the activation signals of a block and the blue and green arrows represent the outputs (respectively vertical and horizontal force).

The GCM block receives the vertical (p_z and v_z) and horizontal (p_x and v_x) positions and velocities of the heel and forefoot of each foot as input. First, a condition is applied on the vertical position that ensures that contact forces are obtained only if there is indeed a contact with the ground. When the model is enabled, first the vertical force is computed, followed by the computation of the horizontal force using the appropriate friction model (static dry friction or dynamic dry friction).

This section is important because it describes the validation of the developed GCM model which is a critical element in the implementation of the global Geyer model. When modeling a multi-body system (MBS), ground contacts are indeed critical elements because the dynamics of the MBS can become very stiff due to the impact of contact forces. The contact forces imply stiffness because of the discrete and non-linear nature of the contacts. This can be explained by 2 phenomena: firstly, the bodies interacting with the ground can undergo very important forces when the contact is established or interrupted (represented by the activation signal of the contact model on Figure 5.11) and secondly, the permutation between static friction mode and kinetic friction mode (represented by the red arrows from the friction switch on Figure 5.11).

These 2 phenomena involve jumps or abrupt oscillations in the dynamics of the system. The stiffness of a dynamic system makes the integration of the dynamic equations more complex because it requires very small-time steps to guarantee the stability of the simulation.

The next two sections cover the validation of the GCM model in simplified cases. First, the validation using a system composed of a three-segmented leg whereby the joints are not actuated and thereafter the validation using the complete model (trunk and 2 three-segmented legs) with non actuated joints.
For each of the simplified cases, the ground reaction forces, and the joint positions are presented and compared with the results from the Geyer model in Simulink [1].

5.3.1 Results of a Non-actuated One-leg Robotran Model

In this section the results obtained from applying the contact model to a simplified case of the multibody system described in section 3.2 are presented. The simplified case consists of a leg composed of three segments connected by unactuated revolute joints. The animation shown in Figure 5.12 illustrates the collapse of the leg arising due to the absence of actuation in the revolute joints. It can be observed that the foot remains static. The immobility is caused by the contact forces at the heel and ball of the foot, which impose constraints on its movement.

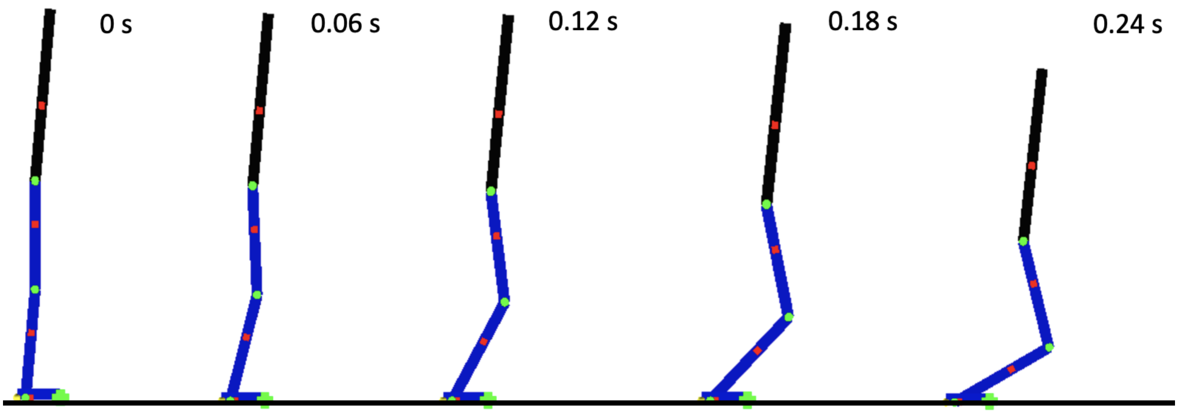

Figure 5.12: Animation of a not-actuated one-leg system on Robotran. Bodies of the leg (thigh, shank, and foot) are represented by blue bodies connected by green dots representing revolute joints. The trunk is represented by a black body.

Both the Robotran and Simulink simulations use the same integrator, namely RK4, with a time step of $125e-7\ s$ (see section 3.1.3 for more details).
The analysis of these results focuses on a duration of $0.239\ s$, as the position values of the joints beyond this time become unrealistic from a bio-mechanical perspective.

[1]Simulink results were obtained from modified models in which the joints were not actuated.

The animation obtained in Robotran is similar to the one obtained in Simulink when using the same integrator. An analysis is performed on the contact forces observed at two specific points, namely the heel and ball of the foot, as well as at the positions of the joints. This analysis aims to provide a comprehensive understanding of the obtained results.

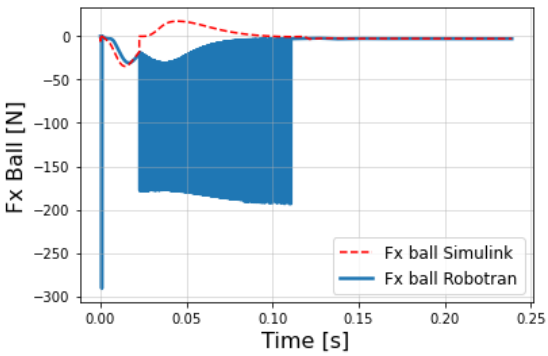

Figure 5.13: F_x Ball

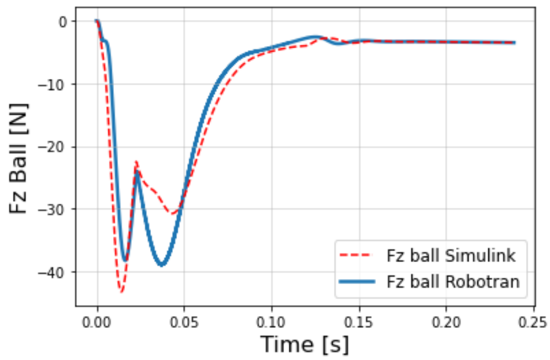

Figure 5.14: F_z Ball

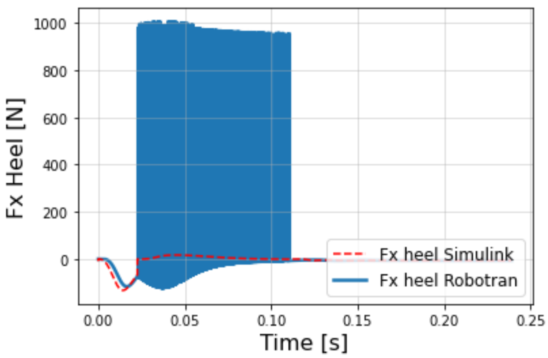

Figure 5.15: F_x Heel

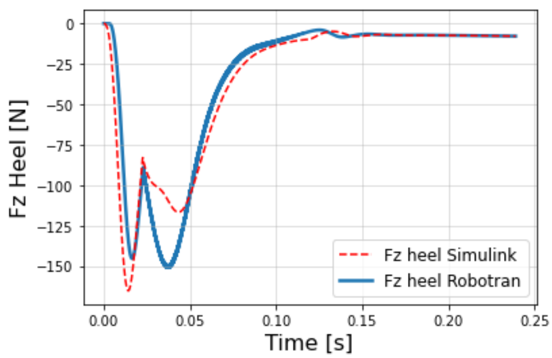

Figure 5.16: F_z Heel

One can observe in Figures 5.13 to 5.16, that the vertical force signals (F_z Ball and F_z Heel) follow a similar shape and have a similar order of magnitude to the signals obtained with Simulink.
However, the general shapes of horizontal forces are different from the signals coming from Simulink presenting undesired oscillations between the two modes of friction, despite using the same integrator method and time step in Robotran and Simulink.
It is important to note that these differences in horizontal contact forces are more likely a result of the model-simulator interaction rather than being indicative of an implementation error in the contact model. This assertion is further supported by validation of the model without interaction with Robotran presented in Appendix E.1.

Although differences are observed in the horizontal forces, it can be demonstrated

that these variations do not have a significant impact on the kinematics of the one-leg system, as conclusive results concerning the positions of the joints can be obtained (as shown in Figures 5.17 to 5.19).
However, one can observe a difference in the position of the hip which seems to increase during the simulation. This tendency is related to the instability of the system. A small variation will lead to an accumulation of the variation and therefore can lead to significant modifications of the global state of the system. In this case, this phenomenon may not be significant, but it can become more pronounced in more complex systems.

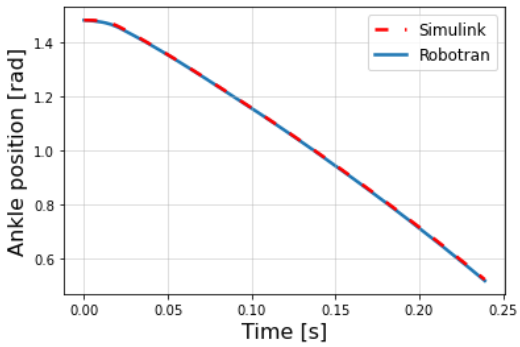

Figure 5.17: Ankle position

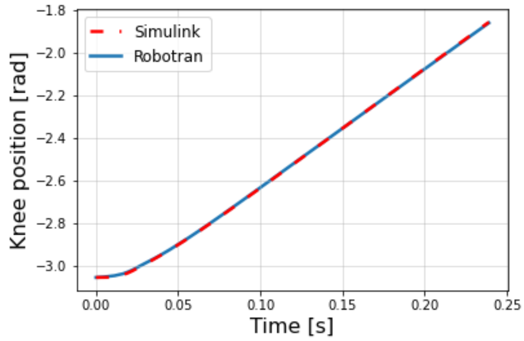

Figure 5.18: Knee position

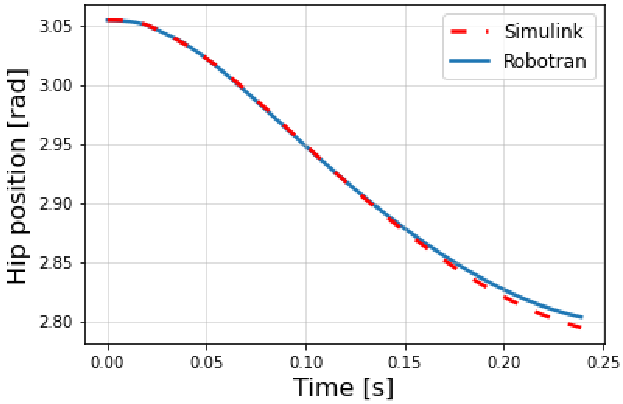

Figure 5.19: Hip position

5.3.2 Results of a Non-actuated Two-leg Robotran Model

After conducting an analysis on a one-leg system, the contact model is extended to a more complex model comprising two three-segmented legs with non-actuated joints. The animation shown in Figure 5.20 illustrates the collapse of the system arising due to the absence of actuation in the revolute joints. It can be observed that the left foot remains almost static while the right foot falls during 0.18 s and then is constrained by ground contact forces.

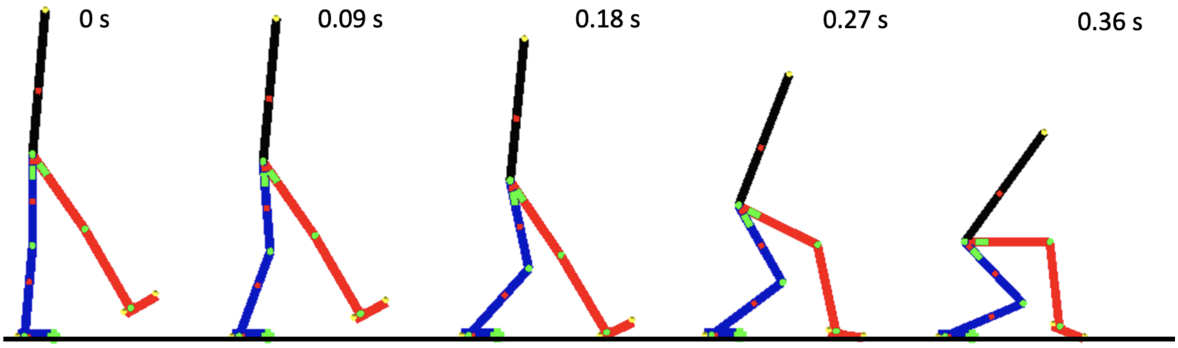

Figure 5.20: Animation of a not-actuated two-leg system on Robotran. The thigh, shank, and foot are represented by red bodies for the right leg and blue bodies for the left leg connected by green dots representing revolute joints. The trunk is represented by a black body.

As for the one leg model, both the Robotran and Simulink simulations use the same integrator, namely RK4, with a time step of $125e-7s$ (see section 3.1.3 for more details).

The forces for heel contact points of both feet are shown in Figures 5.21 to 5.24 below (Results for ball contact points of both feet are included in Appendix E.2).
In the case of the two-leg model, the obtained vertical contact forces on the left foot are similar to those obtained in Simulink whereas there are again considerable differences for the horizontal forces.
For the right foot, both the vertical and horizontal contact forces show significant differences. The peaks of vertical forces obtained in Robotran are approximately twice as high as those obtained in Simulink.
As for the one-leg case, these differences can likely be attributed to the interaction between the GCM model and the simulator given that the model has been validated independently of Robotran (see Appendix E.2).

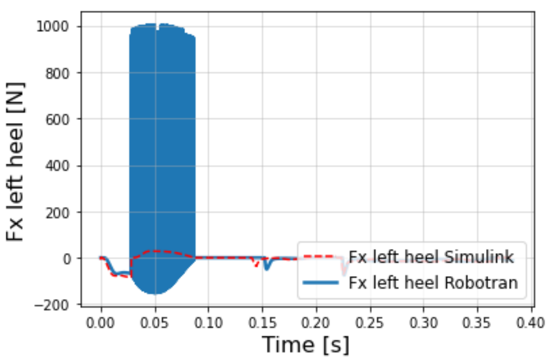

Figure 5.21: F_x Left heel

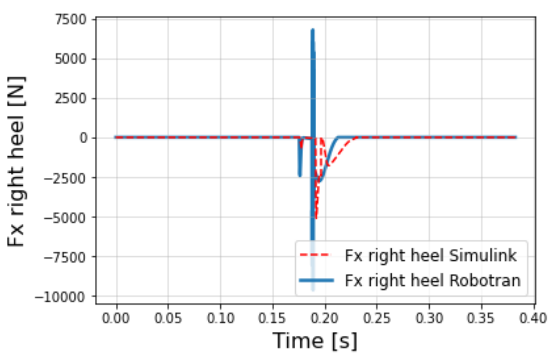

Figure 5.22: F_x Right heel

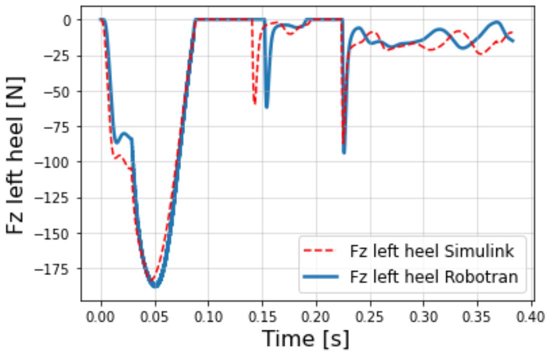

Figure 5.23: F_z Left heel

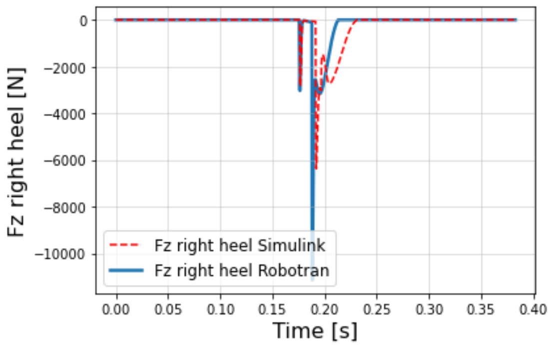

Figure 5.24: F_z Right heel

Figures 5.25 and 5.26 show the temporal evolution of joint positions in Robotran and Simulink. Notably, the two curves demonstrate similar shapes for each joint. However, significant variations start to emerge at 0.18 s of the simulation, corresponding to the moment of contact between the right foot and the ground. This observation is consistent with the occurrence of the greatest differences in contact forces at this time, attributed to their stiffness resulting from the establishment of contact with the ground of the right foot. As for the one-leg system, the instability of the two-leg system induces the increase of the difference throughout the simulation.

In the context of this thesis, the GCM model will act in combination with the reflexe laws of control of the Geyer model which was designed to be robust to small angle differences [2]. The reflexes are influenced by the positions of the joints through the length of the MTC at each time step, which allows it not only to adapt to the differences occurring at the moment of the contact but also to avoid causing too large gaps by difference accumulation in the complete model.

5.4 Conclusion

The implementation of key functions of interest, such as the integrator method, delays, and filters, was subjected to independent testing independently of the Robotran environment. Promising results were obtained, validating the acceptability of these implementations.
However, when testing the contact methods using simplified Robotran models, discrepancies were observed between the results obtained with the contact model and those obtained using the Geyer model in Simulink. This discrepancy suggests that the interaction between our implementation of the contact model and the Robotran simulator may be responsible for these variations.

In the subsequent chapter, we present the results obtained by integrating the specific implementations into a comprehensive Robotran model. The purpose is to evaluate the quality and validity of our model, thus shedding light on its overall performance.

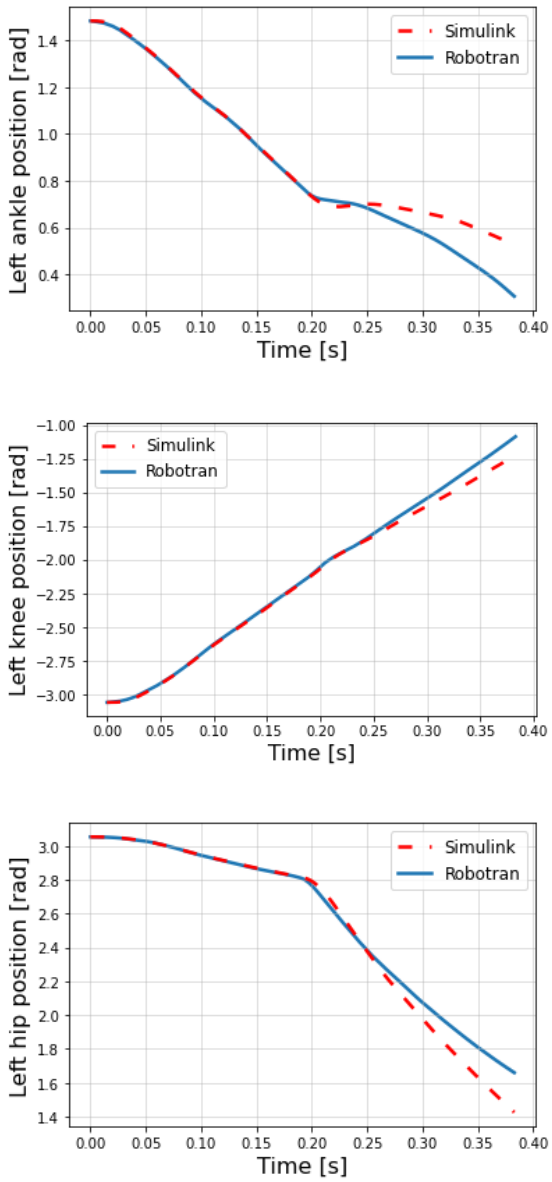

Figure 5.25: Joint positions for each articulations of the left leg. References as presented in section 3.2.1

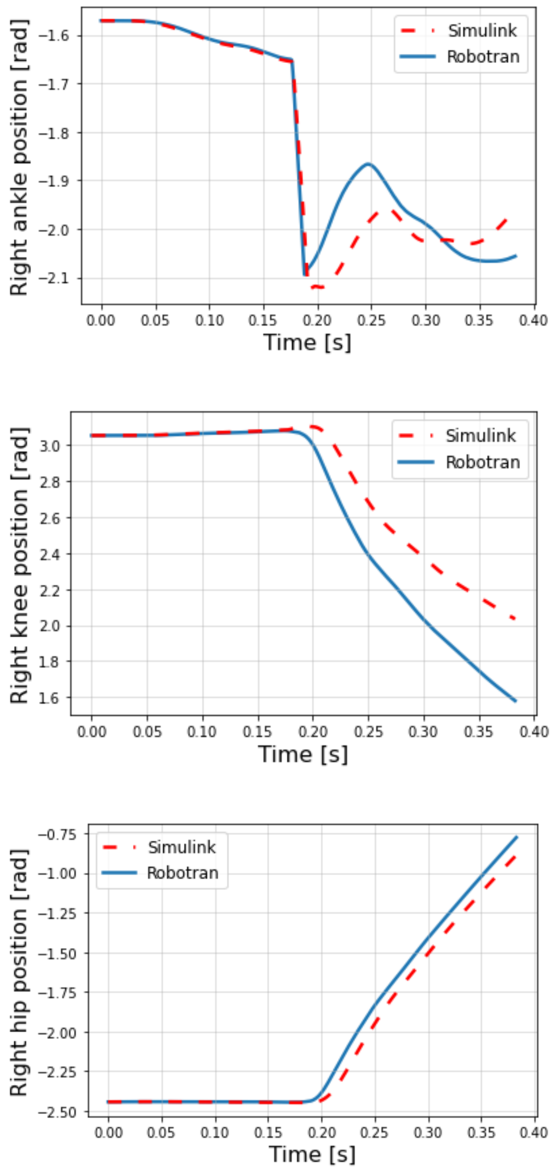

Figure 5.26: Joint positions for each articulations of the right leg. References as presented in section 3.2.1

Chapter 6

Robotran Model: Results and Analysis

The previous chapter presented the intermediate results that drove to specific implementation choices. In this chapter, the results of the human walking simulated on Robotran using Geyer's model are described. The objective is to demonstrate the consistency of the aforementioned results with the results obtained by Geyer on Simulink.

First, a general description of the animation and the behavior observed during the simulation is proposed with the temporal evolution of the joint positions and the results of the walking phase are given.

Thereafter, the results of the main output blocks, based on Figure 4.1, are covered:

- Muscle stimulations for the neural control layer (S_m)
- Joint torques for the muscle actuation layer (τ_{joints})
- External forces for the ground contact force model (F_{ext})

The results were obtained by simulating our model using Robotran for a duration of 2 seconds. The RK4 integrator with a time step of $250e - 7$ has been used for the simulation. On the other hand, Simulink results were obtained by simulating Geyer's model within the Simulink environment. The integrator utilized in Simulink is identical to the one employed in the Robotran simulation, ensuring that the obtained results are under simulation conditions that are as similar as possible. It is worth noting that Geyer's model in Simulink normally runs with the integrator set with a variable time step (ode15s) (see section 3.1.3).

6.1 Simulation Results in Robotran

The overall kinematic behavior of the model representing human walking and gait animation is presented for the first 1.42 seconds of the simulation. Figure 6.1 illustrates the animation of the human walking model, with snapshots representing the critical steps of the left foot gait cycle.

After 1.42s of simulation, a noticeable issue appears during the swing phase of the right leg. The foot gets too close to the ground and therefore enters the stance phase prematurely (see section 6.1.3). This phenomenon is responsible for the collapse of the model after 1.65s of simulation. The characteristics of this collapse are discussed in more details in section 6.1.4.

The analysis presented therefore focuses on the events prior to the model collapse, which occurs within the first 1.65 s of the simulation. While only the left leg performs a complete gait cycle during this time frame, both legs will be analyzed in order to get a comprehensive understanding of the overall behavior of the system and assess potential interactions and dependencies between the legs. This approach allows for identification of similarities or differences in gait patterns, muscle activations and joint torques. The comprehensive analysis will provide insights into the system's behavior and provide us better a understanding off its dynamics, performance while allowing to identify potential causes of the collapse.

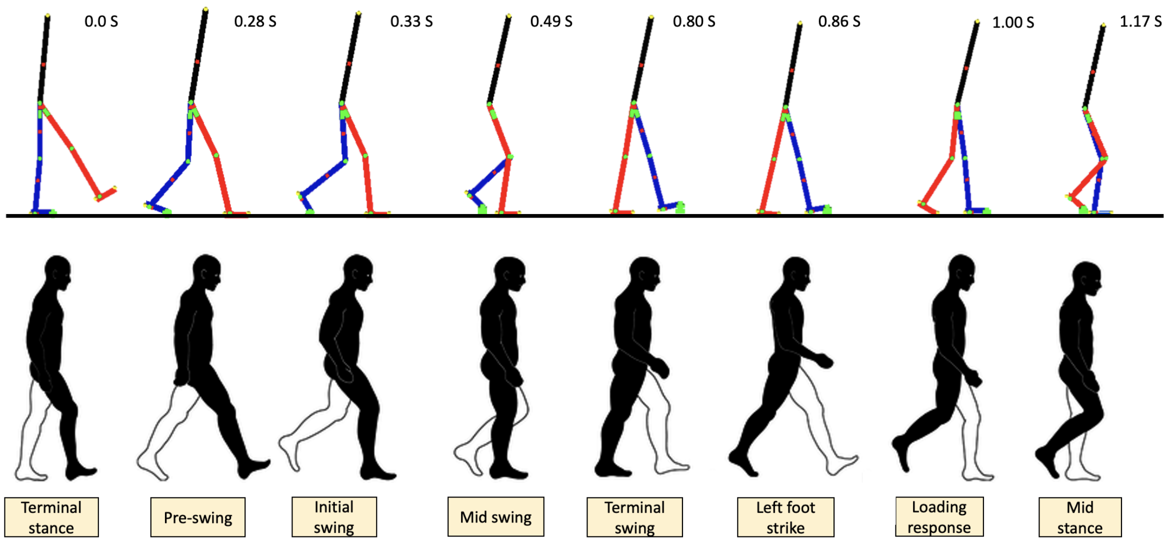

Figure 6.1: Animation of the complete Robotran model for one left foot gait cycle. The snapshots of each critical step of the walking cycle are represented by the drawings, each corresponding to the relevant steps from [8]. Bodies (Thigh, shank, and foot) are represented by blue bodies for the left leg and red bodies for the right leg connected by green dots which represent the revolute joints.

6.1.1 Gait Cycle

The graph displayed in Figure 6.2 illustrates the gait phases for the left leg and right leg, respectively in blue and red. The leg is in stance when the value is 1 and in swing when it is 0. The dashed lines represent the transition moment from one phase to another phase. The orange area corresponds to the moment where both feet are in contact with the ground: the double support phase. The left leg performs a full gait cycle between $0.36s$ and $1.59s$ and the right leg between $0.18s$ and $1.42s$.

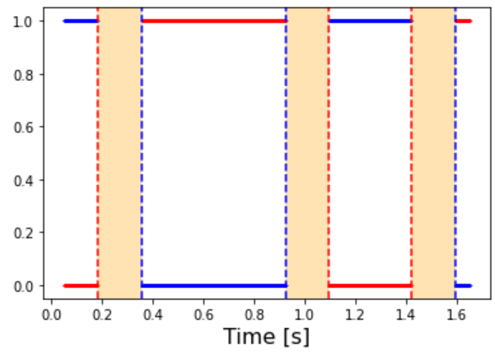

Figure 6.2: Left (blue) and Right (red) leg gait phase. The orange zone represents double support phase.

Theoretically, the average percentage of a gait cycle's time required for the stance phase and swing phase is approximately 60% and 40% as presented in Figure 1.2 [79].
In the developed model, the left leg stance phase accounts for 54% of the first complete gait cycle, while the swing phase represents 46%. For the right leg, the proportions are 73% and 27%. The theoretical percentages do not match the percentages in the developed model. This difference can be explained by the fact that only the first $1.65s$ of the walk are analyzed. Because of the departure position of the model, the first steps allow the system to stabilize. Therefore, during this time frame the system is still undergoing adjustments and the gait pattern is not yet fully stable and periodic. Although this has no significant kinematics consequences on the first two steps, the cycle does not stabilize as expected and the model falls after 1.42 s.

The results graphs presented in this chapter consistently employ the same convention as in Figure 6.2 for representing phase transitions, with blue dashed lines denoting the left leg and red dashed lines denoting the right leg. To indicate the moment corresponding to the collapse of the system, a red zone will be incorporated into the graphs.

6.1.2 Left Joint Positions

Despite slight differences, the joint position signals obtained with Robotran are similar in terms of magnitude and pattern to the signals from Simulink and are in line with the specific characteristics of the gait cycle (see Figure 1.2).

The results are presented in Figure 6.3. The graph compares the joint positions for the left leg obtained in Robotran and in Simulink.

At the start of the left leg swing phase (marked by the first blue dashed line at 0.36 s), the ankle is flexed upwards to reach a 90° angle when hitting the ground (blue dashed line at 0.93 s). At the very beginning of the stance phase, the ankle undergoes a plantar flexion, corresponding to the rolling of the foot from the moment the heel touches the ground to the moment the ball touches the ground. After the rolling movement, the ankle is flexed towards the shank for 50 ms and enters in dorsiflexion, which corresponds to the advancement of the shank. At the end of the stance phase, the heel is lifted off the ground and the ankle undergoes a second peak of plantar flexion in the transition from stance to swing phase.

For the knee, at the beginning of the swing phase, a peak of flexion is observed followed by a return to a quasi-extension position. The latter is maintained from the end of the swing phase until the heel lifts off the ground in the stance phase. The knee will thereafter flex again during the pre-swing and initial swing stages of the cycle.

The hip flexes at the beginning of the swing phase. The hip reaches its maximum flexion angle at $t = 0.5$ s, at the same moment as the knee reaches his maximum flexion angle. The hip then extends to reach a maximum of extension at 1.43 s and finally goes into flexion at the end of the stance phase.

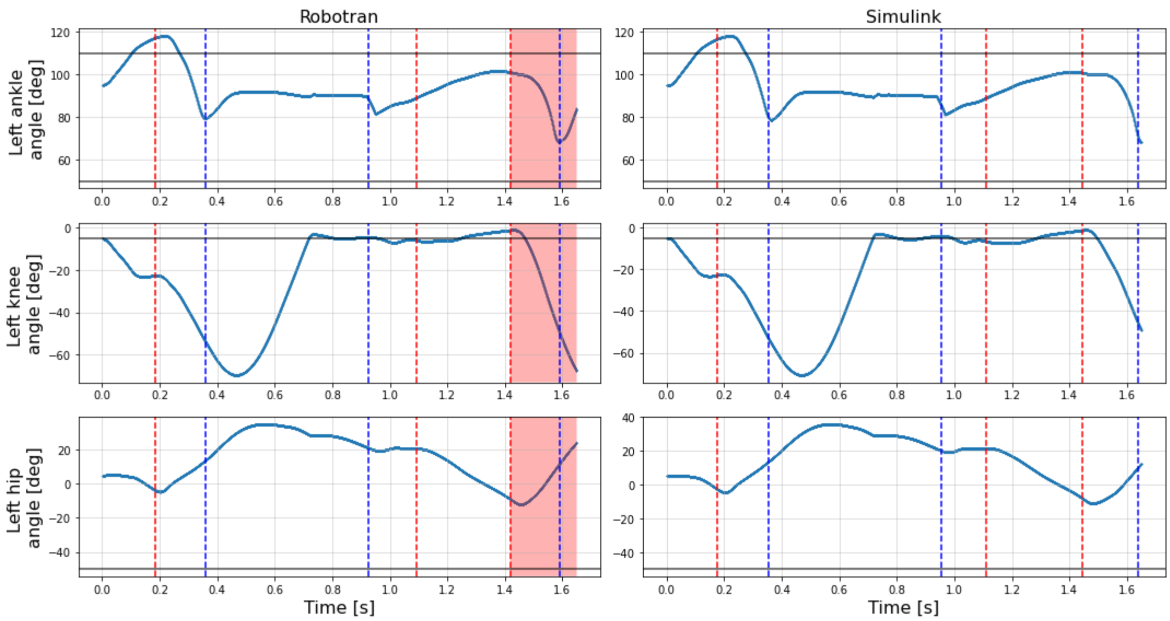

Figure 6.3: Left joint positions, positive angles with respect to the y-axis of the inertial frame: angle between the axis of the tibia and the foot for the ankle, angle between the axis of the thigh and the tibia for the knee, and angle between the axis of the trunk and thigh for the hip. The red and blue dashed lines represent the change of gait phase as explained in Figure 6.2 and the black lines represent limits outside of which joint limits enters in action [2]. The red zone represents the collapse of the system.

6.1.3 Right Joint Positions

For the right leg (Figure 6.4), within the initial 1.42 s of the simulation, the obtained joint positions exhibit characteristics indicative of the theoretical patterns observed during the walking cycle (as explained in section 6.1.2 for the left leg). Nonetheless, differences can be observed.

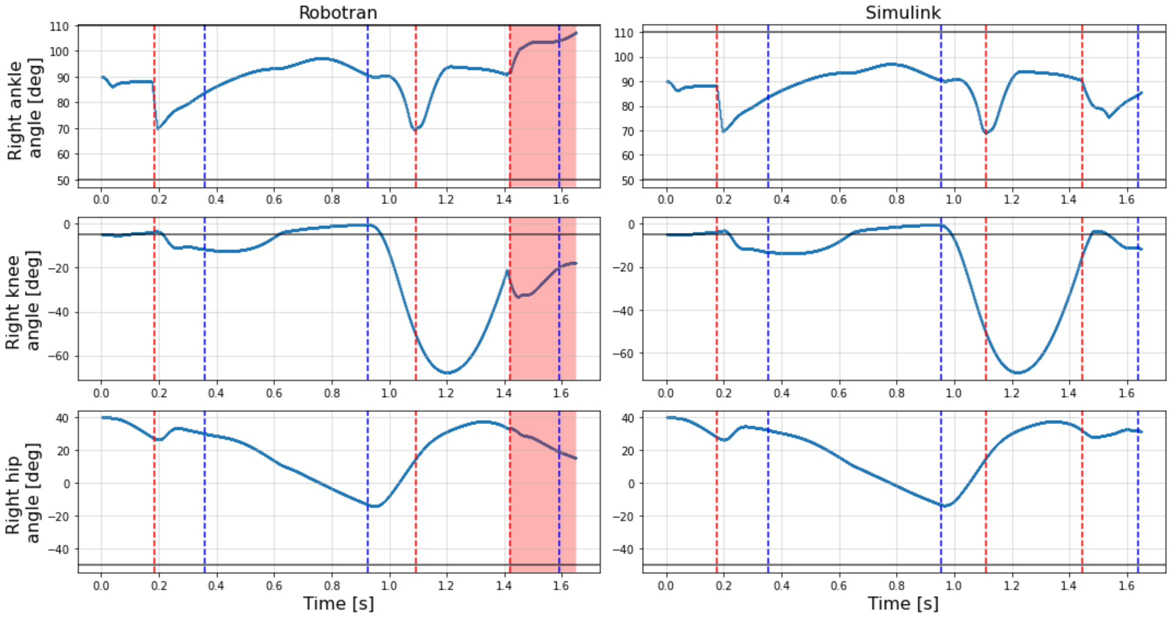

Figure 6.4: Right joint positions (angle's references same as in Figure 6.3). The red and blue dashed lines represent the change of gait phase as explained in Figure 6.2 and the black lines represent limits outside of which joint limits engage [2]. The red zone represents the collapse of the system.

During the onset of the stance phase, the peak of knee flexion, which occurs between 0.25 and 0.6 s, reaches a maximum value of 11.46 deg in Robotran and 14.3 deg in Simulink.

Furthermore, an additional noteworthy distinction arises during the swing phase: the peak flexion of the knee and ankle manifests a temporal shift in the Robotran simulation compared to the knee and ankle flexion results obtained through Simulink. In particular, in Robotran, the flexion maxima occur earlier compared to Simulink. Consequently, the extensions of the knee and ankle following the peak flexion also arise earlier. This temporal shift may explain that the foot is closer to the ground during the swing phase. This phenomenon, whereby the foot grazes the ground, initiates an undesired transition into the stance phase of the right leg after 1.42 s, which is earlier than in Simulink where the right leg enters the stance phase after 1.45 s of simulation.

6.1.4 Collapse of the Model

The model's collapse can be attributed to two distinct phenomena leading to the same outcome.

The first phenomenon is the foot grazing the ground; more specifically, gradual decrease in the distance between the ground and the foot during the swing phases over time. During the swing phase, the foot grazes the ground. But as the model walks, the ball of the foot comes closer and closer to the ground. After a certain number of steps, it transitions from mere contact to actual touch. Figure 6.5 shows the phenomenon for the three first swings. The last point coincides with the moment the model enters its fall.

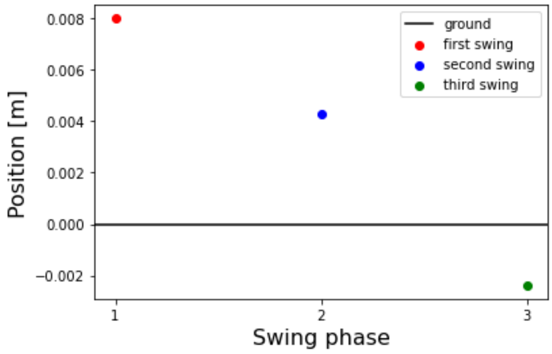

Figure 6.5: Minimum foot distance from the ground for each swing phase.

The second phenomenon is the occurrence of an unlikely event at 1.42s: a bounce of the foot when it touches the ground. Initially, the heel strikes the ground as it has been theoretically described, initiating a downward movement of the ball of the foot. Usually, the heel remains in contact with the ground until the ball touches the ground. Then, both contact points, i.e., the heel and the ball, remain on the ground for a certain period of time before the lift-off of the heel which marks the beginning of a new swing phase. However, in this case, the usual scheme is not observed.

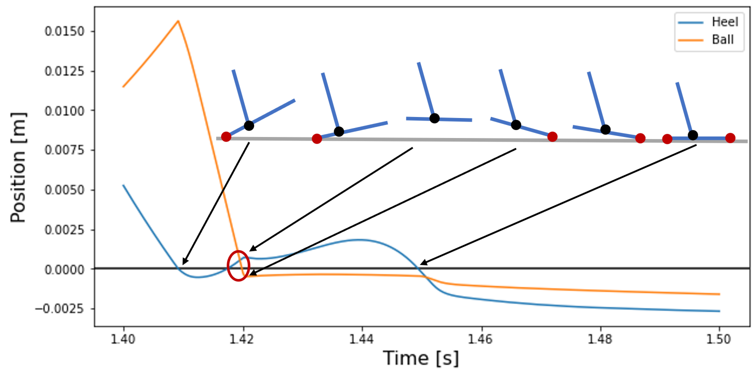

Figure 6.6: Description of the foot kinematics and relationship to the foot position signal

After the heel strikes the ground, it briefly remains in contact before lifting off, as if bouncing off the ground. However, the contact of the heel initiates the downward movement of the sole towards the ground. For a brief moment, neither the heel nor the ball of the foot is in contact with the ground. Then, the ball touches the ground first before the heel makes contact with it again. This pattern is shown in Figure 6.6.

The two described phenomena result in irregularities in phase detection. In the first case, the model detects an erroneously stance phase when the leg should still be swinging. Conversely, in the second case, a brief swing phase is detected when the foot should be in contact with the ground.

It is important to highlight that the phase detection mechanism itself is functioning correctly. However, due to the errors in the foot position, the gait phases occur at times when they theoretically should not.
In both cases, these irregularities of phases compromise the smooth running of the next step. Even though, the phase irregularities are brief, they lead to inaccurate sensory feedback to the muscles. This mismatch in sensory information has implications in the simulation, as the signals for stance and swing are delayed by 0.1 seconds. During this brief period, the muscles have an abnormal behavior, resulting in erratic movements and initiating a series of chain reactions that ultimately leads to the model's collapse.

6.2 Muscle Actuation Layer

The torques of the joints in the left limb in Robotran closely match the torques obtained by Geyer in Simulink (Figure 6.7). Two notable observations can be made. First, there is a time delay which starts at the point the left foot makes contact with the ground (at approximately 0.93 s). The time shift can be attributed to the fact that in the Robotran model, the foot touches the ground slightly earlier than in the Simulink model. However, in terms of torques, this difference has no significant effect. The time lag does not directly impact the torque as the curve continues to follow the Simulink curve without significant deviation.
The second observation pertains to a torque peak at 0.75 s for the left knee. This peak corresponds to a preventive measure against overextension of the knee and is a direct consequence of the joint limit (see section 4.1.3).

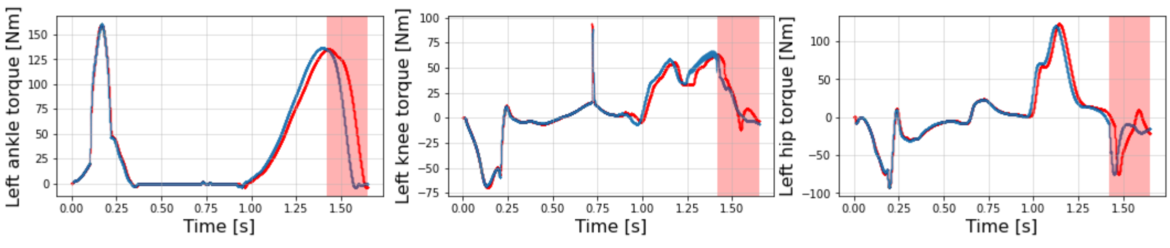

Figure 6.7: Robotran (blue signals) and Simulink (red signals) comparison of left joint torques. The red zone represents the collapse of the system.

For the right leg (Figure 6.8), the observations are similar to those of the left leg. However, it is worth noting that the time lag starts when the right leg initially touches the ground at 0.18 s. Additionally, the peak torque for the knee at 0.2s is approximately half of that observed in Simulink. The impact of the fall is directly visible in the graph.

In particular, in the knee graph, it appears as though the torque induces a movement opposite to what is expected, approximately at 1.5s.

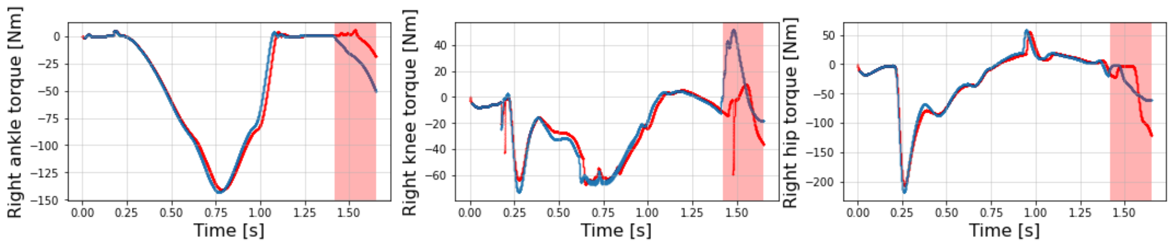

Figure 6.8: Robotran (blue signals) and Simulink (red signals) comparison of right joint torques. The red zone represents the collapse of the system.

6.2.1 Conclusion

While there are some minor differences and deviations in timing and intensity, the general patterns and behavior of the torques align closely to Geyer's results before 1.4s. These findings suggest that the calculation and generation of joint torques in the model are reliable and accurate and are not a plausible cause of the model's collapse.

6.3 Neural Control Layer

The following analysis will primarily concentrate on muscles responsible for hip and knee flexion, namely VAS, GLU, and HFL (as the stimulation of HAM and GLU are interlinked, the focus will be solely on GLU). In the following graphs, the stimulation is represented by the blue curve, while the phase changes of the left and right leg are represented by dotted lines in blue and red, respectively. A comparison of the stimulations obtained with Robotran and those acquired by Geyer for all the muscles can be found in Appendix D.

6.3.1 Left Stimulations

First, it is noteworthy that the overall pattern of the muscle stimulations is preserved. As explained in section 6.1.1, the muscle stimulation is intricately connected to the phase of the gait cycle. From the graphs, several observations can be made. The muscle stimulation is not only impacted by the phase of the corresponding leg but also by the phases of the contralateral leg. Whenever the contralateral leg undergoes a phase change, it immediately affects the stimulation of the ipsilateral leg. Robotran's and Simulink signals remain identical, except for the VAS, until the right leg enters the stance phase at about 1.42s. Particular attention will be given to the events occurring after the left leg has moved into stance at 0.93s.

In Figure 6.9, after 0.93 s, the stimulation of the Vasti muscle in Robotran deviates significantly from the one of the Vasti implemented by Geyer. The stimulation oscillates abruptly between 0.01 and a value close to 0.1 between 1.1 s and 1.2 s. It is worth reiterating that the stimulation values are constrained within the range of 0.01 to 1. This oscillation can be attributed to the inhibitory mechanism at play (see section 4.2). When the inhibition is too important, the stimulation value drops below 0 and is consequently limited to the lower bound of 0.01. Moreover, after the transition of the right leg in the stance phase at 1.42 s, the intensity of the stimulation is considerably lower than in Geyer simulation.

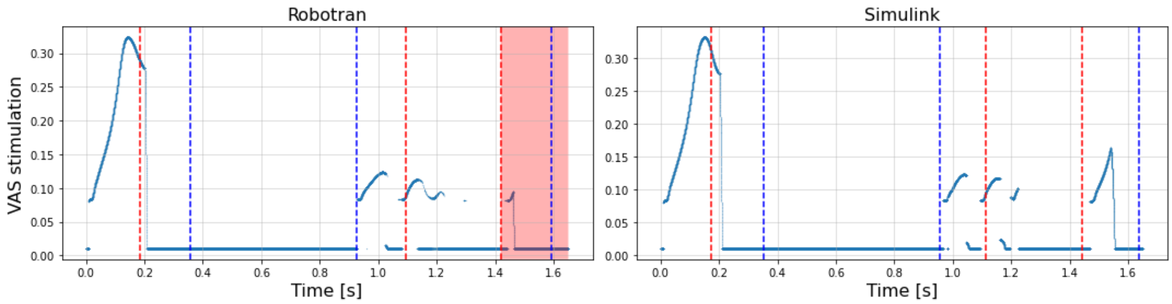

Figure 6.9: Left Vasti stimulations. The red and blue dashed lines represent the change of gait phase as explained in Figure 6.2. The red zone represents the collapse of the system.

For the gluteus muscle similar observations can be made as for the Vast muscle. The shape of the graph obtained in Robotran corresponds to the one obtained by Geyer. However, noticeable differences are observed in the intensities of the peaks. Firstly, the peak intensity before the right foot takeoff (at 1.1s) is lower than expected. Secondly, the intensity of the peak immediately after the takeoff is higher than expected. Lastly, after the last contact of the right foot with the ground at 1.43s, the intensity of the peak is significantly lower than anticipated.

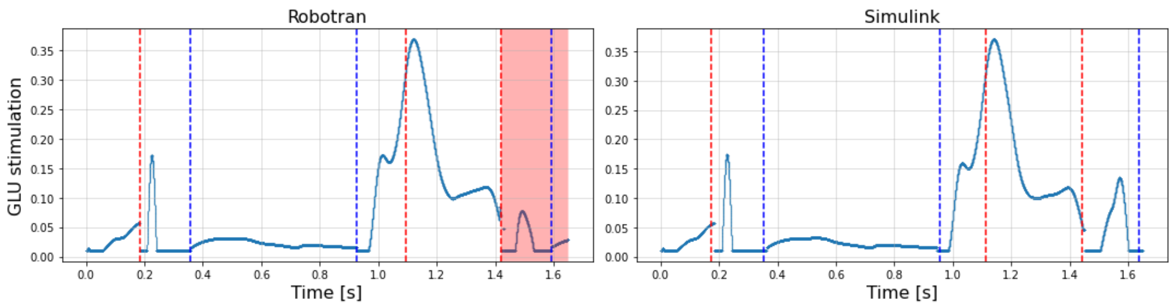

Figure 6.10: Left Gluteus stimulations. The red and blue dashed lines represent the change of gait phase as explained in Figure 6.2. The red zone represents the collapse of the system.

The observations made for the VAS and the GLU are also valid for the hip flexor but, interestingly, their impact is more limited.
As the GLU and HFL are among others responsible for stabilizing the trunk, and as the GLU and HFL are antagonistic muscles, it is logical that when the model starts to lose its balance and as a result the trunk leans forward excessively, this is counterbalanced

by a greater stimulation of the GLU. In this case, the HFL is inhibited which explains why its stimulation is low and why the intensity error visible on the GLU is only slightly visible here.

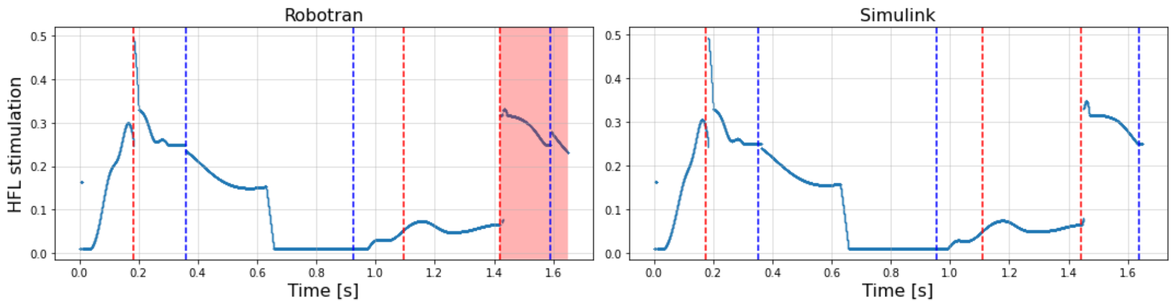

Figure 6.11: Left Hip flexor muscle stimulations. The red and blue dashed lines represent the change of gait phase as explained in Figure 6.2. The red zone represents the collapse of the system.

6.3.2 Right Stimulations

Similar to the left leg, the focus is on the hip and knee flexor muscles. The general pattern of muscle stimulation is respected until the right foot strikes the ground at 1.42 s. The specific characteristics of the gait cycle are present. The activation of the GLU and HFL muscles have an inverse relationship, whereby higher activation of the GLU coincides with lower activation of the HFL, and vice versa. This coordinated modulation of the antagonistic muscles is crucial to ensure the smooth execution of the gait cycle.

In the VAS muscle stimulation (see Figure 6.12), two important observations can be made. First, prior to the swing transition of the left leg at 0.93 s, the VAS stimulation remains limited to 0.01 due to a negative calculated stimulation value. However, when the left foot makes contact with the ground, the model enters the double support phase, causing a sudden change in mass distribution between the legs. Consequently, the factor associated with this distribution also changes, leading to VAS activation during the double support phase. Secondly, immediately after the crucial transition of the right leg into stance at 1.42 s, the model again enters the double support phase. In this phase, one would expect to observe a peak in stimulation followed by a decline. However, the stimulation in Robotran exhibits an abrupt increase, reaching a peak twice as high as that observed in Simulink. Moreover, the stimulation in Robotran does not immediately, i.e., approximately at 1.5s, decrease after the peak as it is observed in Simulink.

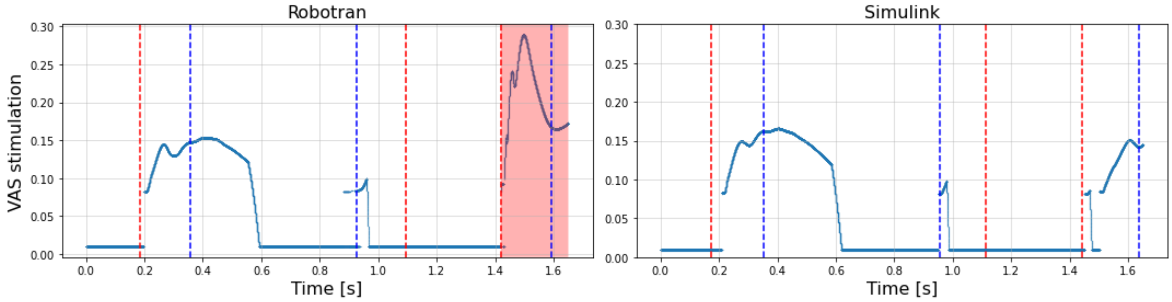

Figure 6.12: Right Vasti stimulations. The red and blue dashed lines represent the change of gait phase as explained in Figure 6.2. The red zone represents the collapse of the system.

For GLU and the HFL, the picture is a little different (see Figures 6.14 and 6.15). During the first double support phase their peak is too high and conversely, their minimum is too low. One hypothesis to explain this would be poor management of the factor taking into account mass distribution. On Figure 6.13, which shows the displacement of the prismatic joint after it has been filtered, it is evident that the error is already present.

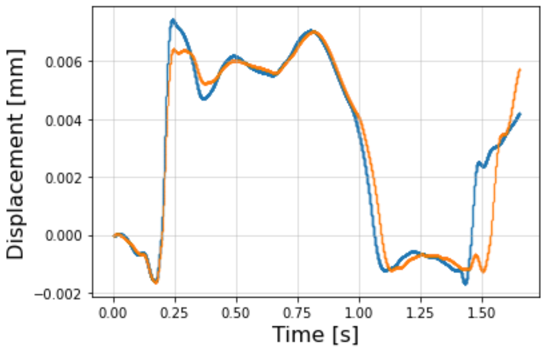

Figure 6.13: Right prismatic joint filtered displacement. The blue signal represents the data obtained from Robotran, while the orange signal represents the data obtained from Simulink.

Another hypothesis explaining the difference in Figure 6.13 is that the filter mismanages the maxima and minima of the signal. However, this hypothesis is challenged by the absence of the same phenomenon during the second stance phase. When examining figures 5.8 and 5.9, it is evident that the Robotran model has a different behavior compared to the Simulink model, particularly during the first double support phase. This contradicts the filter hypothesis as the major factor contributing to the difference in prismatic joint displacement is the kinematic behaviour of the model.
The cause of the kinematic difference remains unclear. It could potentially be related to ground reaction forces or other factors specific to the simulation platforms. Furthermore, during the third phase of double support, similar to the VAS, the observed results deviate from the expected behavior. Despite exhibiting characteristics of antagonistic

muscles, the muscle stimulation no longer corresponds with that of the Simulink model.

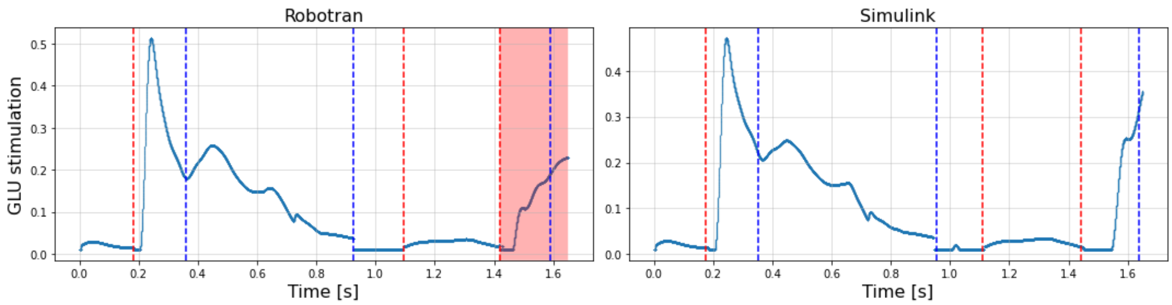

Figure 6.14: Right Gluteus stimulations. The red and blue dashed lines represent the change of gait phase as explained in Figure 6.2. The red zone represents the collapse of the system.

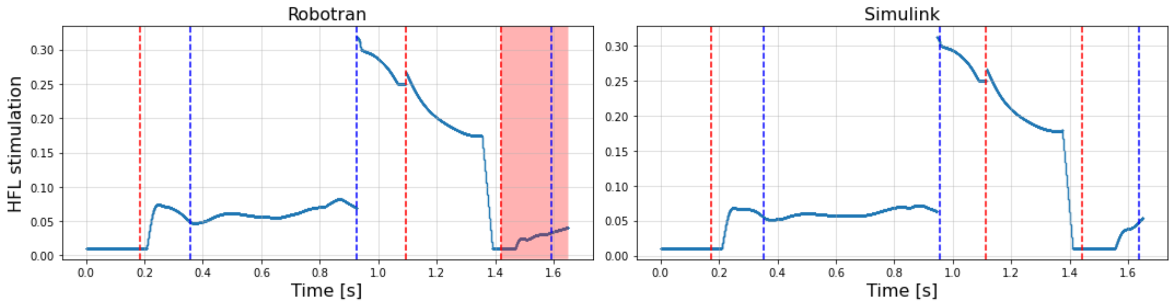

Figure 6.15: Right Hip flexor muscle stimulations. The red and blue dashed lines represent the change of gait phase as explained in Figure 6.2. The red zone represents the collapse of the system.

6.3.3 Conclusion

The analysis showed that the overall pattern of muscle stimulations was respected until the onset of the fall, indicating that the muscles were appropriately responding to the stance, double support, and swing phases of the gait cycle and are in line with the expected coordination during these phases. Additionally, it was observed that even during the fall, the coordination between antagonistic muscles was maintained. This suggests that the model maintains the appropriate coordination between muscles despite the occurrence of unexpected events. Furthermore, it is noteworthy that the muscle stimulations are calculated based on the dynamics and history of the movement to account for the time delay in sensory feedback and therefore do not instantaneously respond to sudden changes such as a fall.
Based on these observations, it can be concluded that the calculation of the muscle stimulations is not responsible for the model's fall and that other factors, such as the ground reaction forces, may be contributing to it.

6.4 External Environment: Ground Contact Model

Because of the transitions between stance and swing phase and vice-versa and the reflexes based on ground contact, the dynamic interaction of the model with its environment is a crucial element. This section presents the results obtained for the forces arising from the interaction between the model and its environment.
The chapter is organized as follows: the vertical and horizontal forces have been separated. For each of the two components, first the general pattern will be analyzed and compared to the results obtained by Geyer with filtered signals. Then, the specific characteristics of unfiltered signals will be explained.

6.4.1 Vertical Ground Contact Forces

The ground reaction forces presented in Figure 6.16 are obtained by adding the heel and ball GRF and normalizing them by the body weight.

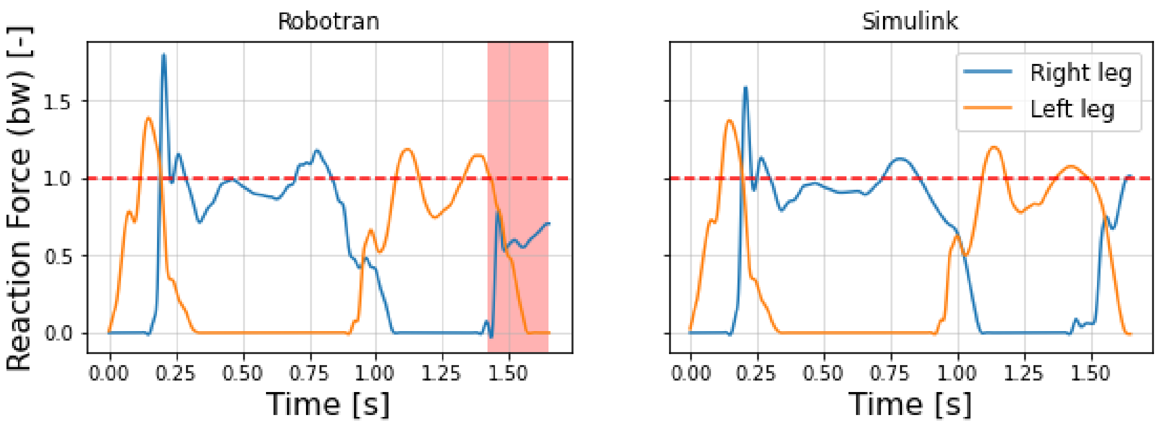

Figure 6.16: Vertical reaction force. Signals have been low pass filtered with a cut-off frequency of 30 Hz and normalized to the model's body weight. (Both graphs have the same scale)

One can observe in Figure 6.16 the specific characteristics of a gait cycle [80].

First during the double stance phase, the body weight is transferred from one leg to the other. For instance, in the second double stance phase between 0.93 and 1.1 s, the reaction force of the right leg decreases until it reaches 0 while during the same period of time, the reaction force of the left leg increases and reaches a first peak. This peak marks the end of the double stance phase and the left leg starts to bear the full body weight.
Secondly, during the stance phase the double bump corresponds to the weight shifting from the back to the front of the foot. As the foot rolls out on the ground, more weight is borne on the front of the foot until the heel lifts off, and the ball of the foot supports all the weight. The force amplitudes during these bumps are expected to exceed body weight, while the minima in between them corresponds to values below body weight, as commonly observed in a gait cycle.

The maximum and minimum values of the contact force are different in the Robotran model compared to Simulink. These variations can be attributed to differences in the kinematics of the model, including divergences in mass repartition, foot position, and velocity, which are significant factors for GRF.

6.4.1.1 Right Leg Vertical Reaction Force

Similar to the non-actuated two-legged model discussed in Section 5.3.2, the initial position and kinematics leading to the first contact of the right heel with the ground at 0.18 s result in a significant force peak upon impact, approximately four times the weight of the model as shown in 6.17. This initial peak creates instability before the force stabilizes.

While the overall shape of the force graph corresponds to the theoretical results, notable oscillations are observed towards the end of the stance phase around 1s. These oscillations primarily occur at the level of the ball of the foot. They occur when the entire weight is concentrated on a single point of support, in this case, the ball of the right foot. When the foot makes contact with the ground again at 1.42 s and the load is redistributed between the two legs, the oscillations appear once again.

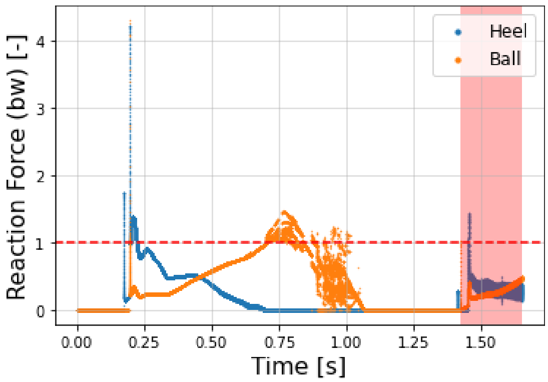

Figure 6.17: Right foot vertical GRFs.

Considering that the vertical reaction force is given by: $F_z = k_z \cdot (-d_z) \cdot (1 + \frac{v_z}{v_{max}})$, these oscillations can be attributed to the fluctuations in vertical position and velocity.

6.4.1.2 Left Leg Vertical Reaction Force

Similarly, to the right leg, the left leg vertical reaction force exhibits a similar oscillation phenomenon during the transition from heel to forefoot (ball) and during the entry of the opposite leg into stance. However, it is important to note that in the case of the left leg, which is initially in contact with the ground, in absence of a heel strike no oscillations are observed during its first stance phase, despite the transfer of body mass to the foot.

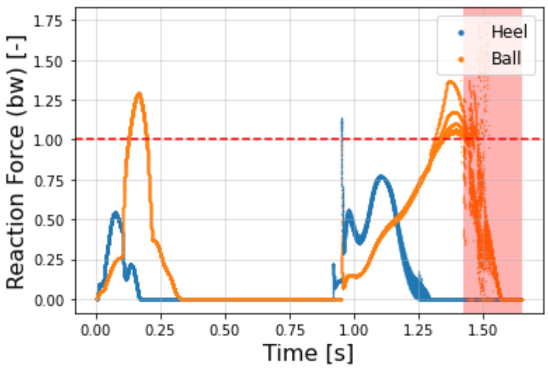

Figure 6.18: Left foot vertical GRFs.

Additionally, it is noteworthy that the oscillations observed in the forces of the forefoot also extend to the forces of the right heel. This indicates that the oscillatory behavior is not limited to a specific region of the foot but affects the entire foot-ground interaction.

Furthermore, it can be observed that the peak force associated with the left heel strike at 0.93 s is less pronounced compared to the right heel strike at 0.18 s. This suggests that the system tends to adopt a more stable configuration or, at least, one that is more resilient to impacts. This reduction in peak force may indicate an improved ability to absorb and distribute the forces generated during the foot-ground contact.

6.4.2 Horizontal Ground Contact Forces

In contrast to the vertical force, the calculation of friction forces is less conclusive, as depicted in Figure 6.19. While the general pattern of force appearance seems to be maintained, the magnitude of the forces is significantly different. Initially, the forces are relatively weak and coordinated, albeit deviating from the theoretical expectations. However, as the simulation progresses, the force values dramatically increase, accompanied by intensified oscillatory behavior.

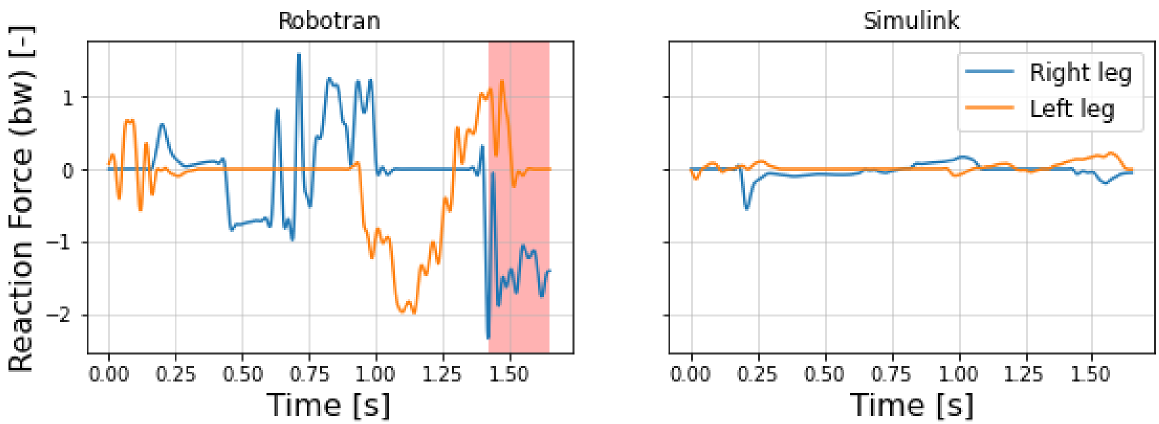

Figure 6.19: Horizontal reaction force. Signals have been low pass filtered with a cut-off frequency of 30 Hz and normalized to the model's body weight. (Both graphs have the same scale)

6.4.2.1 Right Leg Horizontal Reaction Force

The Figure 6.20 illustrates the horizontal force for the right leg. Two outliers are observed at 1.42 s, corresponding to the heel and ball strikes. These outliers have been removed in Figure 6.21 to enhance the clarity of the graph. Notably, the graph shows the oscillatory nature of the force, with fluctuations occurring between negative and positive values.

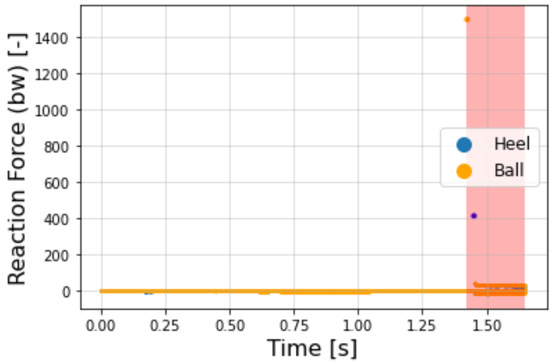

Figure 6.20: Right foot horizontal GRFs with outliers.

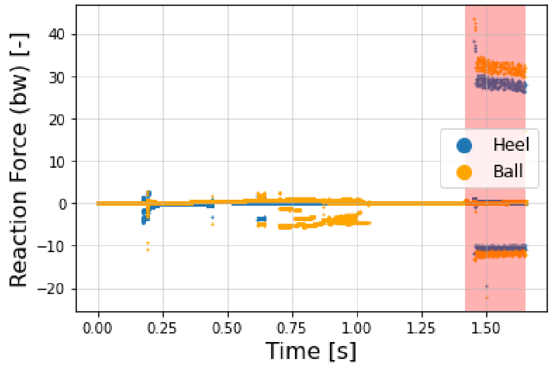

Figure 6.21: Right foot horizontal GRFs without outliers.

The horizontal reaction force, which represents the frictional forces between the ground and the foot, is modeled as $F_{x_{st}} = -k_x \cdot \Delta x \cdot (1 + sgn(\Delta x) \cdot \frac{v_x}{v_{max}}))$ for the static dry friction and as $F_{x_{dyn}} = sgn(v_x) \cdot \mu_{sl} \cdot F_z$ for the dynamic dry friction (see section 4.3). The oscillation phenomenon can therefore, be attributed to three key factors: the foot position, foot speed, and normal force. As discussed in the previous section 6.4.1, it has been demonstrated that even the normal force undergoes oscillations. Therefore, the underlying factor contributing to the oscillation phenomenon is the alteration in the horizontal and vertical velocities of the feet, especially their sign, leading to oscillatory movements in their positions, resembling tremors.

6.4.2.2 Left Leg Horizontal Reaction Force

For the left leg, the same phenomenon can be observed as for the right leg. Once again, outliers are observed when the contact points reach the ground at 0.93 s. However, these outliers are limited to specific moments (0s and 0.9s), and the force values quickly return to a "normal" range afterward. The force oscillates between positive and negative values, and the magnitude of the oscillations has increased compared to the one observed for the right leg horizontal forces, although it appears to remain relatively constant throughout this phase.

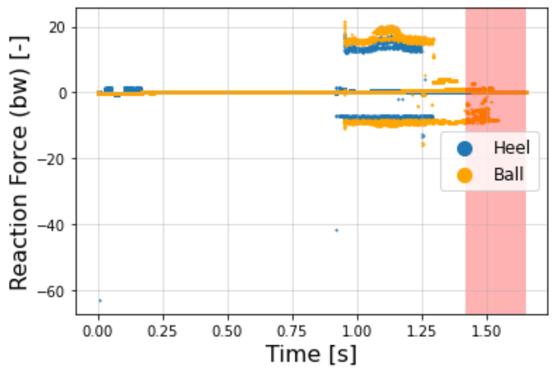

Figure 6.22: Left foot horizontal GRFs.

6.4.3 Conclusion

As observed in the previous sections, the reflex-based control laws of Geyer's model effectively compensate for differences in vertical contact forces, ensuring that the overall kinematics of the system remain relatively stable.

However, it is important to note that the differences in reaction forces, particularly in the horizontal forces, can potentially lead to error accumulation and instability in the model. These differences, as seen in the oscillatory behavior and outliers, are likely due to the tremors of the feet. Eliminating these tremors may have a significant impact on the overall stability of the system and contribute to a fluid and periodic movement without compromising the stability of the model.

Chapter 7

Limitations and Future Perspectives

This chapter aims to present the limitations of the model developed in this thesis, which could be the root of the model's collapse after performing a conclusive gait cycle for the left leg. Several approaches are proposed to improve the model, as well as prospects for future work aimed at continuing this research.

7.1 Limitations and Potential Improvements

Due to the intricate interplay among the various layers of the model, singling out a specific and definitive cause for the model's collapse proves challenging. Three key limitations can be identified and described in the context of the study, namely the horizontal contact model, parameter optimization, and phase detection.

As explained in Chapter 6, the results obtained are conclusive and convincing for the neural control and muscle activation layers. In contrast, the results obtained for the ground contact model, especially for the horizontal friction forces, show significant differences which could be a limitation preventing the model from reproducing stable human walking. The first significant improvement would therefore be to improve the ground contact model in question by reducing its stiffness, to facilitate the integration of the dynamic equations (potential areas for enhancement are given in section 7.1.1).

In the current state of the model, it would be conceivable to allow a greater lifting amplitude for the model's leg, to avoid inappropriate contact with the ground. This could be achieved by optimizing the parameters used in the reflex laws (see section 7.1.2). Hence, although the implementation of suitable muscle stimulation may contribute to an increased number of complete gait cycles, it is important to acknowledge the persistent phenomenon of reduced swing foot height with each cycle. This phenomenon ultimately leads to the eventual collapse of the model after a certain number of cycles.

Another potential improvement could involve revising the phase detection conditions to accurately calculate muscle stimulations for the swing phase instead of the stance phase, even in situations where the foot rubs against the ground during the middle of the swing stroke (see section 7.1.3).

Optimization of the parameters would increase the number of successful walking cycles of the model. However, the complications associated with the contact model would persist. Therefore, a combination of contact model improvement, phase detection refinement, and parameter optimization would be the most optimal solution to obtain a robust and stable walking model.

7.1.1 External Environment: Ground Contact Model

As mentioned above, it is possible that the ground contact model, although the model has been verified theoretically as presented in appendixes E.1 and E.2, is the source of the collapse of the system due to the complexity of its interaction with the Robotran simulator caused by the stiffness of the contact model.

One solution to this limitation could be to reduce the stiffness of the contact model to facilitate the integration of the dynamic equations. To this end, several possibilities can be explored.

First, adjust the stiffness constants of the contact model to make it less stiff. Taking into account the formulas for calculating contact forces:

- $F_z = -k_z \cdot \Delta z \cdot (1 + \frac{v_z}{v_{max}})$
- $F_{x_{st}} = -k_x \cdot \Delta x \cdot (1 + sgn(\Delta x) \cdot \frac{v_x}{v_{max}}))$
- $F_{x_{dyn}} = sgn(v_x) \cdot \mu_{sl} \cdot F_z$

In the realm of vertical forces and static dry friction, stiffness constants play a crucial role. Modifying these constants has a direct impact on the system's response to applied forces. By decreasing these constants, the ground model becomes more deformable, resulting in reduced stiffness. However, excessively lowering these constants can cause the ground behavior to deviate from physical reality, taking on a sponge-like characteristic. Hence, it is imperative to strike a balance between physically consistent values and those that enable the creation of a less stiff model, facilitating the numerical integration of dynamic equations.

Secondly, the incorporation of a hyperbolic tangent function can lead to a less stiff behavior. This is accomplished by constraining the tangential force to a specific maximum threshold. Similar to the reduction in stiffness constants, the inclusion of a hyperbolic tangent function would also decrease the stiffness of the contact model. In his thesis [9], Nicolas Vandernoot calculated the tangential forces using the following approach:

$$F_x = \mu_{max} \cdot F_z \cdot tanh(\beta \cdot v) \tag{7.1}$$

Where μ_{max} is the maximal value for the friction coefficient, β is the inner factor of the hyperbolic tangent $[-]$ and v is the norm of the relative tangential speed between the foot and the ground at the contact point $[m/s]$.

It is worth noting that the specific value of β needs to be carefully chosen to achieve the desired saturation effect. The graph 7.1 illustrates the relationship between β and the behavior of the hyperbolic tangent function. The $tanh(x)$ function has a range of values from -1 to 1. When x is small, close to zero, the $tanh(x)$ function approximates x itself. However, as x increases, $tanh(x)$ tends towards $+/-1$. The function exhibits a "S"-shaped curve and is symmetric around the origin.

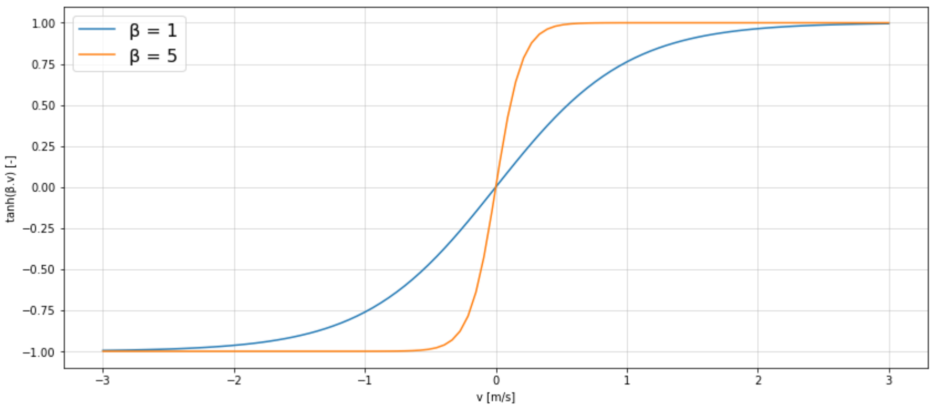

Figure 7.1: Hyperbolic tangent. Impact of the inner factor.

7.1.2 Optimization of Stimulation Parameters

The optimization of parameters used in reflex-based control laws, including gains and length offsets (refer to section 4.2), plays a crucial role in achieving specific characteristics in model simulations. This optimization process can be approached in two ways. The first approach involves a manual method using trial-and-error, where one or two parameters are modified per trial to attain the desired behavior. The second approach employs computational techniques such as Particle Swarm Optimization (PSO) or Covariance Matrix Matching Strategy (CMA-ES). These techniques enable the optimization of all model parameters by maximizing an objective function.

In the manual optimization case, the objective is to improve leg flexion during the swing phase by optimizing the stimulation parameters of the hip and knee flexor muscles (i.e., HFL, HAM, and GAS). An improvement in leg flexion would allow more complete gait cycles, minimizing ground grazing during the middle of the swing stroke compared to the current model. By implementing this, the model would be capable of performing a greater number of cycles compared to its current state.
Conducting a parameter sensitivity analysis beforehand would be optimal in identifying the parameters that have a significant impact on leg flexion and step height. A similar study [81] was conducted on Nicolas Vandernoot's Coman robot model [9], which incorporates additional muscles and a CPG (Central Pattern Generator) model. However, due to these additional components, the findings of that study are not directly applicable to the model presented here.

In the case of set of parameters optimization using computational methods such as PSO and CMA-ES, it is possible to use a fitness function based on successive steps. Each stage can only be unlocked if the expected performance has been achieved in the previous stage. In the case of this thesis, to avoid the collapse of the system due to premature contact with the ground in the swing phase, the objective function could consist in optimizing the length and the height of the step. Similar work has already been done in [81]. A schematic diagram illustrating the consecutive steps is depicted in Figure 7.2, outlining the process as follows:

- The first stage involves determining the minimum distance that the model needs to cover.
- The second stage corresponds to a walking time condition, ensuring that the model operates for a specific duration.
- The third and fourth stages are performed simultaneously and enable the model to perform steps of specific size and length.

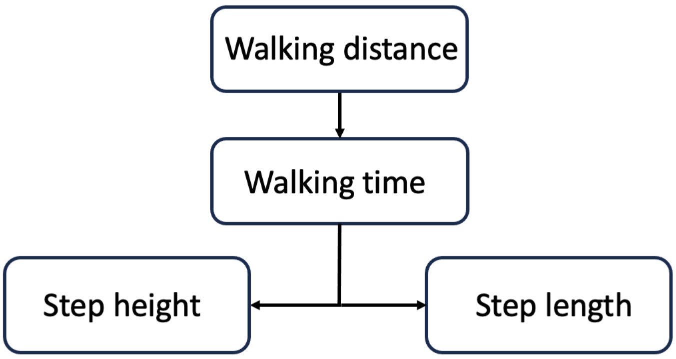

Figure 7.2: Stages of the fitness functions. Figure inspired by [81]

7.1.3 Phase Detection Conditions

In the current state of the model, the detection of stance and swing phases relies on observing whether the heel or ball of the foot is positioned below ground level (stance phase) or above ground level (swing phase). To enhance the detection of these phases and prevent interruptions in the swing phase when the foot brushes the ground, additional detection conditions can be incorporated.

These phase detection conditions could take various forms, such as minimum time requirements for each phase, specific joint angle thresholds during the transition between phases, and/or ground reaction force conditions applied to the foot. These detection conditions can be applied to various situations, taking into consideration that certain data may be more readily available than others. By adapting the detection conditions to different scenarios, researchers can overcome limitations in data collection and leverage

the available information.
A combination of these conditions can further enhance the robustness and stability of the walking model. This combination approach has been used for example in Nicolas Vandernoot's controller, as elaborated by Bruno Somers in his thesis [77].

7.2 Future Perspectives

The following section is a gateway to envision and explore the future endeavors that could extend from this thesis. These forthcoming works hold the promise of unlocking profound understanding, fueling advancements in fields ranging from rehabilitation to robotics.

Three years after his initial work, which served as inspiration for the model presented in this thesis, Hartmut Geyer has developed a 3D generalization of his 2D initial model [23]. This generalization enables the study and comparison of neural controls for three-dimensional movements. Consequently, it would be interesting to apply the same generalization to our Robotran model.
This generalization entails incorporating additional degrees of freedom at the hip joint in the frontal plane, activating these degrees of freedom, and controlling them using adductor and abductor muscles of the hip. Additionally, the contact model would undergo modifications to account for three-dimensional compliant ground contact dynamics.

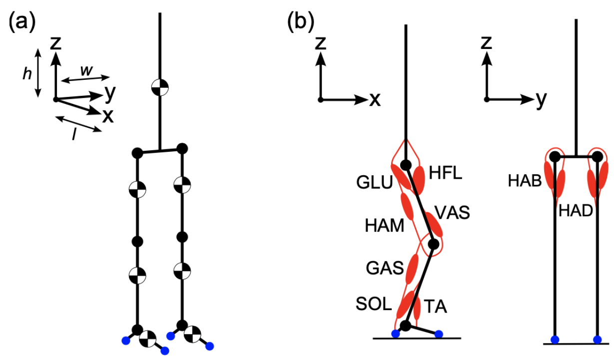

Figure 7.3: Human musculoskeletal model of the 3D generalization of the Geyer's model. (a) Model of 8 DOF composed of 7 segments. (b) Representation of the 9 muscles attached to each leg.

Another potential avenue for improvement involves utilizing a more accurate foot model and applying the contact model to a mesh composed of a higher density of points on the foot. By doing so, it would be possible to obtain a more precise and realistic representation of foot-ground interaction. This enhanced level of detail could provide valuable insights into the mechanics and dynamics of walking, ultimately contributing to the development of more accurate and effective locomotion assistance methods (see Nicolas Vandernoot thesis [9]).

Once the model is complete, stable, and robust, it can serve as a valuable tool for testing and developing assistance methods and strategies. Several potential applications can be explored.
First, rehabilitation devices can be assessed by incorporating a Robotran model of the specific device (e.g., replacing a leg with a prosthetic model) to evaluate their optimality and ability to achieve desired performance and behavior.
Secondly, existing assistive strategies, including high-level and mid-level controller strategies, can be tested within the model. For instance, it is possible to analyze whether the model can replicate the effects of assistance observed in studies such as those investigating oscillation-based assistance [53] or the influence of power delivery timing for hip exoskeletons [26].
Finally, the model can be used to evaluate the impact of novel gait or balance assistance strategies. Subsequently, the obtained results could be experimentally validated using the orthoses available at UCLouvain. This iterative process of testing and experimental verification can provide valuable insights and enhance the development of effective assistance strategies.

Another potential improvement could involve incorporating a central pattern generator model into the existing system. The concept of CPG modeling has been explored in Chapter 2, discussing various approaches and methodologies. By integrating a CPG model, the system can generate rhythmic patterns and control the timing and coordination of leg movements. This can result in more natural and flexible locomotion, enabling the model to adjust its speed and gait pattern according to different conditions and tasks. The addition of speed modulation capabilities to the model, enabling more dynamic and adaptable locomotion, would be a significant enhancement to this Robotran model. Currently, the model operates at a fixed speed determined through parameter optimization.

Chapter 8

Conclusion

This master thesis aimed to replicate and adapt Hartmut Geyer's well-established model of human walking [2] using the multibody simulation environment Robotran. Robotran was developed at UCLouvain [4] with the goal to provide the basis of an accessible tool for developing and conducting virtual tests for new methods of locomotion assistance and control laws.

The results of this project have been highly significant. The Robotran model successfully captures the essential aspects of human walking kinematics. It effectively simulates the coordinated muscular contractions among the different muscle groups, allowing for an accurate reproduction of the stance and swing phases of the gait and the smooth transition between them. It accurately models the flexion of the foot resulting from the heel strike against the ground, as well as the mass transfer between the two legs accordingly to their respective phase and from the heel to the forefoot during the stance phase.

The methodology employed in this thesis was a bottom-up process. First, a comprehensive background of Geyer's model is provided. From this theoretical overview, three points can be highlighted: human walking is complex and requires precision and fine-tuning to execute coordinated movements; interactions between the body and the environment are crucial in walking; Geyer's original article, while providing valuable insights into the control and coordination of human walking, lacks precision in terms of parameter values and clarity regarding some underlying mechanisms of the model.

The next step in this study is the validation of the implementation choices. To maintain a scientific reproduction approach, results obtained using Robotran were compared with the results obtained by Geyer and his Simulink simulation. Rarticular attention was given to the ground contact model. Initially, the contact model was tested on a single non-actuated leg before being extended to a two-legged non-actuated model. While the kinematic aspects of the simulation were correct, some discrepancies in the interactions of the feet and the ground were observed, raising concerns about their impact on the overall model.

Once the complete model was built, the results obtained for the kinematics, muscle actuation, and neural control layers provide conclusive evidence of the model's capabilities. However, after one successful walking cycle for each leg, the model experienced a collapse at approximately 1.42 seconds of simulation time although it demonstrates encouraging results. After investigation, the concerns raised regarding the contact model proved to be justified. The latter emerged as one of the predominant limiting factors in the simulation. In addition, it was observed that with each successive step, the foot grazed closer and closer to the ground during the swing phases, eventually making premature contact before the intended time.

To address these issues and increase the ability of the model to accurately replicate human walking dynamics for a longer period, a combination of three solutions is proposed. First, refining the model of frictional forces between the feet and the ground by eventually reducing the stiffness constants and constraining the forces using a hyperbolic tangent function as threshold. Then, optimizing the parameters of the reflex-based control laws to force the feet to be elevated higher off the ground during the swing phases. Finally, phase detection conditions of various forms, such as specific joint angles thresholds or ground reaction forces, could be added to prevent unforeseen gait events to be detected.

In conclusion, while acknowledging that the current model may not yet be fully stable over a long period of time, this master thesis has achieved its initial objectives. Geyer's walking model has successfully been implemented using Robotran and demonstrates encouraging results. Furthermore, the first two steps could be sufficient to test, for instance, the influence of power delivery timing for hip exoskeletons or the effect of joint angle limitations on the walking kinematic. In the future, further improvements and additional features can be added to the model such as its extension to the three-dimensional world or incorporating a central pattern generator to modulate the walking speed.

In a nutshell, this document sets a solid foundation for the future project of simulating human walking to virtually develop and test new methods for locomotion assistance.

Appendix A

Body Mechanics Characterization

The model's segment are rigid bodies specified by their mass (m_s), inertia (Θ_s), lengths (l_s), position of the local center of mass ($d_{G,s}$), position of the proximal joint measured from the distal end ($d_{J,s}$).

	Feet	Shanks	Thighs	Trunk
l_s	20	50	50	80
$d_{G,s}$	14	30	30	35
$d_{J,s}$	16	50	50	-
m_s	1.25	3.5	8.5	53.5
Θ_s	0.005	0.05	0.15	3

Table A.1: Segment parameters. Values from [2]

Appendix B

Hill Muscles Characterization

B.1 Useful Parameters for Muscle Characterization

B.1.1 Individual MTC Parameters

	VAS	SOL	GAS	TA	HAM	GLU	HFL
F_{max} $[N]$	6000	4000	1500	800	3000	1500	2000
v_{max} $[lopt/s]$	12	6	12	12	12	12	12
l_{opt} $[cm]$	0.08	0.04	0.05	0.06	0.1	0.11	0.11
l_{slack} $[cm]$	0.23	0.26	0.4	0.24	0.31	0.13	0.10

Table B.1: Individual MTC parameters for leg muscles. Values from [2]

B.1.2 MTC Attachment Parameters

	Ankle			Knee			Hip		
	TA	SOL	GAS	GAS	VAS	HAM	HAM	GLU	HFL
$r0$ $[cm]$	0.04	0.05	0.05	0.05	0.06	0.05	0.08	0.1	0.1
ϕ_{max} $[deg]$	80	110	110	140	165	180	-	-	-
ϕ_{ref} $[deg]$	80	110	80	165	125	180	155	150	180
ρ	0.5	0.7	0.7	0.7	0.7	0.7	0.7	0.5	0.5

Table B.2: MTC Attachment parameters. Values from [2]

B.2 Force-length and Force-velocity Relationships of an MTC

The force-length relationship $f_l(l_{ce})$ and force-velocity relationship $f_v(v_{ce})$ can be expressed as follows (adapted from [15]):

$$f_l(l_{ce}) = exp\left(c \cdot \left|\frac{l_{ce} - l_{opt}}{l_{opt}w}\right|^3\right) \tag{B.1}$$

Where $w = 0.56$ represent the width of the $f_l(l_{ce})$ curve, and $c = ln(0.05)$ is such as $f_l(l_{opt}(1 \pm w)) = 0.05$.

$$f_v(v_{ce}) = \begin{cases} \frac{v_{max} - v_{ce}}{v_{max} + K \cdot v_{ce}} & \text{if } v_{ce} < 0 \\ \\ N(N+1) \cdot \frac{v_{max} + v_{ce}}{7.56 K v_{ce} - v_{max}} & \text{if } v_{ce} \geq 0 \end{cases} \tag{B.2}$$

Where $K = 5$ is a curve constant, $N = 1.5$ is the amount of force F_{MTC}/F_{max} obtained at a velocity $v_{ce} = -v_{max}$, and the maximum contraction velocity $v_{max} = -12$ $[l_{opt}s^{-1}]$.

Appendix C

Neural Control Characterization

C.1 Synthesis of Stimulations

C.1.1 Laws of Control based on Reflexes

STANCE	
SOL	$S_{SOL} = S^{St}_{SOL,0} + G_{SOL,n} \cdot F_{SOL}(t - \Delta t_l)$
TA	$S_{TA} = S^{St}_{TA,0} + [G_{TA,n} \cdot (l^{ce}_{TA}(t - \Delta t_l) - l_{off,TA})] - G_{SOLTA,n} \cdot F_{SOL}(t - \Delta t_l)$
GAS	$S_{GAS} = S^{St}_{GAS,0} + G_{GAS,n} \cdot F_{GAS}(t - \Delta t_l)$
VAS	$S_{VAS} = S^{St}_{VAS,0} + G_{VAS,n} \cdot F_{VAS}(t - \Delta t_m) - K_{VAS} \cdot (\theta_{knee}(t - \Delta t_m) - 170°) - k_{bw} \cdot \lvert F^{contra}_{leg}(t - \Delta t_s)\rvert$
HAM	$S_{HAM} = S^{St}_{HAM,0} + [K_{HAM} \cdot (\theta(t - \Delta t_s) - \theta_{ref}) + D_{HAM} \cdot \dot{\theta}(t - \Delta t_s)] + k_{bw} \cdot \lvert F^{ipsi}_{leg}(t - \Delta t_s)\rvert$
GLU	$S_{GLU} = S^{St}_{GLU,0} + [K_{GLU} \cdot (\theta(t - \Delta t_s) - \theta_{ref}) + D_{GLU} \cdot \dot{\theta}(t - \Delta t_s)] + k_{bw} \cdot \lvert F^{ipsi}_{leg}(t - \Delta t_s)\rvert - \Delta S$
HFL	$S_{HFL} = S^{St}_{HFL,0} - [K_{HFL} \cdot (\theta(t - \Delta t_s) - \theta_{ref}) + D_{HFL} \cdot \dot{\theta}(t - \Delta t_s)] - k_{bw} \cdot \lvert F^{ipsi}_{leg}(t - \Delta t_s)\rvert + \Delta S$
SWING	
SOL	$S_{SOL} = S^{Sw}_{SOL,0}$
TA	$S_{TA} = S^{Sw}_{TA,0} + [G_{TA,n} \cdot (l^{ce}_{TA}(t - \Delta t_l) - l_{off,TA})]$
GAS	$S_{GAS} = S^{Sw}_{GAS,0}$
VAS	$S_{VAS} = S^{Sw}_{VAS,0}$
HAM	$S_{HAM} = S^{Sw}_{HAM,0} + G_{HAM,n} \cdot F_{HAM}(t - \Delta t_s)$
GLU	$S_{GLU} = S^{Sw}_{GLU,0} + G_{GLU,n} \cdot F_{GLU}(t - \Delta t_s)$
HFL	$S_{HFL} = S^{Sw}_{HFL,0} + [G_{HFL,n} \cdot (l^{ce}_{HFL}(t - \Delta t_s) - l_{off,HFL})] + k_{lean} \cdot (\theta - \theta_{ref})_{TO}$ $-[G_{HAMHFL,n} \cdot (l^{ce}_{HAM}(t - \Delta t_s) - l_{off,HAM})]$

Table C.1: Summary table of the stimulations according to the phase. Red parts correspond to double support. θ correspond to the trunk pitch.

C.1.2 Reflex Parameters

The parameters listed in the table below are the parameters that govern the operation of muscle reflexes. The optimization of these parameters is crucial to achieve the desired gait behavior. Please refer to Chapter 7 for further details.

Pre-stimulations		**Gain and offsets**		**Parameters**		**Delays**	
S^{st}_{SOl}	0.01	$G_{SOL,n}$	$3e-4$	K_{VAS}	2	Δt_l $[ms]$	20
S^{st}_{TA}	0.01	$G_{TA,n}$	1.1	K_{HAM}	1.91	Δt_m $[ms]$	10
S^{st}_{GAS}	0.01	$G_{SOLTA,n}$	$1e-4$	D_{HAM}	0.2	Δt_s $[ms]$	5
S^{st}_{VAS}	0.08	$G_{GAS,n}$	$7.333e-4$	K_{GLU}	1.91		
S^{st}_{HAM}	0.05	$G_{VAS,n}$	$2e-4$	D_{GLU}	0.2		
S^{st}_{GLU}	0.05	$G_{HAM,n}$	$2.17e-4$	K_{HFL}	1.91		
S^{st}_{HFL}	0.05	$G_{GLU,n}$	$3.33e-4$	D_{HFL}	0.2		
S^{sw}_{SOL}	0.01	$G_{HFL,n}$	0.5	k_{bw}	1.2		
S^{sw}_{TA}	0.01	$G_{HAMHFL,n}$	4	k_{lean}	1.146		
S^{sw}_{GAS}	0.01	$l_{off,TA}$	0.72	ΔS	0.25		
S^{sw}_{VAS}	0	$l_{off,HFL}$	0.65	θ_{ref}	0.105		
S^{sw}_{HAM}	0.01	$l_{off,HAM}$	0.85				
S^{sw}_{GLU}	0.01						
S^{sw}_{HFL}	0.01						

Table C.2: Reflexes parameter. The gains (G_m) are normalized to the maximum isometric force F^{max}_m of the muscle and the offsets are normalized to the optimal length of the contractile element l^{opt}_m. Values taken from the Geyer's Simulink model, based on [2].

C.2 Representation of Muscle Activity during a Gait Cycle

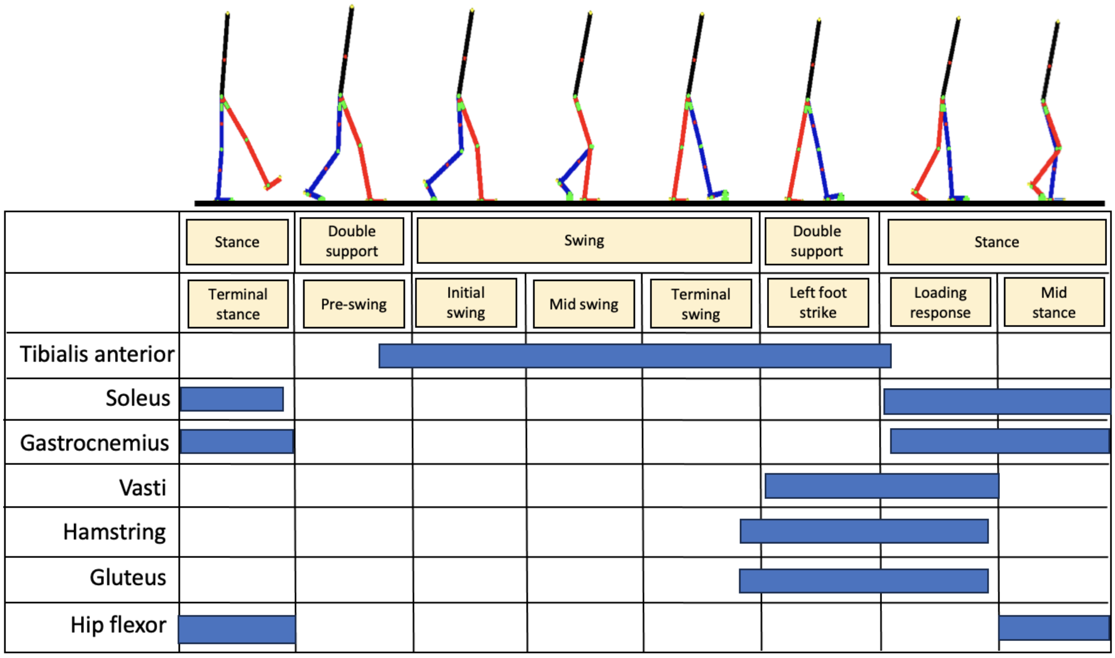

Figure C.1: Representation of muscle activity during a gait cycle. The blue color indicates periods where the muscles are active during the gait cycle. Figure inspired from [80].

Appendix D

Stimulations Results

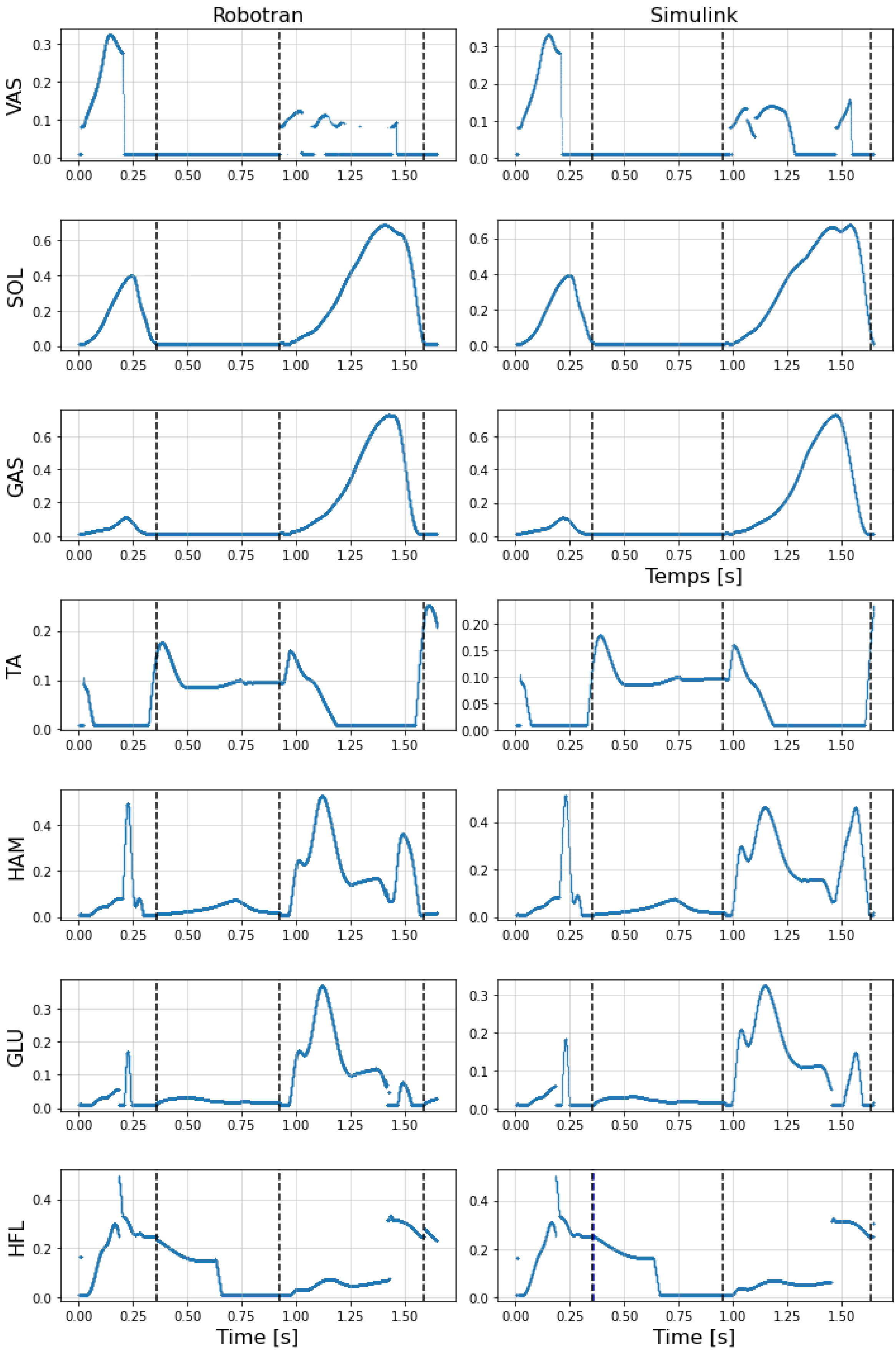

Figure D.1: Left leg muscle stimulations. The black dashed lines represent the change of gait phase.

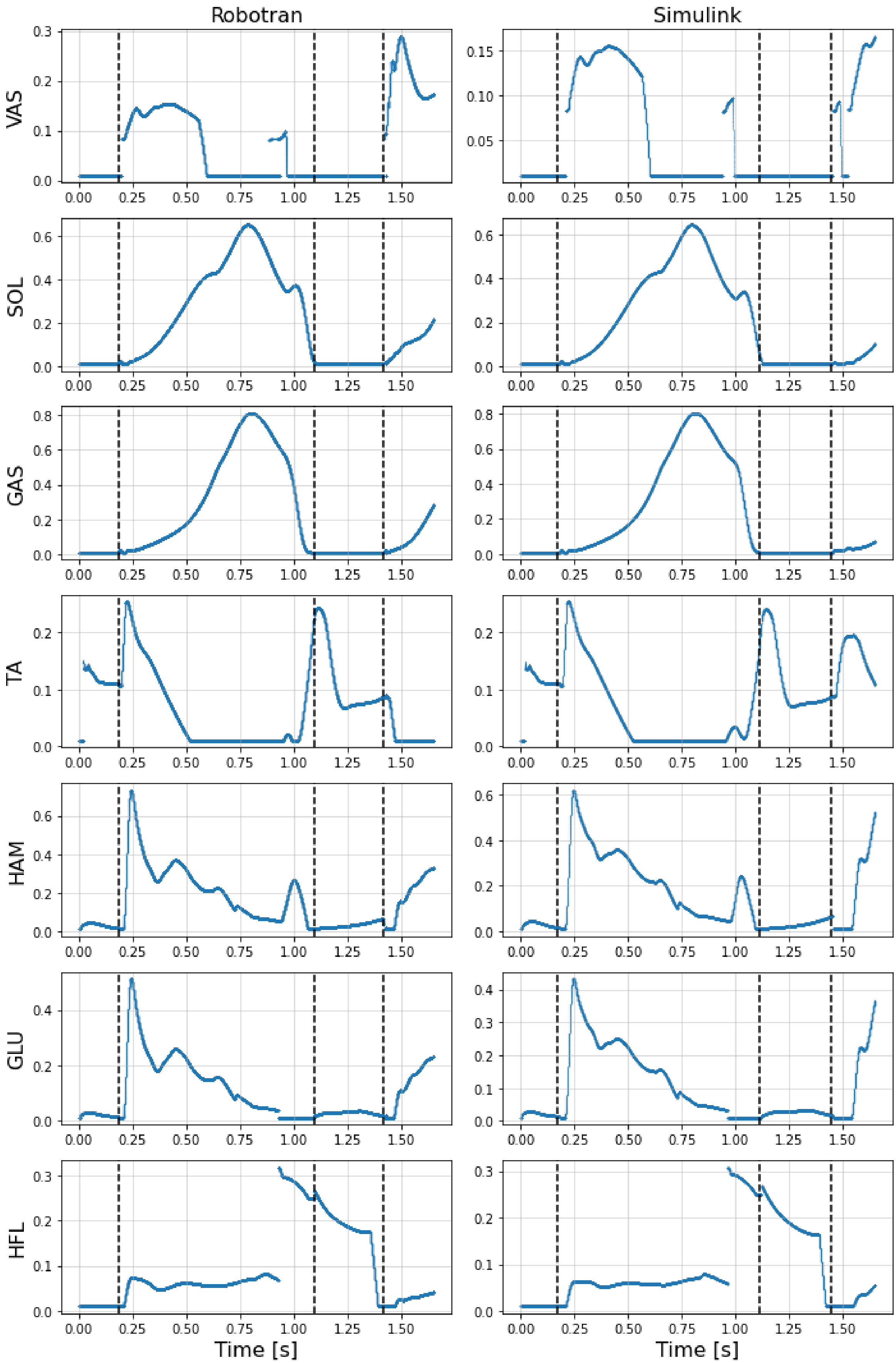

Figure D.2: Right leg muscle stimulations. The black dashed lines represent the change of gait phase.

Appendix E

Ground Contact Model Results

In order to justify that the differences in the forces obtained by the contact model do not come from an error in the implementation of the model, the results presented in this appendix were obtained through testing the implemented model independently, without direct interaction with the Robotran model. Inputs were exported from Simulink, and the outputs obtained from our implementation of the contact model were compared with the outputs of the contact model implemented by Geyer in Simulink.

E.1 One-leg Unactuated Model

The results presented in this section correspond to GRF of the ball point of the foot from the position and velocity signals exported from a system with a single non-actuated leg in Simulink.

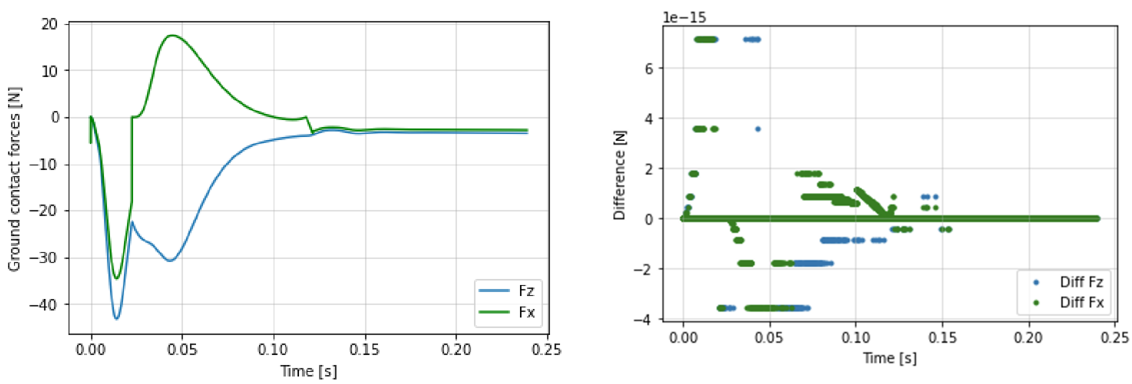

(a) Ground contact forces obtained with the implemented model when no interaction with Robotran

(b) Differences between ground contact forces from the implemented model and from Simulink

The difference obtained is about $7e - 15$ which corresponds to a difference in rounding management between Simulink and Robotran. The implemented ground contact force model is therefore theoretically validated.

E.2 Two-leg unactuated model

The results presented in this section correspond to GRF of the heel point of left foot from the position and velocity signals exported from a system with two non-actuated leg in Simulink.

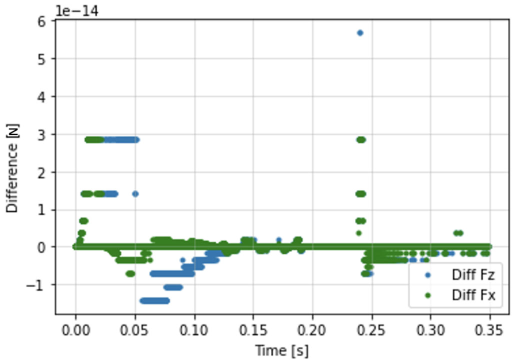

(a) Ground contact forces obtained with the implemented model when no interaction with Robotran

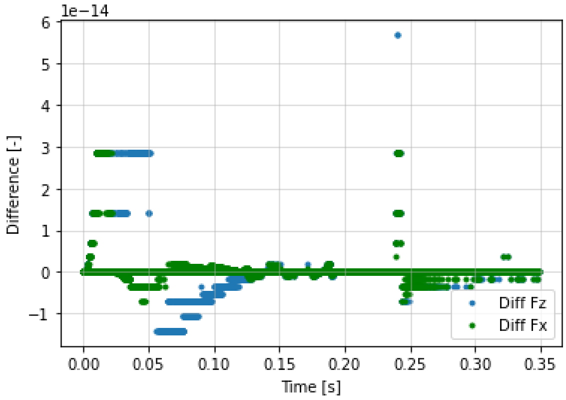

(b) Differences between ground contact forces from the implemented model and from Simulink

The difference obtained is about $6e-14$ which corresponds to a difference in rounding management between Simulink and Robotran. The implemented ground contact force model is therefore theoretically validated.

The following graphs represent results for ball contact points of both feet:

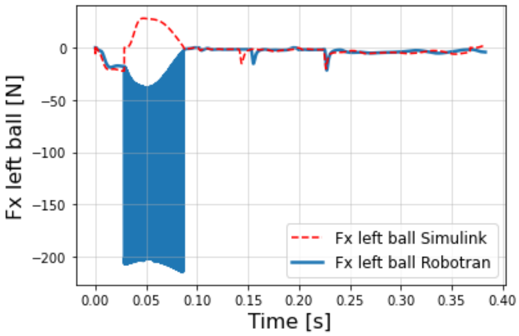

Figure E.3: F_x Left ball

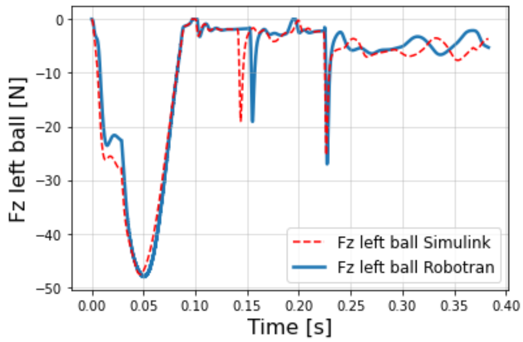

Figure E.4: F_z Left ball

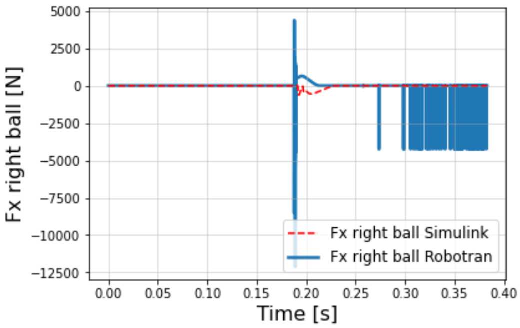

Figure E.5: F_x Right ball

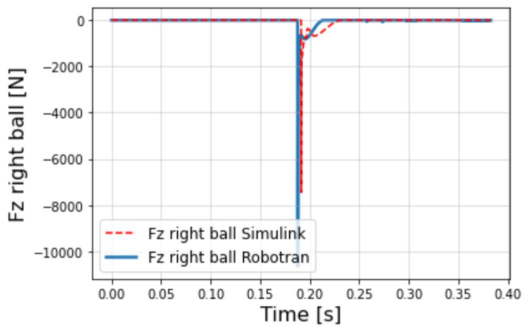

Figure E.6: F_z Right ball

Bibliography

1. *Ageing Europe - statistics on population developments* `https://ec.europa.eu/eurostat/statistics-explained/index.php?title=Ageing_Europe_-_statistics_on_population_developments#Older_people_.E2.80.94_increasingly_old_and_with_growing_dependency` (2023).
2. Geyer, H. & Herr, H. A Muscle-Reflex Model That Encodes Principles of Legged Mechanics Produces Human Walking Dynamics and Muscle Activities. *IEEE Transactions on Neural Systems and Rehabilitation Engineering* **18,** 263–273 (2010).
3. Geyer, H. *Hartmut Geyer's Website* `https://www.cs.cmu.edu/~hgeyer/index.html`. 2015.
4. iMMC, U. .-. *Robotran Website* `https://www.robotran.be`. 2020.
5. Aussems, M. & Dineur, N. *Github repository of the code used in this thesis* `https://github.com/Matthieu2209/Simulating-human-walking-to-virtually-devellop-and-test-new-methods-of-assistanc`. 2023.
6. Gorney, M. *How to Increase Exercise Difficulty | Move Through 3-Planes of Motion* Brain Meets Brawn. `https://www.bmbfitnesssolutions.com/post/how-to-increase-exercise-difficulty-move-through-three-planes-of-motion` (2023).
7. Kharb, A., Saini, V., Jain, Y. & Dhiman, S. A review of gait cycle and its parameters. *IJCEM International Journal of Computational Engineering & Management* **13,** 78–83 (2011).
8. Adelaar, R. S. The practical biomechanics of running. *The American journal of sports medicine* **14,** 497–500 (1986).
9. Van der Noot, N. Rich and robust bio-inspired locomotion control for humanoid robots (2017).
10. Geyer, H., Seyfarth, A. & Blickhan, R. Compliant leg behaviour explains basic dynamics of walking and running. English. *Proceedings of the Royal Society. B, Biological sciences* **273,** 2861–2867 (2006).
11. Martin, W. C., Wu, A. & Geyer, H. *Robust spring mass model running for a physical bipedal robot* in *2015 IEEE International Conference on Robotics and Automation (ICRA)* (2015), 6307–6312.
12. Seyfarth, A., Günther, M. & Blickhan, R. Stable operation of an elastic three-segment leg. *Biological cybernetics* **84,** 365–82 (June 2001).

13. Oconnor, S. & Kuo, A. Direction-Dependent Control of Balance During Walking and Standing. *Journal of neurophysiology* **102,** 1411–9 (July 2009).

14. Silva, M. & Ambrósio, J. Kinematic Data Consistency in the Inverse Dynamic Analysis of Biomechanical Systems. *Multibody System Dynamics* **8,** 219–239 (Aug. 2002).

15. Geyer, H., Seyfarth, A. & Blickhan, R. Positive force feedback in bouncing gaits? *Proc Biol Sci.* **270,** 2173–2183 (2003).

16. Hill, A. V. The Heat of Shortening and the Dynamic Constants of Muscle. *Proceedings of the Royal Society of London. Series B, Biological Sciences* **126,** 136–195. ISSN: 00804649. `http://www.jstor.org/stable/82135` (2023) (1938).

17. G. Taga, Y. Y. H. S. Self-organized control of bipedal locomotion by neural oscillators in unpredictable environment. *Biological Cybernetics* **65,** 147–159 (1991).

18. HASE, K. & OBINATA, G. Computer Simulation Study of Human Locomotion with a Three-Dimensional Entire-Body Neuro-Musculo-Skeletal Model. *JSME International Journal Series C Mechanical Systems, Machine Elements and Manufacturing* **45,** 1051–1057 (2002).

19. Farley, C. T. & González, O. Leg stiffness and stride frequency in human running. *Journal of Biomechanics* **29,** 181–186. ISSN: 0021-9290. `https://www.sciencedirect.com/science/article/pii/0021929095000291` (1996).

20. Ackermann, M. & van den Bogert, A. J. Optimality principles for model-based prediction of human gait. *Journal of Biomechanics* **43,** 1055–1060. ISSN: 0021-9290. `https://www.sciencedirect.com/science/article/pii/S0021929009007210` (2010).

21. Scott, S. H. & Winter, D. A. Biomechanical model of the human foot: Kinematics and kinetics during the stance phase of walking. *Journal of Biomechanics* **26,** 1091–1104. ISSN: 0021-9290. `https://www.sciencedirect.com/science/article/pii/S0021929005800089` (1993).

22. Van Hulle, R. *et al.* A foot/ground contact model for biomechanical inverse dynamics analysis. *Journal of Biomechanics* **100,** 109412. ISSN: 0021-9290. `https://www.sciencedirect.com/science/article/pii/S0021929019306591` (2020).

23. Song, S. & Geyer, H. *Generalization of a muscle-reflex control model to 3D walking* in *2013 35th Annual International Conference of the IEEE Engineering in Medicine and Biology Society (EMBC)* (2013), 7463–7466.

24. Rajagopal, A. *et al.* Full-Body Musculoskeletal Model for Muscle-Driven Simulation of Human Gait. *IEEE Transactions on Biomedical Engineering* **63,** 2068–2079 (2016).

25. *Opensim's site* `https://simtk.org`.

26. Young, A. J., Foss, J., Gannon, H. & Ferris, D. P. Influence of Power Delivery Timing on the Energetics and Biomechanics of Humans Wearing a Hip Exoskeleton. English. *Frontiers in bioengineering and biotechnology* **5,** 4–4 (2017).

27. Asif, M. *et al.* Advancements, Trends and Future Prospects of Lower Limb Prosthesis. *IEEE Access* **9,** 85956–85977 (2021).
28. Gastaldi, L. *Active orthosis for rehabilitation and passive exercise* in (June 1997).
29. Newman, D. *1.7M to build everyday exoskeletons to assist with lifting, walking and climbing stairs* `https://news.engin.umich.edu/2021/10/1-7m-to-build-everyday-exoskeletons-to-assist-with-lifting-walking-and-climbing-stairs/`. 2021.
30. *Lower Limb Prosthesis* `https://www.drugs.com/cg/lower-limb-prosthesis.html`. 2023.
31. *Human leg orthosis medical equipment* `https://www.freepik.com/premium-vector/human-leg-orthosis-medical-equipment_2338397.htm`.
32. He, Y., Luu, T. P., Nathan, K., Nakagome, S. & Contreras-Vidal, J. A mobile brain-body imaging dataset recorded during treadmill walking with a brain-computer interface. *Scientific Data* **5,** 180074 (Apr. 2018).
33. Bortole, M. *et al.* The H2 robotic exoskeleton for gait rehabilitation after stroke: early findings from a clinical study. *Journal of NeuroEngineering and Rehabilitation* (June 2015).
34. Farris, R. J., Quintero, H. A. & Goldfarb, M. Preliminary Evaluation of a Powered Lower Limb Orthosis to Aid Walking in Paraplegic Individuals. *IEEE Transactions on Neural Systems and Rehabilitation Engineering* **19,** 652–659 (2011).
35. Chen, B. *et al.* A wearable exoskeleton suit for motion assistance to paralysed patients. *Journal of Orthopaedic Translation* **11,** 7–18. ISSN: 2214-031X. `https://www.sciencedirect.com/science/article/pii/S2214031X16303023` (2017).
36. Vouga, T., Baud, R., Fasola, J., Bouri, M. & Bleuler, H. *TWIICE — A lightweight lower-limb exoskeleton for complete paraplegics* in *2017 International Conference on Rehabilitation Robotics (ICORR)* (2017), 1639–1645.
37. Chen, B. *et al.* Reference Joint Trajectories Generation of CUHK-EXO Exoskeleton for System Balance in Walking Assistance. *IEEE Access* **7,** 33809–33821 (2019).
38. Yeung, L.-F. *et al. Design of an exoskeleton ankle robot for robot-assisted gait training of stroke patients* in *2017 International Conference on Rehabilitation Robotics (ICORR)* (2017), 211–215.
39. Gao, S., Wang, Y., Fang, C. & Xu, L. A Smart Terrain Identification Technique Based on Electromyography, Ground Reaction Force, and Machine Learning for Lower Limb Rehabilitation. *Applied Sciences* **10.** ISSN: 2076-3417. `https://www.mdpi.com/2076-3417/10/8/2638` (2020).
40. Villa-Parra, A. *et al.* Control of a robotic knee exoskeleton for assistance and rehabilitation based on motion intention from sEMG. *Research on Biomedical Engineering* **34** (July 2018).
41. Shim, M. *et al.* Terrain Feature Estimation Method for a Lower Limb Exoskeleton Using Kinematic Analysis and Center of Pressure. *Sensors* **19.** ISSN: 1424-8220. `https://www.mdpi.com/1424-8220/19/20/4418` (2019).

42. Krausz, N. E. & Hargrove, L. J. *Recognition of ascending stairs from 2D images for control of powered lower limb prostheses* in *2015 7th International IEEE/EMBS Conference on Neural Engineering (NER)* (2015), 615–618.
43. Al-Dabbagh, A. *Visual-inertial prediction of terrain-specific human locomotion modes* Thesis (École polytechnique de Louvain (EPL), 2022).
44. Baud, R., Manzoori, A. R., Ijspeert, A. & Bouri, M. Review of control strategies for lower-limb exoskeletons to assist gait. English. *Journal of neuroengineering and rehabilitation* **18,** 119–119 (2021).
45. Choi, J., Na, B., Jung, P.-G., Rha, D.-w. & Kong, K. WalkON Suit: A Medalist in the Powered Exoskeleton Race of Cybathlon 2016. *IEEE Robotics Automation Magazine* **24,** 75–86 (2017).
46. Jackson, R. W. & Collins, S. H. An experimental comparison of the relative benefits of work and torque assistance in ankle exoskeletons. *Journal of Applied Physiology* **119.** PMID: 26159764, 541–557. eprint: `https://doi.org/10.1152/japplphysiol.01133.2014`. `https://doi.org/10.1152/japplphysiol.01133.2014` (2015).
47. Esquenazi, A., Talaty, M., Packel, A. & Saulino, M. The ReWalk Powered Exoskeleton to Restore Ambulatory Function to Individuals with Thoracic-Level Motor-Complete Spinal Cord Injury. *American Journal of Physical Medicine Rehabilitation* **91,** 911–921 (2012).
48. Sanz-Merodio, D., Cestari, M., Arevalo, J. C. & Garcia, E. Control Motion Approach of a Lower Limb Orthosis to Reduce Energy Consumption. *International Journal of Advanced Robotic Systems* **9,** 232 (2012).
49. Gams, A., Petrič, T., Debevec, T. & Babič, J. Effects of Robotic Knee Exoskeleton on Human Energy Expenditure. *IEEE Transactions on Biomedical Engineering* **60,** 1636–1644 (2013).
50. Sanz-Merodio, D., Cestari, M., Arevalo, J. C. & Garcia, E. Control Motion Approach of a Lower Limb Orthosis to Reduce Energy Consumption. *International Journal of Advanced Robotic Systems* **9,** 232 (2012).
51. Mooney, L. M. & Herr, H. M. Biomechanical walking mechanisms underlying the metabolic reduction caused by an autonomous exoskeleton. English. *Journal of neuroengineering and rehabilitation* **13,** 4–4 (2016).
52. Wang, S. *et al.* Design and Control of the MINDWALKER Exoskeleton. *IEEE Transactions on Neural Systems and Rehabilitation Engineering* **23,** 277–286 (2015).
53. Ronsse, R. *et al.* Oscillator-based assistance of cyclical movements: model-based and model-free approaches. English. *Medical biological engineering computing* **49,** 1173–1185 (2011).
54. Quintero, D., Villarreal, D. J., Lambert, D. J., Kapp, S. & Gregg, R. D. Continuous-Phase Control of a Powered Knee–Ankle Prosthesis: Amputee Experiments Across Speeds and Inclines. *IEEE Transactions on Robotics* **34,** 686–701 (2018).

55. Kang, I., Kunapuli, P. & Young, A. J. Real-Time Neural Network-Based Gait Phase Estimation Using a Robotic Hip Exoskeleton. *IEEE Transactions on Medical Robotics and Bionics* **2,** 28–37 (2020).

56. Thongsook, A., Nunthawarasilp, T., Kraypet, P., Lim, J. & Ruangpayoongsak, N. *C4.5 Decision Tree against Neural Network on Gait Phase Recognition for Lower Limp Exoskeleton* in *2019 First International Symposium on Instrumentation, Control, Artificial Intelligence, and Robotics (ICA-SYMP)* (2019), 69–72.

57. Xu, D., Liu, X. & Wang, Q. Knee Exoskeleton Assistive Torque Control Based on Real-Time Gait Event Detection. *IEEE Transactions on Medical Robotics and Bionics* **1,** 158–168 (2019).

58. Pasinetti, S., Fornaser, A., Lancini, M., De Cecco, M. & Sansoni, G. Assisted Gait Phase Estimation Through an Embedded Depth Camera Using Modified Random Forest Algorithm Classification. *IEEE Sensors Journal* **20,** 3343–3355 (2020).

59. Manchola, M. D. S., Mayag, L. J. A., Munera, M. & García, C. A. C. *Impedance-based Backdrivability Recovery of a Lower-limb Exoskeleton for Knee Rehabilitation* in *2019 IEEE 4th Colombian Conference on Automatic Control (CCAC)* (2019), 1–6.

60. Pehlivan, A. U., Losey, D. P. & O'Malley, M. K. Minimal Assist-as-Needed Controller for Upper Limb Robotic Rehabilitation. *IEEE Transactions on Robotics* **32,** 113–124 (2016).

61. Auberger, R., Russold, M. F., Riener, R. & Dietl, H. Patient Motion Using a Computerized Leg Brace in Everyday Locomotion Tasks. *IEEE Transactions on Medical Robotics and Bionics* **1,** 106–114 (2019).

62. Yao, S., Zhuang, Y., Li, Z. & Song, R. Adaptive Admittance Control for an Ankle Exoskeleton Using an EMG-Driven Musculoskeletal Model. *Frontiers in Neurorobotics* **12.** ISSN: 1662-5218. `https://www.frontiersin.org/articles/10.3389/fnbot.2018.00016` (2018).

63. Fernandes, P. N. *et al. EMG-based Motion Intention Recognition for Controlling a Powered Knee Orthosis* in *2019 IEEE International Conference on Autonomous Robot Systems and Competitions (ICARSC)* (2019), 1–6.

64. Grazi, L. *et al.* Gastrocnemius Myoelectric Control of a Robotic Hip Exoskeleton Can Reduce the User's Lower-Limb Muscle Activities at Push Off. *Frontiers in Neuroscience* **12.** ISSN: 1662-453X. `https://www.frontiersin.org/articles/10.3389/fnins.2018.00071` (2018).

65. Nasr, A., Laschowski, B. & McPhee, J. *Myoelectric Control of Robotic Leg Prostheses and Exoskeletons: A Review* in (Nov. 2021).

66. Eilenberg, M., Geyer, H. & Herr, H. Control of a Powered Ankle–Foot Prosthesis Based on a Neuromuscular Model. *IEEE transactions on neural systems and rehabilitation engineering : a publication of the IEEE Engineering in Medicine and Biology Society* **18,** 164–73 (Apr. 2010).

67. Ruiz Garate, V. *et al.* Walking Assistance Using Artificial Primitives: A Novel Bioinspired Framework Using Motor Primitives for Locomotion Assistance Through a Wearable Cooperative Exoskeleton. English. *IEEE Robotics and Automation Magazine* (2016).

68. Pinto-Fernandez, D. *et al.* Performance Evaluation of Lower Limb Exoskeletons: A Systematic Review. *IEEE Transactions on Neural Systems and Rehabilitation Engineering* **28,** 1573–1583 (2020).

69. Cifrek, M., Medved, V., Tonković, S. & Ostojić, S. Surface EMG based muscle fatigue evaluation in biomechanics. *Clinical Biomechanics* **24,** 327–340. ISSN: 0268-0033. `https://www.sciencedirect.com/science/article/pii/S0268003309000254` (2009).

70. Bhargava, L. J., Pandy, M. G. & Anderson, F. C. A phenomenological model for estimating metabolic energy consumption in muscle contraction. *Journal of Biomechanics* **37,** 81–88. ISSN: 0021-9290. `https://www.sciencedirect.com/science/article/pii/S0021929003002392` (2004).

71. Kim, J. H. & Roberts, D. A joint-space numerical model of metabolic energy expenditure for human multibody dynamic system. *International Journal for Numerical Methods in Biomedical Engineering* **31.** e02721 CNM-Nov-14-0190.R1, e02721. eprint: `https://onlinelibrary.wiley.com/doi/pdf/10.1002/cnm.2721`. `https://onlinelibrary.wiley.com/doi/abs/10.1002/cnm.2721` (2015).

72. Silva, F. & Tenreiro Machado, J. *Energy analysis during biped walking* in *Proceedings 1999 IEEE International Conference on Robotics and Automation (Cat. No.99CH36288C)* **1** (1999), 59–64 vol.1.

73. Ramanujam, A. *et al. Center of mass adaptations and its interaction between the trunk and lower-extremity during exoskeleton walking* in *2019 Wearable Robotics Association Conference (WearRAcon)* (2019), 57–62.

74. Shamaei, K. *et al.* Biomechanical Effects of Stiffness in Parallel With the Knee Joint During Walking. *IEEE Transactions on Biomedical Engineering* **62,** 2389–2401 (2015).

75. *Taille moyenne des hommes et des femmes* `https://www.donneesmondiales.com/taille-moyenne.php`.

76. Wang, J. M., Hamner, S. R., Delp, S. L. & Koltun, V. Optimizing Locomotion Controllers Using Biologically-Based Actuators and Objectives. *ACM Trans. Graph.* **31.** ISSN: 0730-0301. `https://doi.org/10.1145/2185520.2185521` (July 2012).

77. Somers, B. *Course bio-inspirée pour un robot humanoïde* Master's thesis (École polytechnique de Louvain (EPL), 2015).

78. Günther, M. & Rudder, H. Synthesis of two-dimensional human walking: a test of the -model. *Biol. Cybern.* **89,** 89–106 (2003).

79. Godha, S. & Lachapelle, G. Foot mounted inertial system for pedestrian navigation. *Measurement Science and Technology* **19,** 075202 (2008).

80. Bonnefoy-Mazure, A. & Armand, S. in, 199–214 (Jan. 2015).

81. Greiner, P. *Gait modulation of a humanoid robot, using bio-inspired mechanisms* Thesis (École polytechnique de Louvain (EPL), 2017).

UNIVERSITÉ CATHOLIQUE DE LOUVAIN
École polytechnique de Louvain
Rue Archimède, 1 bte L6.11.01, 1348 Louvain-la-Neuve, Belgique | **www.uclouvain.be/epl**